

Numerical Simulation of Natural Fire in an Industrial Building

Kalliopi K. Zografopoulou

Supervisor: Prof. Euripidis Mistakidis

Master of Science in

Applied Mechanics and Systems Modeling and Simulation

Dept. of Civil Engineering - University of Thessaly

Volos, June 2013

Summary

Post-earthquake non-structural damage can alter significantly the fire behaviour of a building which, if not taken under consideration, could downgrade the structural safety and pose a threat for the fire fighting and rescue crews. The target of this study is to examine the impact of the damage of the non-structural members on the development of natural fire in a industrial building. Several fire scenarios that correspond to different levels of damage are simulated and the temperatures arising in the vicinity of the steel structural members are discussed. The simulation is performed on a 3-D model, using the Fire Dynamics Simulator (FDS), a Computational Fluid Dynamics code for the simulation of thermally driven flows with an emphasis on smoke and heat transport from fires. The fire spread within the compartment is simulated using a temperature controlled activation of heat release devices representing the combustible materials. The intensity of the fire scenarios is discussed in correlation to the existing non-structural damage.

Keywords: natural fire, non-structural damage, CFD, FDS

Summary

(Greek)

Οι μετασεισμικές βλάβες των μη δομικών μελών μπορεί να αλλάξουν σημαντικά την συμπεριφορά ενός κτιρίου σε συνθήκες πυρκαγιάς, και αν δεν ληφθεί μέριμνα, μπορεί να υποβαθμίσουν την στατική ασφάλεια του κτιρίου και να αποτελέσουν απειλή για την ασφάλεια των συνεργείων διάσωσης και πυρόσβεσης. Ο στόχος της παρούσας μελέτης είναι να εξετάσει την επίδραση των μη δομικών βλαβών στην ανάπτυξη φυσικής πυρκαγιάς σε ένα βιομηχανικό κτίριο. Διάφορα σενάρια φυσικής πυρκαγιάς που αντιστοιχούν σε διαφορετικό επίπεδο μη δομικών βλαβών προσομοιώνονται αριθμητικά και στη συνέχεια καταγράφονται οι θερμοκρασίες που αναπτύσσονται στην περιοχή των δομικών μελών. Η προσομοίωση εκτελείται σε ένα 3-διάστατο αριθμητικό προσομοίωμα του κτιρίου, κάνοντας χρήση του Fire Dynamics Simulator, ενός έναρ κώδικα Υπολογιστικής Ρευστοδυναμικής για την προσομοίωση θερμικά οδηγούμενων ροών, με έμφαση στην μεταφορά καπνού και θερμότητας προερχόμενων από φωτιά. Η διάδοση της πυρκαγιάς εντός του πυροδιαμερίσματος προσομοιώνεται μέσω ειδικών, θερμοκρασιακά ελεγχόμενων συσκευών απελευθέρωσης θερμότητας οι οποίες αντιπροσωπεύουν τα εύφλεκτα υλικά. Η ένταση της κάθε πυρκαγιάς εξετάζεται σε συσχέτιση με το επίπεδο των μη δομικών βλαβών.

Λέξεις κλειδιά: φυσική πυρκαγιά, μη δομικές βλάβες, υπολογιστική ρευστοδυναμική

Table of Contents

1. INTRODUCTION	1
2. NATURAL FIRE BEHAVIOR IN AN ENCLOSURE	3
2.1 Stages of the Fire Development	3
<i>Pre-flashover period</i>	3
<i>Post-flashover period</i>	4
<i>Decay period</i>	4
2.3 Factors affecting fire development in an enclosure	5
<i>Ignition source</i>	5
<i>Fuel</i>	5
<i>Geometry of the enclosure</i>	7
<i>Compartment openings</i>	7
<i>Material properties of the enclosure boundaries</i>	8
3. EUROCODE’S GUIDELINES FOR FIRE DESIGN	9
3.1 Structural fire design procedure	9
3.2 Thermal Actions	10
3.2.1 <i>General rules</i>	10
3.2.2. <i>Nominal temperature-time curves</i>	11
3.2.2.1. <i>Standard temperature- time curve</i>	11
3.2.2.2. <i>External fire curve</i>	11
3.2.2.3. <i>Hydrocarbon curve</i>	11
3.2.3. <i>Natural fire models</i>	13
3.2.3.1. <i>Simplified fire models</i>	13
3.2.3.2. <i>Advanced fire models</i>	17
4. COMPUTATIONAL FLUID DYNAMICS	20
4.1 Application	20
4.2 Governing Equations	20
4.3 Turbulence modeling	22
<i>Reynolds-averaged Navier–Stokes equations</i>	22
<i>Large Eddy Simulation</i>	22
<i>Direct Numerical Simulation</i>	22

5. FIRE DYNAMICS SIMULATOR AND SMOKEVIEW	23
5.1 General description	23
5.2 Input parameters	23
5.3 Output parameters	24
5.4 Governing Equations, Assumptions and Numerics	25
5.5 Limitations and assumptions	26
6. BUILDING DESCRIPTION	29
7. PARAMETRIC FIRE SCENARIOS.....	33
8. SIMULATION.....	36
8.1 Computational domain – Grid Sensitivity	36
8.2 Structural materials	38
8.3 Modeling of fire and fire spread	40
<i>Fire modeling</i>	41
<i>Modeling of the fire spread</i>	44
8.4 Sprinklers and particle materials.....	45
8.5 Boundary conditions	46
8.6 Results data acquisition	47
<i>Temperature time histories</i>	47
<i>Plane slices</i>	48
<i>Smoke production and movement</i>	49
9. SIMULATION RESULTS.....	50
9.1 Processing of the temperature time-histories	50
9.2 Total Heat Release Rate.....	55
9.3 Pressure, velocity and temperature spatial distributions.....	56
10. DISCUSSION.....	69
11. CONCLUSIONS.....	75
12. REFERENCES.....	76

List of Figures

Fig. 2.1 Enclosure fire development in terms of gas temperatures (Karlsson and Quintiere,2000)	3
Fig. 2.2 Variation of flame spread over a thin paper card as a function of angle of inclination $\theta=90$ vertically downwards to $\theta=0$ horizontal, (Drysdale, 1999).....	6
Fig. 2.3 Interaction between a spreading flame and the surface of a thick combustible solid (Drysdale, 1999)	6
Fig. 2.4 The temperature in the fire plume as a function of height above a burning stack of wood pallets. A, B, and C indicate burning away from walls, by a wall, and in a corner, respectively (Karlsson and Quintiere,2000)	6
Fig. 2.5 Compartment fire burning rate data of Hägglund et al. (1974) as a function of the ventilation parameter $A_w H^{1/2}$ (Drysdale, 1999).....	8
Fig. 3.1 Nominal temperature – time curves	12
Fig. 3.2 Flame not impacting the ceiling (EN 1991-1-2)	14
Fig. 3.3 Flame impacting the ceiling (EN 1991-1-2)	15
Fig. 5.1 Oxygen-temperature phase space showing where combustion is allowed and not allowed to take place.	27
Fig. 6.1 Internal view of the industrial building.....	29
Fig. 6.2 External view of the industrial building.....	29
Fig. 6.3 Building description (dimensions in meters)	30
Fig. 6.4 Position of the sprinkler heads in the storage compartment.....	30
Fig. 6.5 Architectural Plane view (dimensions in meters)	31
Fig. 6.6 Elevation views (dimensions in meters)	32
Fig. 7.1 Parametric Fire Scenarios	34
Fig. 7.2 Position of the 50% functional part of the water sprinkler system	35
Fig 8.1 Point temperature histories for different mesh-cell dimensions.....	37
Fig. 8.2 Heat Release Rate for different mesh-cell dimensions	37
Fig. 8.3 Typical insulation panel cross section.....	39
Fig. 8.4 Combustion and pyrolysis (Gissi,2010).....	40
Fig. 8.5 Experimental setup of the rack units (Lönnermak and Ingason,2005)	41
Fig. 8.6 Experimental setup of the rack units (Lönnermak and Ingason,2005)	42
Fig. 8.7 Experimental setup of the rack units (Lönnermak and Ingason,2005)	42
Fig. 8.8 Experiment Heat Release Rate curve	43
Fig. 8.9 Experiment and Real scale Heat Release Rate curves	44
Fig. 8.10 Layout of the 156 Heat Release Rate sections	44
Fig. 8.11. Mesh of the type 2 was applied extending the computational domain beyond the windows and limits of the building in all directions (Gissi,2010)	47
Fig 8.12 Points where the gas temperatures time histories were recorded around the structural members during the fire simulation at a distance of 1.00 m.....	47
Fig. 8.13 Slices where the temperature distribution, velocity vector field and pressure is recorded with the evolution of time.....	48
Fig. 9.1 Fluctuation in the temperature time-histories.	50
Fig. 9.2 Total heat release rate of all the considered fire scenarios.....	55
Fig. 9.3 Total heat release rate of the seven most representative fire scenarios.....	55

Fig. 9.4 Slice of temperature distribution in the compartment – SC-00.....	56
Fig. 9.5 Area of Heat Release Rate per Unit Volume $> 27 \text{ kW/m}^3$ – SC-00.....	56
Fig. 9.6 Slice of temperature distribution in the compartment – SC-07.....	57
Fig. 9.7 Slice of temperature distribution under the roof – SC-07.....	57
Fig. 9.8 Area of Heat Release Rate per Unit Volume $> 27 \text{ kW/m}^3$ – SC-07.....	57
Fig. 9.9 Slice of temperature distribution in the compartment – SC-015a.....	58
Fig. 9.10 Slice of temperature distribution under the roof – SC-015a.....	58
Fig. 9.11 Area of Heat Release Rate per Unit Volume $> 27 \text{ kW/m}^3$ – SC-015a.....	58
Fig. 9.12 Slice of temperature distribution in the compartment – SC-015b.....	59
Fig. 9.13 Slice of temperature distribution under the roof – SC-015b.....	59
Fig. 9.14 Area of Heat Release Rate per Unit Volume $> 27 \text{ kW/m}^3$ – SC-015b.....	59
Fig. 9.15 Slice of temperature distribution in the compartment – SC-015c.....	60
Fig. 9.16 Slice of temperature distribution under the roof – SC-015b.....	60
Fig. 9.17 Area of Heat Release Rate per Unit Volume $> 27 \text{ kW/m}^3$ – SC-015c.....	60
Fig. 9.18 Slice of temperature distribution in the compartment – SC-030a.....	61
Fig. 9.19 Slice of temperature distribution under the roof – SC-030a.....	61
Fig. 9.20 Area of Heat Release Rate per Unit Volume $> 27 \text{ kW/m}^3$ – SC-030a.....	61
Fig. 9.21 Slice of temperature distribution in the compartment – SC-030b.....	62
Fig. 9.22 Slice of temperature distribution under the roof – SC-030b.....	62
Fig. 9.23 Area of Heat Release Rate per Unit Volume $> 27 \text{ kW/m}^3$ – SC-030b.....	62
Fig. 9.24 Slice of temperature distribution in the compartment – SC-030c.....	63
Fig. 9.25 Slice of temperature distribution under the roof – SC-030c.....	63
Fig. 9.26 Area of Heat Release Rate per Unit Volume $> 27 \text{ kW/m}^3$ – SC-030c.....	63
Fig. 9.27 Slice of temperature distribution in the compartment – SC-045.....	64
Fig. 9.28 Slice of temperature distribution under the roof – SC-045.....	64
Fig. 9.29 Area of Heat Release Rate per Unit Volume $> 27 \text{ kW/m}^3$ – SC-045.....	64
Fig. 9.30 Slice of temperature distribution in the compartment – SC-060a.....	65
Fig. 9.31 Slice of temperature distribution under the roof – SC-060a.....	65
Fig. 9.32 Area of Heat Release Rate per Unit Volume $> 27 \text{ kW/m}^3$ – SC-060a.....	65
Fig. 9.33 Slice of temperature distribution in the compartment – SC-060b.....	66
Fig. 9.34 Slice of temperature distribution under the roof – SC-060b.....	66
Fig. 9.35 Area of Heat Release Rate per Unit Volume $> 27 \text{ kW/m}^3$ – SC-060b.....	66
Fig. 9.36 Slice of temperature distribution in the compartment – SC-100.....	67
Fig. 9.37 Slice of temperature distribution under the roof – SC-100.....	67
Fig. 9.38 Area of Heat Release Rate per Unit Volume $> 27 \text{ kW/m}^3$ – SC-100.....	67
Fig. 9.39 Slice of temperature distribution in the compartment – SC-100SP50 50% operational water sprinkler system.....	68
Fig. 9.40 Slice of temperature distribution under the roof – SC-100SP50 50% operational water sprinkler system.....	68
Fig. 10.1 Fire scenarios SC-030a/b/c and steel frames' position.....	70
Fig. 10.2 Temperature distribution under the roof of the building for scenarios SC-030a/b/c	71
Fig. 10.3 Temperature distribution under the roof of the building for scenarios SC-07, SC- 015a/b/c and SC-045.....	71
Fig. 10.4 Temperature distribution under the roof of the building for scenarios SC-060a/b...	72

Fig. 10.5 Average gas temperature time-histories around the beam of the most affected frame by the fire.....	74
Fig. 10.6 Average gas temperature time-histories around the beam of the most affected frame by the fire.....	74

List of Tables

Table 7.1 Parametric Fire Scenarios.....	33
Table 8.1 Grid size and corresponding computational time required for the analysis of one fire scenario.....	37
Table 8.2 Thermal properties of insulation.....	38
Table 8.3 Thermal properties of concrete.....	38
Table 8.4 Thermal properties of steel.....	39
Table 8.5 Scale comparison between experiment setup and real building.....	42
Table 8.6 Properties of the water particles.....	45
Table 8.7 Plane slices and recorded quantities.....	48
Table 9.1 Duration (min) of temperature exceeding 600°C near the steel frames for every fire scenario.....	51
Table 9.2 Duration (min) of temperature exceeding 700°C near the steel frames for every fire scenario.....	52
Table 9.3 Duration (min) of temperature exceeding 800°C near the steel frames for every fire scenario.....	52
Table 9.4 Duration (min) of temperature exceeding 900°C near the steel frames for every fire scenario.....	53
Table 9.5 Duration (min) of temperature exceeding 900°C near the steel frames for every fire scenario.....	53
Table 9.6 Average duration (min) and st. deviation of temperature levels near the steel frames.....	54
Table 10.1 Duration (min) of temperature exceeding 600°C near the steel frames for fire scenarios SC-030a/b/c.....	70
Table 10.2 Duration (min) of temperature exceeding 600°C near the steel frames for fire scenarios SC-07, SC-015a/b/c and SC-045.....	71
Table 10.3 Duration (min) of temperature exceeding 800°C near the steel frames for fire scenarios SC-060a/b.....	72
Table 10.4 Average duration (min) and st. deviation of temperature levels near the steel frames for scenario SC-100.....	73

Acknowledgements

I would like to thank, first and foremost, my teacher, Professor Euripidis Mistakidis, initially for introducing me to the fascinating field of fire engineering and fire dynamics by offering me the opportunity to work on the present thesis, and secondly for his encouragement and continuous guidance and support until its completion.

Secondly, I would like to thank doctoral candidate and member of the Laboratory of Structural Analysis and Design, Daphne Pantousa, for her assistance, friendly collaboration and very helpful insights.

Last but not least, my family for all their love and encouragement.

“Essentially, all models are wrong, but some are useful.”

George E. P. Box (1919 – 2013), Mathematician

1. Introduction

Post earthquake non-structural damage is a definite result of middle to high intensity earthquakes, even in the case that the structural system remains intact. A subsequent fire after the seismic event in a structurally sound, though functionally damaged building, could eventually lead to unpredicted temperatures, which can cause the deterioration of the structural system and collapse of the structure, in addition to the potential loss of human lives.

Eurocode 1, part 1-2 (EN 1991-1-2) provides the current European normative basis for the appropriate procedures that should be followed regarding the fire design process and assessment of actions on structures exposed to fire. According to Eurocode, the analytical fire design procedure for the structure needs to take into account the behavior of the structural system at elevated temperatures, the potential heat exposure and the beneficial effects of any active and passive fire protection systems. Along with the above mentioned features, it is pointed also that the uncertainties associated with them ought to be taken into consideration with respect to the consequences of their failure. This study concentrates on this last part, the consequences of a failure of some of the building's features. This failure is not considered as an error in the structural design process, but as a corollary of an earthquake event, a situation not so rare, as history has shown in the numerous large fires that have occurred after earthquakes (Scawthorn Ch., 1996), (Ohnishi K., 1996). These fires can be caused by broken gas lines, destruction of the power grid, humans evacuating buildings hurriedly without switching off heating devices and any kind of short circuits that can act as ignition.

An aid in the fire design of buildings is the implementation of advanced modeling tools for the simulation of the natural fire phenomenon, like the one/two-zone models or the use of Computational Fluid Dynamics (CFD). Simpler methods such as the parametric temperature-time curves given in Eurocode1, part1-2 (EN 1991-1-2) are only valid for small compartments and only with specific occupancies. So, for the fire analysis and design, the engineer can either use the prescriptive method of the codes, if the building meets the criteria for its use, or if one is interested in a performance based design or evaluation, a numerical study of the fire phenomenon that takes into account its dynamic nature is the only available option.

The idea that the dynamics of a fire might be studied numerically, dates back to the beginning of the computer age. The equations that describe fluid motion are known since the 1840s (Navier-Stokes equations), but only with the introduction of computers a more consistent attempt was made to solve them numerically. However, in contrast to sole fluid motion, fire involves many other concepts such as body aerodynamics, multi-phase flow, turbulent mixing and combustion, radiative transport, and conjugate heat transfer. Therefore, the parameters that need to be known are many, and most of them are not well known. For example, the fuel, that is one of the necessary parameters to mathematically describe fire and combustion, is rarely explicitly known because, usually, the materials that act as fuel in most of the accidental fires were never intended as such.

A first attempt to numerically describe fire in a compartment and predict the arising temperatures for engineering purposes was performed with the use of the zone models, in which the compartment is divided in two zones (upper/hot and lower cooler) and mass and energy balances are enforced on both layers. In these models homogenous temperature, density, internal energy and pressure of gas within each layer are assumed.

A more advanced approach to numerical simulation of fire is the use of Computational Fluid Dynamics (CFD) which solves numerically a form of the Navier-Stokes equation, in addition to combustion and radiative heat transport modeling. The solution of the partial differential equations provides results of the thermo-dynamic and aero-dynamic variables in all points of the computational domain.

In this study, a CFD analysis is performed on an industrial building used as a storage facility and the aim is to examine the impact of non-structural damage on the development of natural fire. Several potential fire scenarios that correspond to different levels of damage of the non-structural members are considered and the temperature distributions arising in the vicinity of the steel structural members are recorded.

The fire development in the storage compartment is modelled with the Fire Dynamics Simulator (FDS) and Smokeview (SMV) software. FDS is a CFD code for the simulation of low mach, thermally driven flows with an emphasis on smoke and heat transport from fires. The CFD-FDS method has two main advantages over the two-zone model: the ability to describe a detailed geometry of the compartment/building with a custom-defined burn behaviour of the combustible materials and, secondly, the capability of providing time-history temperature results at any position of the modelled structure.

Finally, by the post processing, study and analysis of the gathered simulation results, conclusions regarding the severity of each fire scenario are determined.

2. Natural Fire Behavior in an Enclosure

2.1 Stages of the Fire Development

The development of natural fire can be divided in three main stages:

- the Pre-flashover period
- the Post- flashover period
- the Decay period of the fire

The term “flashover” that defines the two stages is the transition from the fire growth period to the fully developed stage in the enclosure fire development (Drysdale, 1999). The formal definition from the International Standards Organization is “the rapid transition to a state of total surface involvement in a fire of combustible material within an enclosure.”

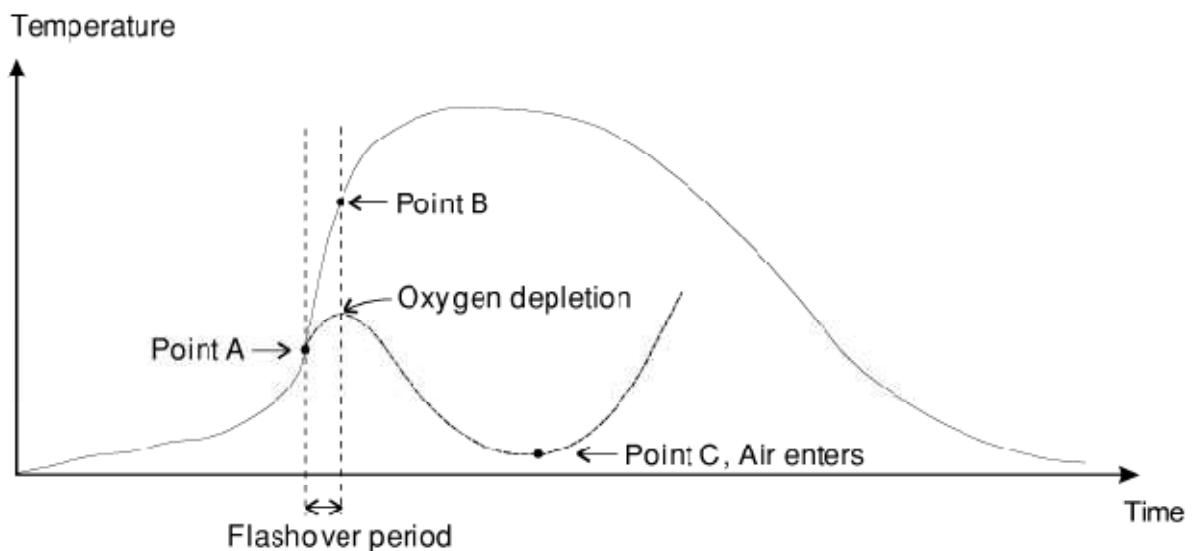


Fig. 2.1 Enclosure fire development in terms of gas temperatures (Karlsson and Quintiere, 2000)

PRE-FLASHOVER PERIOD

In the pre-flashover period the fire is localized and remains near the ignition point with minor spread in the neighborhood area. After the ignition the fire burns freely and the rate of burning depends only on the fuel characteristics and geometry, with the boundaries of the compartment having no effect on it. The temperature in the compartment is still very near the ambient temperature, although in the vicinity of the fire the temperature may start to be substantial. In this phase the fire may start to grow, depending mainly on the fuel supply, as the oxygen within the compartment in this stage is usually adequate to support the chemical reaction. As the temperature of the compartment is still low, there is no immediate effect in

the structural members and the engineering aim in this stage is the fire detection and safe evacuation of humans.

The pre-flashover stage can lead to:

- flashover and post flashover period,
- burn out of the fire without any involvement of the other combustible materials, or
- continuation of the burning at a very low rate with the danger of backdraught occurrence, depending on the air supply conditions of the compartment.

If there is enough ventilation during the process, assuming that fuel is present, the fire will start to spread and eventually will cease to be a local phenomenon and will ignite all the available combustible materials within the compartment. From this point, the interaction with the compartment boundaries will affect greatly the fire development. The flashover will then lead to the fully developed fire.

From the structural engineering point of view the pre-flashover period is not of great importance temperature wise as the increase in the compartment is relatively low, although depending on the compartment characteristics its duration can be comparable to the duration of the fully developed fire. The duration of the pre-flashover period defines a slow, medium or fast growing fire.

POST-FLASHOVER PERIOD

After the occurrence of the flashover, the fire has spread to almost all available exposed surfaces of the combustible materials in the compartment, becoming a global phenomenon, and the heat release rate reaches its peak, producing very high temperatures in the whole enclosure. This is also described as a *fully developed fire*. During this period the structural elements of the building are mostly affected by the heat produced and, depending on their fire resistance a number of the elements can fail and lead to local or general structure collapse. By this time if any of the occupants haven't evacuated the compartment the chances of survival are almost zero as a result of the temperatures that can exceed 1000°C, or due to asphyxiation caused by the smoke or CO produced by the fire. This is the important stage of the fire in regard to the structural safety of the structure in contrast to the pre-flashover stage which is important regarding the people's safety and evacuation.

The compartment boundaries at this time play a major role in the fire development. In this stage the fire will burn at a rate that is controlled either by the oxygen supply (*ventilation controlled fire*) or by the fuel supply if the oxygen levels are enough to support the combustion of the available combustible materials (*fuel controlled*). Usually, for typical compartment formations without extensive openings the fire is ventilation controlled. The factors that affect the fire behavior will be presented in more detail in the next section.

DECAY PERIOD

In the decay phase, as the fuel is consumed, the rate of combustion decreases, and with some time delay the compartment temperature will start to lower. This delay in the compartment temperature decrease depends on the thermal inertia, which can lead for a short period to further temperature increase in the compartment elements, even though the burning rate decreases. The fire will probably become from ventilation controlled to fuel controlled at this point.

2.3 Factors affecting fire development in an enclosure

The factors that define the development of natural fire in a compartment are the enclosure properties and the fuel characteristics.

These factors are (Karlsonn and Quintiere, 2000):

- the size and location of the ignition source
- the type, amount, position, spacing, orientation, and surface area of the fuel packages
- the geometry of the enclosure
- the size and location of the compartment openings
- the material properties of the enclosure boundaries.

IGNITION SOURCE

The ignition of a fire can be a chemical, electrical or mechanical supply of energy of a low value. It is usually a spark occurring accidentally, but can also be a pilot flame, to induce fire. In the accidental category can be included a glowing cigarette which can cause smoldering combustion and consequently flame, or an electrical spark due to a short circuit. The energy of the ignition can vary from very low (spark, cigarette) to high (pilot flame), and it can define the growth rate of the combustion.

The location of the ignition source is also important as buoyancy can cause more rapid fire development when the ignition is positioned at a lower level of the combustible material.

FUEL

The fuel available in buildings is either solid, in the majority of the cases, or liquid, usually only in industrial facilities.

For the combustion to occur, a mixture of flammable gases and oxygen (air) is necessary. For liquid fuels, evaporation creates the necessary flammable gases and for highly volatile substances is a respectively quick process, driven by the surrounding pressure and temperature. For solid fuels that are usually of cellulosic nature, (i.e. wood) the generation of flammable volatiles involves chemical decomposition of the solid (pyrolysis), which is an irreversible process and requires a source of energy in the form of heat.

The orientation of the surface of the fuel is of high importance as the flame spread is controlled by the way heat is transferred ahead of the burning zone. In liquid pool fires there is only a horizontal surface for the flame to spread, but in solid fuels any orientation configuration can be achieved. If the hot gases rise in the direction of the available material (upwards) the rate of spread is many times higher than if spread is allowed to occur downwards. In addition, the placement and spacing of the fuel packages can influence the fire growth. In a vertically spaced arrangement, upward flame spread will occur much more rapidly than lateral spread along a horizontal configuration (Fig. 2.2 and 2.3).

Also the placement of the available fuel within the compartment is a major factor as burning in the vicinity of a wall can lead to higher temperatures and higher flames. If the fire has no surrounding obstacles, cold air can be introduced from all directions, and hot air can be dispersed either. If there is an obstacle (i.e. wall) air is blocked from entering the combustion from this direction, and also the hot gases are forced to burn over a greater distance, thus causing higher flames (Fig. 2.4).

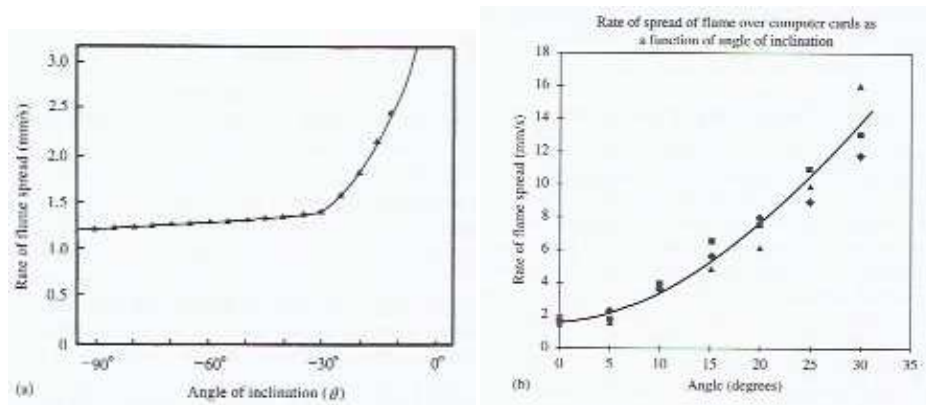


Fig. 2.2 Variation of flame spread over a thin paper card as a function of angle of inclination $\theta=-90$ vertically downwards to $\theta=0$ horizontal, (Drysdale, 1999)

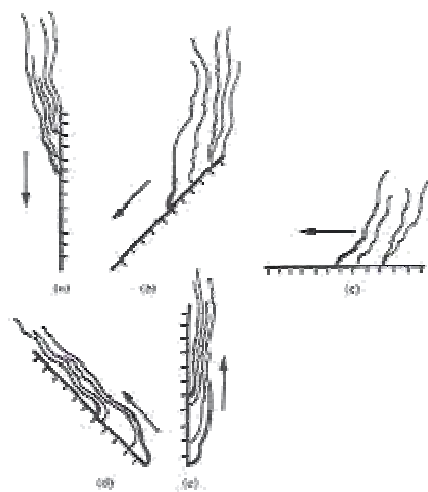


Fig. 2.3 Interaction between a spreading flame and the surface of a thick combustible solid (Drysdale, 1999)

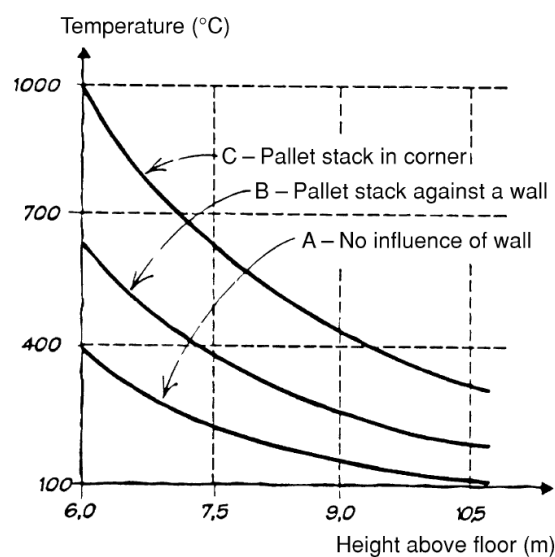


Fig. 2.4 The temperature in the fire plume as a function of height above a burning stack of wood pallets. A, B, and C indicate burning away from walls, by a wall, and in a corner, respectively (Karlsson and Quintiere,2000)

GEOMETRY OF THE ENCLOSURE

The geometry of the compartment is a key factor in the way the fire develops, as it defines the boundaries of the volume in which it is allowed to extend. As the fire grows, smoke and hot gases build up under the ceiling, creating a hot layer which heats the boundary surfaces and radiates heat back to the fire and the remaining combustible materials, enhancing the evaporation or pyrolysis rate, causing the fire to propagate. It is evident that a small compartment with a certain fuel load, will lead to higher gas temperatures and faster fire growth, than a larger compartment containing the same fuel load, as there is more air to be heated up and the formation of a thick hot layer will take longer. Also, the proximity of the boundaries and especially the upper boundary to the fire and the fire plumes will impact the rate of the fire growth, and the heat exposure of the structural elements, as the plume may start spreading horizontally due to the ceiling obstacle. A direct result is the increase in the burning rate as the heat feedback of the ceiling is greater and comes directly from the fire plumes.

In large enclosures with high ceilings, such as industrial buildings, the flames will probably not be high enough to reach the ceiling, and the long distance between the fire and the hot upper layer will not provide much heat through radiation back to the fire, thus decreasing the fire growth rate. The fire spread in this case is aided solely from the heat released directly from the burning adjacent materials.

COMPARTMENT OPENINGS

Along with the fuel supply the other major factor that defines the behavior and development of a compartment fire is the ventilation. After the fire has developed, the available oxygen in the initial air volume of the enclosure will be consumed. Then, depending on the ventilation conditions, the fire will either self-extinguish, if there is not any fresh air introduced to the compartment, or will continue to burn at a rate defined by the oxygen input through the openings. In the early stages of the fire development, the openings apart from providing air from the exterior into the compartment, also act as vents removing hot gases and smoke from the interior due to the difference in the pressure inside and outside of the enclosure.

For the ventilation controlled fires, provided that fuel is available, the *ventilation factor* of the compartment $A_w H^{1/2}$, has been found to influence greatly the fire's behavior (A_w is the area of the opening and H is the opening's height (originally studied by Kawagoe, 1958)). In a series of experiments by Hägglund et al. (1974), the ventilation factor was studied in correlation to the rate of burning and the occurrence or not of a flashover in the compartment. The test results, presented in Figure 2.5, show that an increase in the ventilation factor increases the rate of burning. Also the pair of burning rate and ventilation factor defines whether flashover will occur or not, noted that flashover in the context of the experiments was defined by ceiling temperatures greater than 600°C and visible flames through the openings.

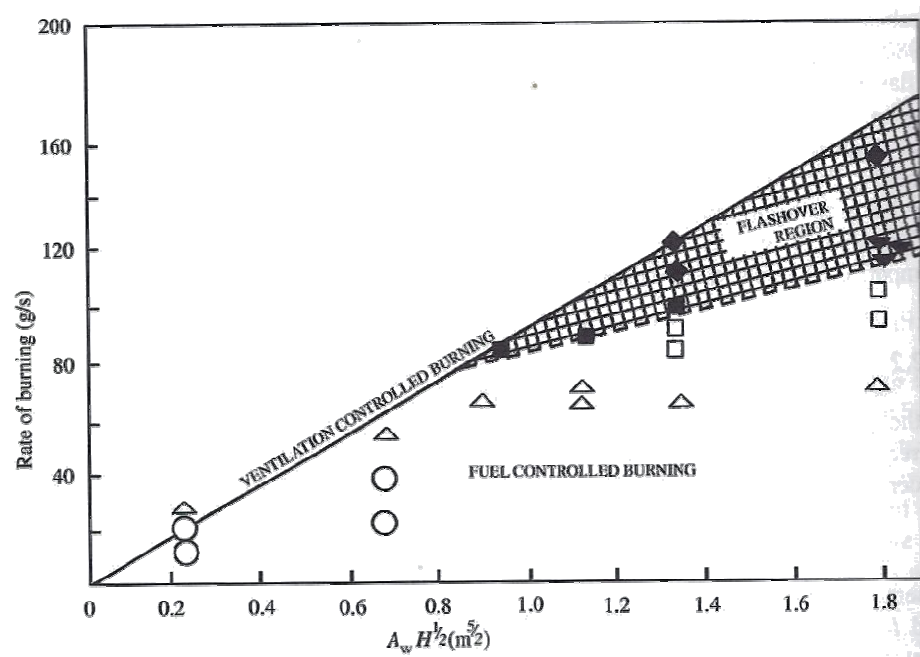


Fig. 2.5 Compartment fire burning rate data of Hägglund et al. (1974) as a function of the ventilation parameter $A_w H^{1/2}$ (Drysdale, 1999)

MATERIAL PROPERTIES OF THE ENCLOSURE BOUNDARIES

As mentioned earlier, some of the heat that is produced by the fire is redirected back to the compartment through radiation, enhancing the combustion. This process is highly affected by the material properties of the compartment boundaries. Materials with low conductivity (thermal insulators) reduce considerably the heat that is conducted through the bounding surfaces away from the enclosure causing the hot gases to retain most of their energy, increasing at the same time feedback radiation to the fire and the rest of the combustible materials.

3. Eurocode's guidelines for fire design

3.1 Structural fire design procedure

According to Eurocode 1, part 1-2 (EN 1991-1-2) a structural fire design analysis should take into account the following steps:

- Selection of the relevant design fire scenarios
- Determination of the corresponding design fires
- Calculation of the temperature evolution within the structural members
- Calculation of the mechanical behavior of the structure exposed to fire.

The design process can be considered as a two part procedure. The first two steps of fire design process correspond to the assessment of the fire loads that the structural members are eventually exposed to and the last two consider the consequent structural - mechanical analysis.

The design fire scenario that defines the accidental design situation should be determined on the basis of a fire risk assessment.

Fire is classified as an accidental action, thus time- and load-dependent structural behavior need not be taken into account, unless the fire risk arises as a consequence of other accidental actions, which then should be considered as a whole.

Regarding the fire scenario, the design fire should be applied only to one fire compartment of the building at a time, unless otherwise specified in the design fire scenario.

After the fire situation is considered and the temperatures are estimated, the mechanical analysis follows.

3.2 Thermal Actions

3.2.1 GENERAL RULES

(adapted from EN 1991-1-2, Section 3: Thermal actions for temperature analysis)

(1) On the fire exposed surfaces the net heat flux \dot{h}_{net} should be determined by considering heat transfer by convection and radiation as

$$\dot{h}_{\text{net}} = \dot{h}_{\text{net,c}} + \dot{h}_{\text{net,r}} \quad [\text{W/m}^2] \quad (3.1)$$

where

$\dot{h}_{\text{net,c}}$ is given by e.q. (3.2)

$\dot{h}_{\text{net,r}}$ is given by e.q. (3.3)

(2) The net convective heat flux component should be determined by:

$$\dot{h}_{\text{net,c}} = a_c \times (\Theta_g - \Theta_m) \quad [\text{W/m}^2] \quad (3.2)$$

where

a_c is the coefficient of heat transfer by convection $[\text{W/m}^2\text{K}]$

Θ_g is the gas temperature in the vicinity of the fire exposed member $[\text{°C}]$

Θ_m is the surface temperature of the member $[\text{°C}]$

(4) On the unexposed side of separating members, the net heat flux \dot{h}_{net} should be determined by using equation (3.1), with $a_c = 4 [\text{W/m}^2\text{K}]$. The coefficient of heat transfer by convection should be taken as $a_c = 9 [\text{W/m}^2\text{K}]$, when assuming it contains the effects of heat transfer by radiation.

(5) The net radiative heat flux component per unit surface area is determined by:

$$\dot{h}_{\text{net,r}} = \Phi \times e_m \times e_f \times \sigma \times [(\Theta_r + 273)^4 - (\Theta_m + 273)^4] \quad [\text{W/m}^2] \quad (3.3)$$

where

Φ is the configuration view factor

e_m is the surface emissivity of the member

e_f is the emissivity of the fire

σ is the Stephan Boltzmann constant ($= 5,67 \times 10^{-8} \text{ W/m}^2\text{K}^4$)

Θ_r is the effective radiation temperature of the fire environment $[\text{°C}]$

Θ_m is the surface temperature of the member $[\text{°C}]$

NOTE: Unless given in the material related fire design Parts of prEN 1992 to prEN 1996 and prEN 1999, $e_m = 0.8$ may be used.

3.2.2. NOMINAL TEMPERATURE-TIME CURVES

3.2.2.1. Standard temperature- time curve

The most usual method for the fire design of the structural members and the determination of their fire resistance is the direct use of the nominal temperature-time curves and specifically the standard temperature-time curve:

$$\Theta_g = 20 + 345 \log_{10}(8t + 1) \quad [^{\circ}\text{C}] \quad (3.4)$$

where

Θ_g is the gas temperature in the fire compartment [$^{\circ}\text{C}$]
 t is the time [min]

The coefficient of heat transfer by convection is $a_c = 25 \text{ W/m}^2\text{K}$

This curve provides the gas temperature time history around the structural member and is considered to be the same for all the members of the structural system.

3.2.2.2. External fire curve

The external fire curve can be used for external structural members that are subjected to fire through openings. The external fire curve is given by

$$\Theta_g = 660 (1 - 0.687 e^{-0,32 t} - 0.313 e^{-3,8 t}) + 20 \quad [^{\circ}\text{C}] \quad (3.5)$$

where

Θ_g is the gas temperature in the fire compartment [$^{\circ}\text{C}$]
 t is the time [min]

The coefficient of heat transfer by convection is $a_c = 25 \text{ W/m}^2\text{K}$

3.2.2.3. Hydrocarbon curve

The hydrocarbon temperature-time curve is given by

$$\Theta_g = 1080 (1 - 0.325 e^{-0,167 t} - 0.675 e^{-2,5 t}) + 20 \quad [^{\circ}\text{C}] \quad (3.6)$$

where

Θ_g is the gas temperature in the fire compartment [$^{\circ}\text{C}$]
 t is the time [min]

The coefficient of heat transfer by convection is $a_c = 50 \text{ W/m}^2\text{K}$

The temperature evolution for the three curves is given in Fig. 3.1.

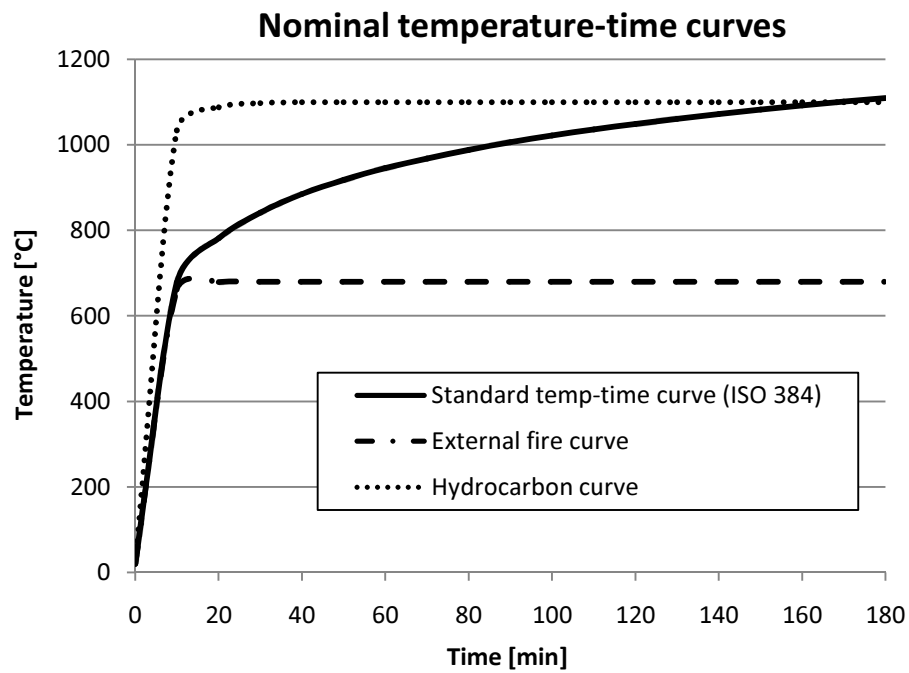


Fig. 3.1 Nominal temperature – time curves

3.2.3. NATURAL FIRE MODELS

3.2.3.1. Simplified fire models

The simplified fire models have a limited field of application, are based on specific physical parameters, and either provide a uniform temperature distribution as a function of time in the compartment (compartment fires), or a non uniform temperature distribution (localized fires).

Compartment Fires

(the equations are taken from Annex A of EN 1991-1-2)

In the case of compartment fires the temperature time history that is used is applicable only to

- compartments up to 500 m²,
- without roof openings and
- for a maximum compartment height of 4 m.

The time-temperature curve is given by

$$\Theta_g = 20 + 1325(1 - 0.324 e^{-0.2t^*} - 0.204 e^{-1.7 t^*} - 0.472 e^{-19t^*}) \quad (3.7)$$

where

Θ_g is the gas temperature in the fire compartment [°C]

$$t^* = t \cdot \Gamma \quad [\text{h}] \quad (3.8a)$$

with

t time [h]

$$\Gamma = [O/b]^2 / (0.04/1160)^2 \quad [-]$$

$$b = (\sqrt{\rho c \lambda})$$

with the following limits: $100 \leq b \leq 2\,200$ [J/m²s^{1/2} K]

ρ density of boundary of enclosure [kg/m³]

c specific heat of boundary of enclosure [J/kgK]

λ thermal conductivity of boundary of enclosure [W/mK]

O opening factor: $A_v \sqrt{h_{eq}} / A_t$ [m^{1/2}]

with the following limits: $0.02 \leq O \leq 0.20$

A_v total area of vertical openings on all walls [m²]

h_{eq} weighted average of window heights on all walls [m]

A_t total area of enclosure (walls, ceiling and floor, including openings) [m²]

NOTE In case of $\Gamma = 1$, equation (3.7) approximates the standard temperature-time curve.

Localized Fires

(the equations are taken from Anex C of EN 1991-1-2)

Localized fires ought to be considered where flashover is unlikely to occur.

The heat flux from a localized fire to a structural element is calculated with expression (3.1), along with the configuration factor.

The flame lengths L_f of a localized fire (see Figure 3.2) is given by:

$$L_f = -1.02D + 0.0148Q^{2/5} \quad [\text{m}] \quad (3.9)$$

When the flame is not impacting the ceiling of a compartment ($L_f < H$) or in case of fire in open air, the temperature $\Theta(z)$ in the plume along the symmetrical vertical flame axis is given by:

$$\Theta(z) = 20 + 0.25Q_c^{2/3} (z-z_0)^{-5/3} \leq 900 \quad [^\circ\text{C}] \quad (3.10)$$

where

D is the diameter of the fire [m], see Figure 3.2

Q is the rate of heat release [W] of the fire according to EN 1991-1-2-E.4

Q_c is the convective part of the rate of heat release [W], with $Q_c = 0.8 Q$ by default

z is the height [m] along the flame axis, see Figure 3.2

H is the distance [m] between the fire source and the ceiling, see Figure 3.2

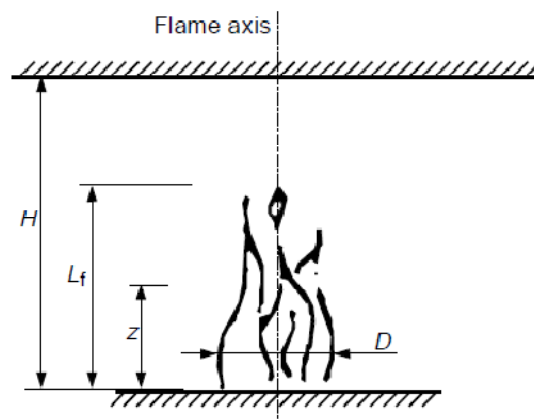


Fig. 3.2 Flame not impacting the ceiling (EN 1991-1-2)

The virtual origin z_0 of the axis is given by:

$$z_0 = -1.02D + 0.00524Q^{2/5} \quad [\text{m}] \quad (3.11)$$

When the flame is impacting the ceiling ($L_f \geq H$) the heat flux \dot{h} [W/m^2] received by the fire exposed unit surface area at the level of the ceiling is given by:

$$\begin{aligned} \dot{h} &= 100000 & \text{if } y &\leq 0.30 \\ \dot{h} &= 136300 \text{ to } 121000 y & \text{if } 0.30 < y < 1.0 \\ \dot{h} &= 15000 y^{-3.7} & \text{if } y &\geq 1.0 \end{aligned}$$

where

y is a parameter [-] given by :

r is the horizontal distance [m] between the vertical axis of the fire and the point along the ceiling where the thermal flux is calculated, see Figure 3.3

H is the distance [m] between the fire source and the ceiling, see Figure 3.3

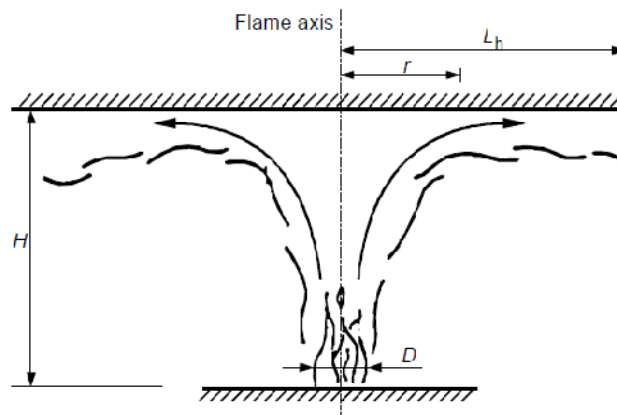


Fig. 3.3 Flame impacting the ceiling (EN 1991-1-2)

L_h is the horizontal flame length (Figure 3.3) given by the following relation:

$$L_h = (2.9 H (Q_H^*)^{0.33}) - H \quad [\text{m}] \quad (3.12)$$

Q_H^* is a non-dimensional rate of heat release given by:

$$Q_H^* = Q / (1.11 \cdot 10^6 \cdot H^{2.5}) \quad [-] \quad (3.13)$$

z' is the vertical position of the virtual heat source [m] and is given by:

$$z' = 2.4D(Q_D^{*2/5} - Q_D^{*2/3}) \text{ when } Q_D^* < 1,0 \quad (3.14)$$

$$z' = 2.4D(1,0 - Q_D^{*2/5}) \text{ when } Q_D^* \geq 1,0$$

where

$$Q_D^* = Q/1.11 \cdot 10^6 \cdot D^{2.5} \quad (3.15)$$

The net heat flux \dot{h}_{net} received by the fire exposed unit surface area at the level of the ceiling, is given by :

$$\dot{h}_{\text{net}} = \dot{h} - \alpha_c \cdot (\Theta_m - 20) - \Phi \cdot \varepsilon_m \cdot \varepsilon_f \cdot \sigma \cdot [(\Theta_m + 273)^4 - (293)^4] \quad (3.16)$$

where the various coefficients depend on expressions (3.2), (3.3) and (3.12).

The rules given are valid if the following conditions are met:

- the diameter of the fire is limited by $D \leq 10$ m;
- the rate of heat release of the fire is limited by $Q \leq 50$ MW.

In case of several separate localized fires, expression (3.16) may be used in order to get the different individual heat fluxes $\dot{h}_1, \dot{h}_2 \dots$ received by the fire exposed unit surface area at the level of the ceiling.

The total heat flux may be taken as:

$$\dot{h}_{\text{tot}} = \dot{h}_1 \dots \leq 100\,000 \quad [\text{W/m}^2] \quad (3.17)$$

3.2.3.2. Advanced fire models

(the equations are taken from Annex D of EN 1991-1-2)

The advanced fire models according to Eurocode 1 should take into account the gas properties, the mass exchange and the energy exchange. The models that should be used are:

- One zone models
- Two-zone models
- Computational Fluid Dynamic models

One-zone models

A one-zone model should apply for post-flashover conditions. Homogeneous temperature, density, internal energy and pressure of the gas are assumed in the compartment.

The temperature should be calculated considering:

- the resolution of mass conservation and energy conservation equations;
- the exchange of mass between the internal gas, the external gas (through openings) and the fire (pyrolysis rate);
- the exchange of energy between the fire, internal gas, walls and openings.

The ideal gas law considered is:

$$P_{int} = \rho_g R T_g \quad [\text{N/m}^2] \quad (3.18)$$

The mass balance of the compartment gases is written as

$$\frac{dm}{dt} = \dot{m}_{in} - \dot{m}_{out} + \dot{m}_{fi} \quad [\text{kg/s}] \quad (3.19)$$

where

$\frac{dm}{dt}$ is the rate of change of gas mass in the fire compartment

\dot{m}_{out} is the rate of gas mass going out through the openings

\dot{m}_{in} is the rate of gas mass coming in through the openings

\dot{m}_{fi} is the rate of pyrolysis products generated

The rate of change of gas mass and the rate of pyrolysis may be neglected. Thus

$$\dot{m}_{in} = \dot{m}_{out}$$

These mass flows may be calculated based on static pressure due to density differences between air at ambient and high temperatures, respectively.

The energy balance of the gases in the fire compartment may be taken as:

$$\frac{dE_g}{dt} = Q - Q_{out} - Q_{in} - Q_{wall} - Q_{rad}$$

where

E_g is the internal energy of gas [J]

Q is the rate of heat release of the fire [W]

$$Q_{out} = \dot{m}_{out} c T_f$$

$$Q_{in} = \dot{m}_{in} c T_{amb}$$

$Q_{wall} = (A_t - A_{h,v}) \dot{h}_{net}$, is the loss of energy to the enclosure surfaces

$Q_{rad} = A_{h,v} \sigma T_f^4$, is the loss of energy by radiation through the openings

with:

c is the specific heat [J/kgK]

\dot{h}_{net} is given by expression (3.1)

\dot{m} is the gas mass rate [kg/s]

T is the temperature [K]

Two-zone models

A two-zone model is based on the assumption of accumulation of combustion products in a layer beneath the ceiling, with a horizontal surface. Different zones are defined: the upper layer, the lower layer, the fire and its plume and the external gas and walls. In the upper layer the characteristics of the gas are assumed to be uniform and the exchanges of mass, energy and chemical substance are calculated between these different zones. In a fire compartment with uniformly distributed fire load, a two zone model may develop into a one zone fire:

- if the gas temperature of the upper layer gets higher than 500°C or
- if the upper layer is growing so to cover 80% of the compartment height.

Computational Fluid Dynamic models (CFD)

Computational Fluid Dynamic models solve numerically the partial differential equations giving in all points of the compartment the thermodynamic and aerodynamic variables. These models analyze systems involving fluid flow, heat transfer and associated phenomena by solving the fundamental equations of the fluid flow. These equations represent the mathematical statements of the conservation laws of physics:

- the mass of a fluid is conserved;
- the rate of change of momentum equals the sum of the forces on a fluid particle (Newton's second law);
- the rate of change of energy is equal to the sum of the rate of heat increase and the rate of work done on a fluid particle (first law of thermodynamics).

A more detailed description of the Computational Fluid Dynamic models is given in the next chapter.

4. Computational Fluid Dynamics

4.1 Application

Computational Fluid Dynamics (CFD) is a branch of fluid mechanics, which uses numerical methods to obtain solutions of the equations of motion of fluids and describe their interaction with solid bodies. The equations have been introduced since the 1840s (Navier – Stokes), but due to the fact that they were closely coupled they were very difficult to be solved. Some explicit solutions were given only for very low Reynolds numbers and for very simple geometries. The potential for solution of turbulent flows was invoked with the appearance of computers powerful enough to allow computations, at least nominally, to be extended to considerably higher Reynolds numbers. Since then, with the advance both in computer capabilities and numerical methods CFD methods are applied in every discipline that involves flow movement.

Nowadays, it is used both as a research and design tool in

- Aerospace
- Automobile and engine applications
- Industrial manufacturing
- Chemical engineering
- Civil engineering applications
- Environmental engineering
- Naval Architecture
- Fire engineering

With the aid of CFD the various problems can be modeled and studied without extensive need of experimental testing -it will always be needed in addition to theory-, but at least much lesser in quantity and, most important, of better design. With CFD simulations a problem can be studied in infinite forms or scenarios, without any expenses apart from computational or programming time. Moreover it is the only solution for the study of certain problems, such as aircrafts in supersonic speeds that cannot be accommodated by wind tunnels.

In the last 10-20 years the CFD method has been used for fire and combustion modeling with the development of appropriate codes, incorporating combustion and radiation transport modeling for the solution of thermally driven flows.

4.2 Governing Equations

The equations that describe the motion of fluids are the complete system of Navier –Stokes equations. These are a set of partial differential equations that are derived from the three fundamental principles of physics:

- Mass is conserved
- Newton's second law , $F = m a$
- Energy is conserved

That's why they are also referred as the continuity, momentum and energy equations.

The equations are presented in brief and more details about their forms and solution can be found in the FDS Technical Reference Guide Volume 1- Mathematical Model.

The Continuity Equation

Mass conservation can be expressed in terms of the density, ρ

$$\frac{\partial \rho}{\partial t} + \nabla \cdot (\rho \mathbf{V}) = 0 \quad (4.1)$$

The Momentum Equation(s)

in conservation form

x component

$$\frac{\partial(\rho u)}{\partial t} + \nabla \cdot (\rho u \mathbf{V}) = - \frac{\partial p}{\partial x} + \frac{\partial \tau_{xx}}{\partial x} + \frac{\partial \tau_{yx}}{\partial y} + \frac{\partial \tau_{zx}}{\partial z} + \rho f_x \quad (4.2a)$$

y component

$$\frac{\partial(\rho v)}{\partial t} + \nabla \cdot (\rho v \mathbf{V}) = - \frac{\partial p}{\partial y} + \frac{\partial \tau_{xy}}{\partial x} + \frac{\partial \tau_{yy}}{\partial y} + \frac{\partial \tau_{zy}}{\partial z} + \rho f_y \quad (4.2b)$$

z component

$$\frac{\partial(\rho w)}{\partial t} + \nabla \cdot (\rho w \mathbf{V}) = - \frac{\partial p}{\partial z} + \frac{\partial \tau_{zx}}{\partial x} + \frac{\partial \tau_{yz}}{\partial y} + \frac{\partial \tau_{zz}}{\partial z} + \rho f_z \quad (4.2c)$$

The Energy Equation

in conservation form

$$\begin{aligned} \frac{\partial}{\partial t} \left[\rho \left(e + \frac{V^2}{2} \right) \right] + \nabla \cdot \left[\rho \left(e + \frac{V^2}{2} \right) \mathbf{V} \right] &= \rho \dot{q} + \frac{\partial}{\partial x} \left(k \frac{\partial T}{\partial x} \right) + \frac{\partial}{\partial y} \left(k \frac{\partial T}{\partial y} \right) \\ &+ \frac{\partial}{\partial z} \left(k \frac{\partial T}{\partial z} \right) - \frac{\partial(u p)}{\partial x} - \frac{\partial(v p)}{\partial y} - \frac{\partial(w p)}{\partial z} + \frac{\partial(u \tau_{xx})}{\partial x} \\ &+ \frac{\partial(u \tau_{yx})}{\partial y} + \frac{\partial(u \tau_{zx})}{\partial z} + \frac{\partial(v \tau_{xy})}{\partial x} + \frac{\partial(v \tau_{yy})}{\partial y} \\ &+ \frac{\partial(v \tau_{zy})}{\partial z} + \frac{\partial(w \tau_{xz})}{\partial x} + \frac{\partial(w \tau_{yz})}{\partial y} + \frac{\partial(w \tau_{zz})}{\partial z} + \rho \mathbf{f} \cdot \mathbf{V} \end{aligned} \quad (4.3)$$

4.3 Turbulence modeling

In contrast to laminar flow, turbulent flow is described by the chaotic motion of the molecules of the fluid along complex irregular paths causing the various layers of the fluid to mix intensely. The simulation of such flow is very difficult, although the fluctuations in the flow variables are of deterministic nature.

There are many turbulence models available. Here will be presented briefly the three most widely used models in the applications of fire simulation.

REYNOLDS-AVERAGED NAVIER–STOKES EQUATIONS

The Reynolds-averaged form of the Navier – Stokes equations (RANS) is a time-averaged approximation of the conservation equations of fluid dynamics. The averaging time is long enough to require the introduction of large eddy transport coefficients to describe the unresolved fluxes of mass, momentum and energy. Due to the averaging in the basic equations the results of the simulations are more smooth, because the smallest resolvable length scales are determined by the product of the local velocity and the averaging time rather than the spatial resolution of the underlying computational grid. The evolution of large eddy structures, characteristic of most fire plumes, is lost and the method lacks in the prediction of local transient events.

LARGE EDDY SIMULATION

Large Eddy Simulation (LES) is based on the observation that the small turbulent structures are more universal in character than the large eddies. Therefore, there is no need to compute the momentum and energy transfer of these small turbulent structures, but only the momentum and energy transfer of the large eddies. The effect of the small scale structures can be modeled separately. Specifically in the case of combustion modeling the idea is that the eddies that account for most of the mixing of the gaseous fuels and combustion products with the atmosphere of the fire can be calculated with reasonable accuracy from the equations of fluid dynamics, without the simultaneous calculation of the small scale eddies in the computational mesh.

DIRECT NUMERICAL SIMULATION

Direct Numerical Simulation (DNS) is the most straightforward approach. The solution is obtained by solving directly the Navier-Stokes equations without any turbulence model. This means that the turbulence must be resolved in the computational mesh. A mesh capable of such a task would have to account for the whole range of spatial and temporal scales of the turbulence. This approach requires very high computational recourses, which are still unavailable for the usual problems of engineering, such as the simulation of building fires.

5. Fire Dynamics Simulator and Smokeview

(based on the FDS Technical Reference guide)

5.1 General description

Fire Dynamics Simulator (FDS) is a Computational Fluid Dynamics model of fire driven fluid flow. It is a Large Eddy Simulation (LES) code for low speed thermally driven flow with an emphasis on smoke and heat transport from fires. The partial derivatives of the conservation equations of mass, momentum and energy are approximated as finite differences, and the solution is updated in time on a three-dimensional, rectilinear grid. Thermal radiation is computed using a finite volume technique on the same grid as the flow solver. Lagrangian particles are used to simulate smoke movement, sprinkler discharge, and fuel sprays.

Smokeview is an accompanying visualization program to FDS that produces images and animations of the results. Smokeview is able to visualize fire and smoke in a fairly realistic way. It can produce three-dimensional realistic renderings of the fire and smoke development along with the described geometry.

The code was originally developed by the National Institute of Standards and Technology (NIST) and the first version was publicly released in 2000.

The aim of the software is to solve practical fire problems in fire engineering, but it is also used as a tool to analyze and study fire dynamics and combustion. As a fire engineering tool it can be implemented in the analysis of:

- Low speed transport of heat and combustion products of fire
- Radiative and convected heat transfer between gas and solid surfaces
- Sprinkler, heat detector and smoke detector activation.

It can also be used to model more advanced physical phenomena such as pyrolysis, flame spread and fire growth, sprinkler activation and fire suppression by water.

All the above characteristics make it a suitable candidate for the study and analysis of residential and industrial fires by engineers, and other fire related professions such as the fire service. However, due to the complexity of the phenomena that are modeled and the large number of parameters that need to be provided, it should not be treated as software with conclusive predictive capability, but as a supplement to the informed and qualified engineer. To date, about half of the applications of the model have been for design of smoke control systems and sprinkler/detector activation studies. The other half consists of residential and industrial fire reconstructions.

5.2 Input parameters

All the necessary input parameters of the model and corresponding fire scenario are described in a text file. The basic parameters are information regarding the numerical grid, ambient environment, building geometry, material properties, combustion kinetics, and desired output quantities. The numerical grid consists of one or more rectilinear meshes with (usually) uniform cells. All geometric features must conform to the specified grid, and objects that are smaller than the grid, are ignored or approximated as a single cell. Due to the

rectilinear grid all the building's entities are described as a series of rectangle blocks, and the detail of the geometric description is defined by the mesh refinement. Boundary conditions are applied to solid surfaces. Materials are defined by their thermal conductivity, specific heat, density, thickness, and burning behavior.

For the simulation of real fire scenarios in real structures, the properties of the building's walls, floors, ceilings and furnishings need to be provided. FDS treats all of these objects as multi-layered solids, thus the physical parameters for many real objects can only be viewed as approximations to the actual properties. The properties of these materials govern the fire development and their accurate and appropriate description is the part that requires the most effort and attention by the user. Thermal properties such as conductivity, specific heat, density, and thickness can be found in various handbooks, or in manufacturers' literature, or from bench-scale measurements. The burning behavior of materials at different heat fluxes is more difficult to be described, and the properties more difficult to be obtained. Despite the many scripted or online material properties databases, the description of a particular item in most of the cases is very challenging.

5.3 Output parameters

As output parameters can be almost all of the variables described in the equations that are used to perform the numerical calculations, such as temperature, density, pressure, velocity and chemical composition. These variables are available in every grid cell for every discrete simulation time step. Also, FDS computes at solid surfaces the temperature, heat flux, mass loss rate, and various other quantities. Because of the large number of grid cells and time steps, which are usually in the magnitude of thousands or millions, the storage of all the quantities would require enormous data files, so the user must choose from the beginning which output quantities to record, as it would be done in the case of a real experiment.

Typical output quantities for the gas phase include:

- Gas temperature
- Gas velocity
- Gas species concentration (water vapor, CO₂, CO, N₂)
- Smoke concentration and visibility estimates
- Pressure
- Heat release rate per unit volume
- Mixture fraction (or air/fuel ratio)
- Gas density
- Water droplet mass per unit volume

On solid surfaces, FDS predicts additional quantities associated with the energy balance between gas and solid phase, such as:

- Surface and interior temperature
- Radiative and convective heat flux,
- Burning rate
- Water droplet mass per unit area

Global quantities recorded by the program include:

- Total Heat Release Rate (HRR)
- Sprinkler and detector activation times
- Mass and energy fluxes through openings or solids

The various quantity time histories at single points are simple data sets that can be easily plotted. The more complex field or surface data are visualized with the use of Smokeview in 3-d surfaces or section slices.

5.4 Governing Equations, Assumptions and Numerics

For the calculation of the thermal flows FDS implements various models which deal with the aspects of the corresponding governing equations that are associated with all the different phenomena that constitute fire development and heat transport.

Hydrodynamic Model

FDS solves numerically a form of the Navier-Stokes equations appropriate for low speed, thermally-driven flow with an emphasis on smoke and heat transport from fires. The core algorithm is an explicit predictor-corrector scheme that is second order accurate in space and time. Turbulence is treated by means of the Smagorinsky form of Large Eddy Simulation (LES). It is possible to perform a Direct Numerical Simulation (DNS) if the underlying numerical grid is fine enough. LES is the default mode of operation.

Combustion Model

For most applications, FDS uses a combustion model based on the mixture fraction concept. The mixture fraction is a conserved scalar quantity that is defined as the fraction of gas at a given point in the flow field that originates as fuel. The reaction of fuel and oxygen is not necessarily instantaneous and complete, and there are several optional schemes that are designed to predict the extent of combustion in under-ventilated spaces. The mass fractions of all of the major reactants and products can be derived from the mixture fraction by means of “state relations,” expressions arrived at by a combination of simplified analysis and measurement.

Radiation Transport

Radiative heat transfer is included in the model via the solution of the radiation transport equation for a gray gas. In a limited number of cases, a wide band model can be used in place of the gray gas model to provide a better spectral accuracy. The radiation equation is solved using a technique similar to a finite volume method for convective transport, thus the name given to it is the Finite Volume Method (FVM). Using approximately 100 discrete angles, the finite volume solver requires about 20 % of the total CPU time of a calculation, a modest cost given the complexity of radiation heat transfer. Water droplets can absorb and scatter thermal radiation. This is important in cases involving mist sprinklers, but also plays a role in all sprinkler cases. The absorption and scattering coefficients are based on Mie theory (Wiscombe,1980). The scattering from the gaseous species and soot is not included in the model.

Geometry

FDS approximates the governing equations on one or more rectilinear grids. The user prescribes rectangular obstructions that are forced to conform with the underlying grid.

Boundary Conditions

All solid surfaces are assigned thermal boundary conditions, plus information about the burning behavior of the material. Heat and mass transfer to and from solid surfaces is usually handled with empirical correlations, although it is possible to compute directly the heat and mass transfer when performing a Direct Numerical Simulation (DNS).

Sprinklers and Detectors

The activation of sprinklers and heat and smoke detectors is modeled using fairly simple correlations of thermal inertia for sprinklers and heat detectors, and transport lag for smoke detectors. Sprinkler sprays are modeled by Lagrangian particles that represent a sampling of the water droplets ejected from the sprinkler.

5.5 Limitations and assumptions

Although FDS can address most fire scenarios, there are limitations in all of its various algorithms.

Low Speed Flow Assumption

The use of FDS is limited to low-speed flow with an emphasis on smoke and heat transport from fires. This assumption rules out using the model for any scenario involving flow speeds approaching the speed of sound, such as explosions, choke flow at nozzles, and detonations.

Rectilinear Geometry

The efficiency of FDS is due to the simplicity of its rectilinear numerical grid and the use of a fast, direct solver for the pressure field. This can be a limitation in some situations where certain geometric features do not conform to the rectangular grid, although most building components do. There are techniques in FDS to lessen the effect of “sawtooth” obstructions used to represent nonrectangular objects, but these cannot be expected to produce good results if, for example, the intent of the calculation is to study boundary layer effects. For most practical large-scale simulations, the increased grid resolution afforded by the fast pressure solver offsets the approximation of a curved boundary by small rectangular grid cells.

Fire Growth and Spread

Because the model was originally designed to analyze industrial-scale fires, it can be used reliably when the heat release rate (HRR) of the fire is specified and the transport of heat and exhaust products is the principal aim of the simulation. In these cases, the model predicts flow velocities and temperatures to an accuracy within 10 % to 20 % of experimental measurements, depending on the resolution of the numerical grid. However, for fire scenarios where the heat release rate is predicted rather than specified, the uncertainty of the model is higher. There are several reasons for this:

- properties of real materials and real fuels are often unknown or difficult to be obtained,
- the physical processes of combustion, radiation and solid phase heat transfer are more complicated than their mathematical representations in FDS,
- the results of calculations are sensitive to both the numerical and physical parameters.

Modeling fire growth and spread will always require a higher level of user skill and judgment than that required for modeling the transport of smoke and heat from specified fires.

Combustion

For most applications, FDS uses a mixture fraction-based combustion model. The mixture fraction is a conserved scalar quantity that is defined as the fraction of gas at a given point in the flow field that originated as fuel. In its simplest form, the model assumes that combustion is mixing controlled, and that the reaction of fuel and oxygen is infinitely fast, regardless of the temperature. For large-scale, well-ventilated fires, this is a good assumption. However, if a fire is in an under-ventilated compartment, or if a suppression agent like water mist or CO₂ is introduced, fuel and oxygen are allowed to mix and not burn, according to a few empirically-based criteria. The physical mechanisms underlying these phenomena are complex, and are tied closely to the flame temperature and local strain rate, neither of which is readily-available in a large scale fire simulation. Subgrid-scale modeling of gas phase suppression and extinction is still an area of active research in the combustion community. Until reliable models can be developed for building-scale fire simulations, simple empirical rules can be used that prevent burning from taking place when the atmosphere immediately surrounding the fire cannot sustain the combustion.

Simple empirical rules can be used to predict local extinction based on the oxygen concentration and temperature of the gases in the vicinity of the flame sheet. Figure 5.1 shows values of temperature and oxygen concentration for which burning can or cannot take place.

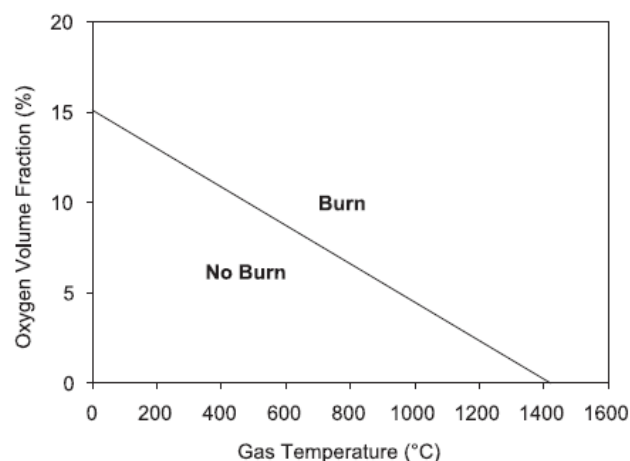


Fig. 5.1 Oxygen-temperature phase space showing where combustion is allowed and not allowed to take place.

Radiation

Radiative heat transfer is included in the model via the solution of the radiation transport equation (RTE) for a gray gas, and in some limited cases using a wide band model. The RTE is solved using a technique similar to finite volume methods for convective transport, thus the name given to it is the Finite Volume Method (FVM). There are several limitations of the model. First, the absorption coefficient for the smoke-laden gas is a complex function of its composition and temperature. Because of the simplified combustion model, the chemical composition of the smoky gases, especially the soot content, can affect both the absorption and emission of thermal radiation. Second, the radiation transport is discretized via

approximately 100 solid angles, although the user may choose to use more angles. For targets far away from a localized source of radiation, like a growing fire, the discretization can lead to a non-uniform distribution of the radiant energy. This error is called “ray effect” and can be seen in the visualization of surface temperatures, where “hot spots” show the effect of the finite number of solid angles. The problem can be lessened by the inclusion of more solid angles, but at a price of longer computing times. In most cases, the radiative flux to far-field targets is not as important as those in the near-field, where coverage by the default number of angles is much better.

6. Building description

The building under examination is an industrial building which is mainly used as a storage facility, and partly as an office and exhibition area. The overall dimensions of the structure are 80.00 x 40.00m, with a height of 10.00m plus a 2.00m high two ridged roof (Figures 6.1 and 6.2).

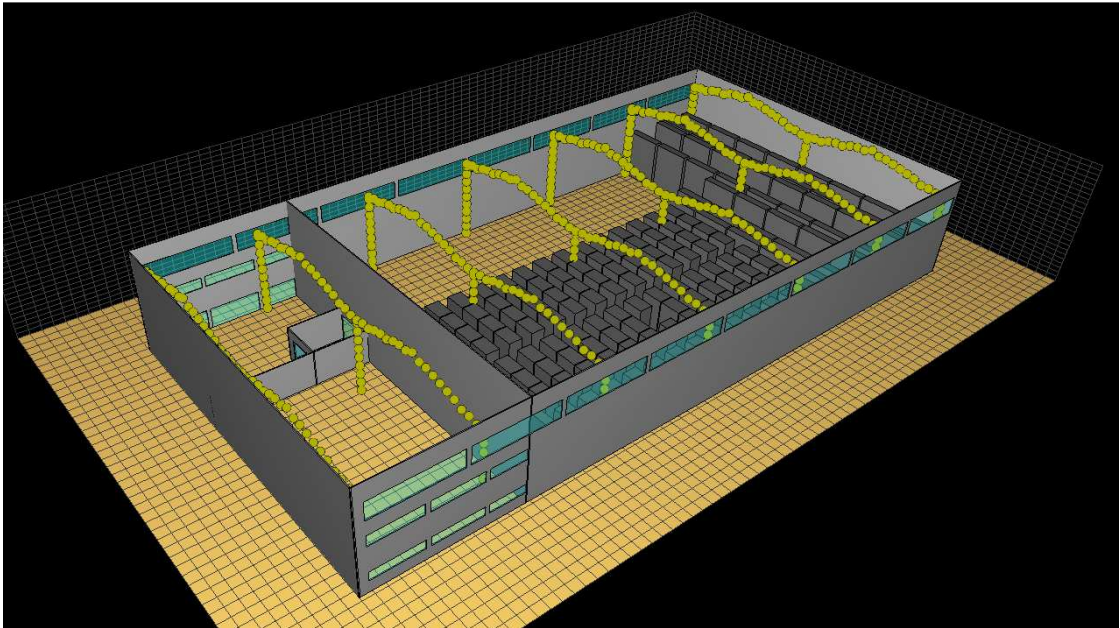


Fig. 6.1 Internal view of the industrial building

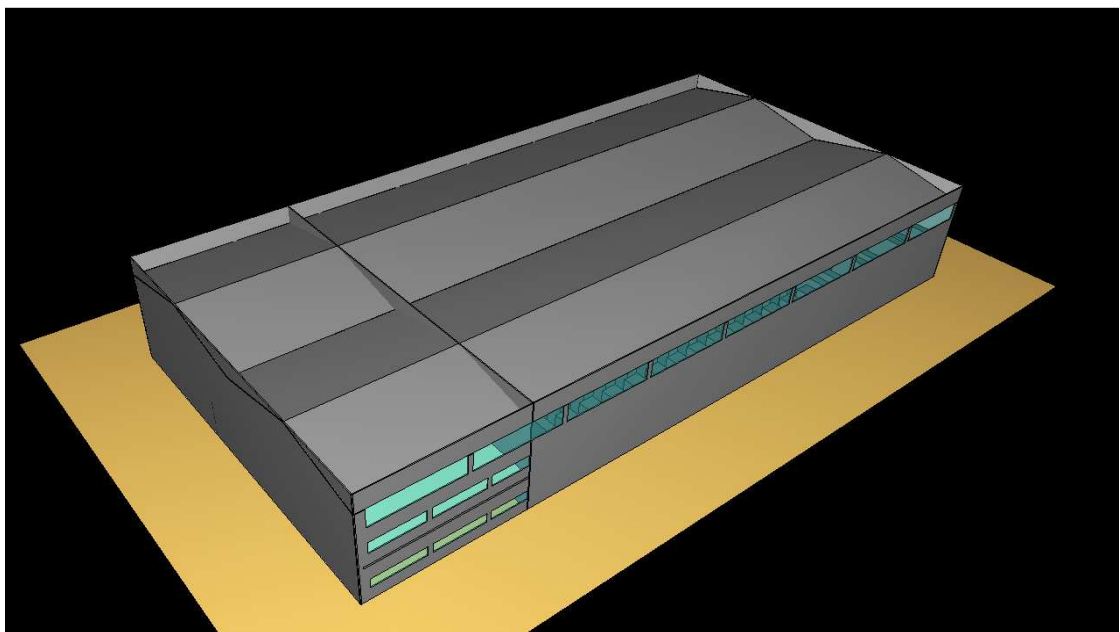


Fig. 6.2 External view of the industrial building

The space is divided into two main compartments, the storage area with dimensions 63.00 x 40.00 m and a 2-storey office/exhibition area of 17.00 x 40.00 m with heights 4.00 and 6.00 meters respectively. The storage compartment has a total of 247m² of windows located in a high row on each of the 63.00 m walls. On the ground and first floor of the office/exhibition area are additional 94.00 m² and 58.00 m² of windows. In the storage area the supplies are stored in 6.25m high racks (industrial shelving units), comprised mainly of electrical appliances and spare parts stored inside cardboard boxes. The structural system of the building consists of seven double-span steel frames. The walls and roof are composed of typical insulation panels. The base is standard industrial concrete flooring and the slab of the two-storey compartment is also made of concrete. The two compartments communicate through a 5.00x3.00m fireproof door. Also, there is a water sprinkler system installed in the storage area (Fig 6.4). The architectural plans are displayed in Figures 6.5 and 6.6, where the layout of the storage units is displayed in detail.

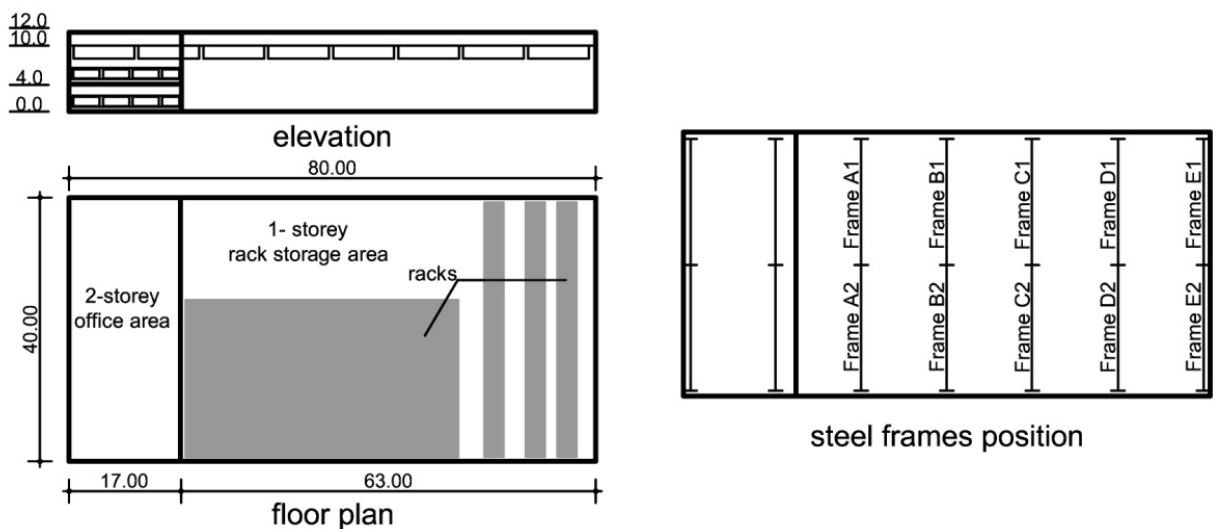


Fig. 6.3 Building description (dimensions in meters)

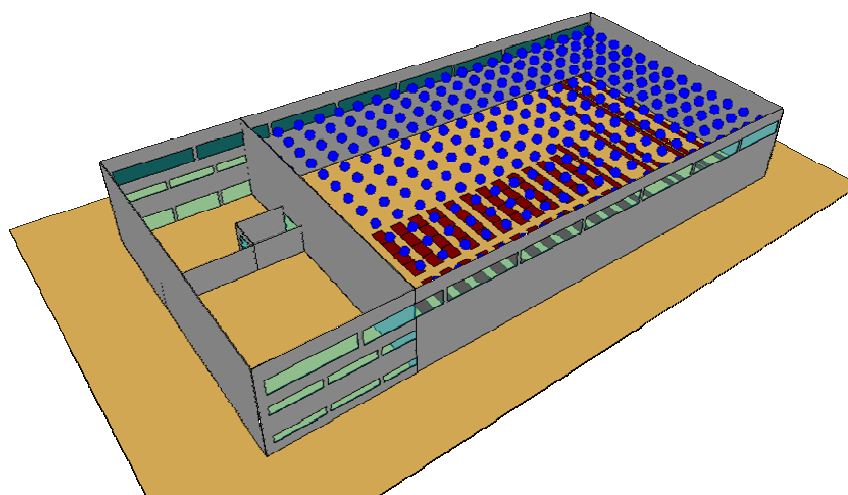


Fig. 6.4 Position of the sprinkler heads in the storage compartment

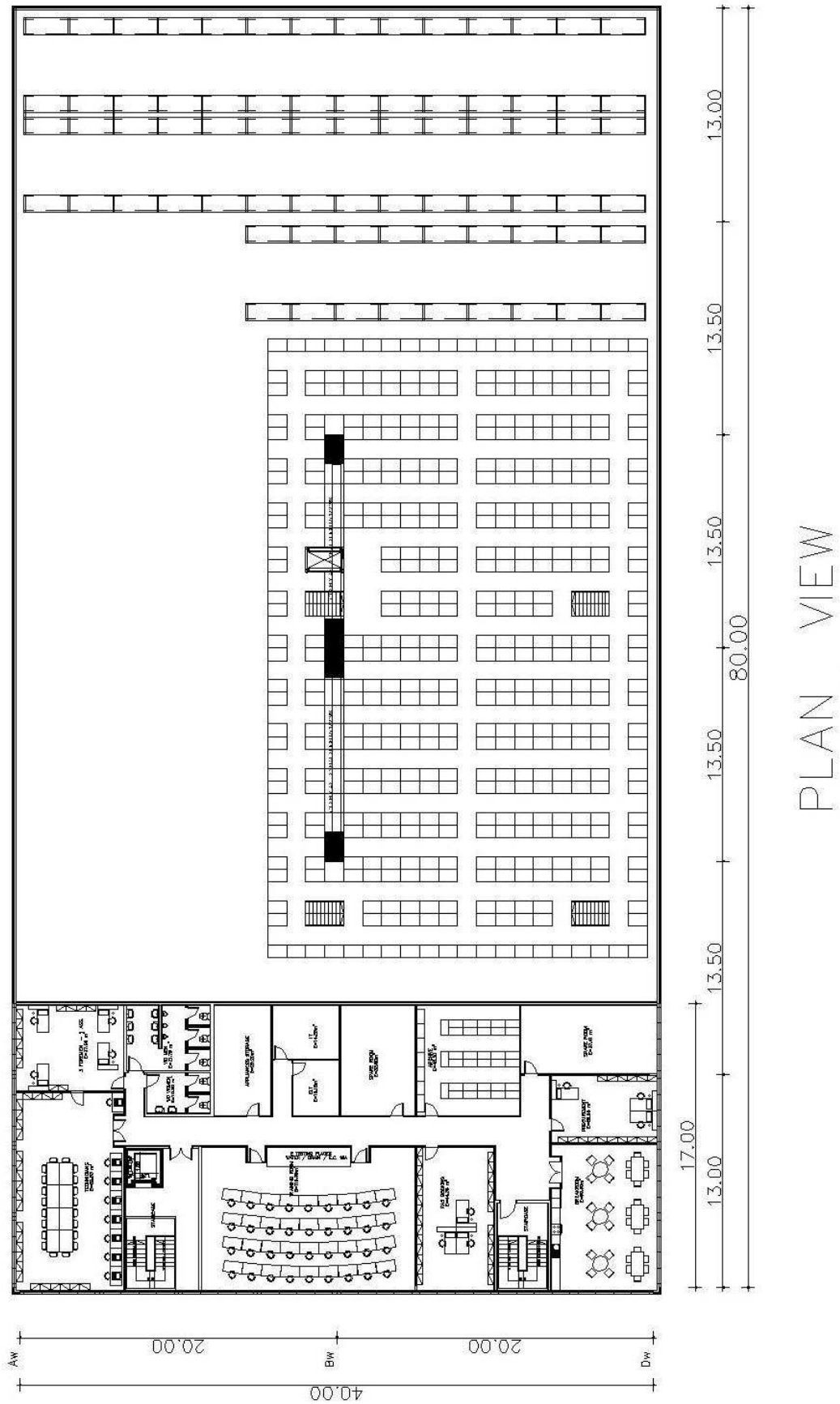


Fig. 6.5 Architectural Plan view (dimensions in meters)

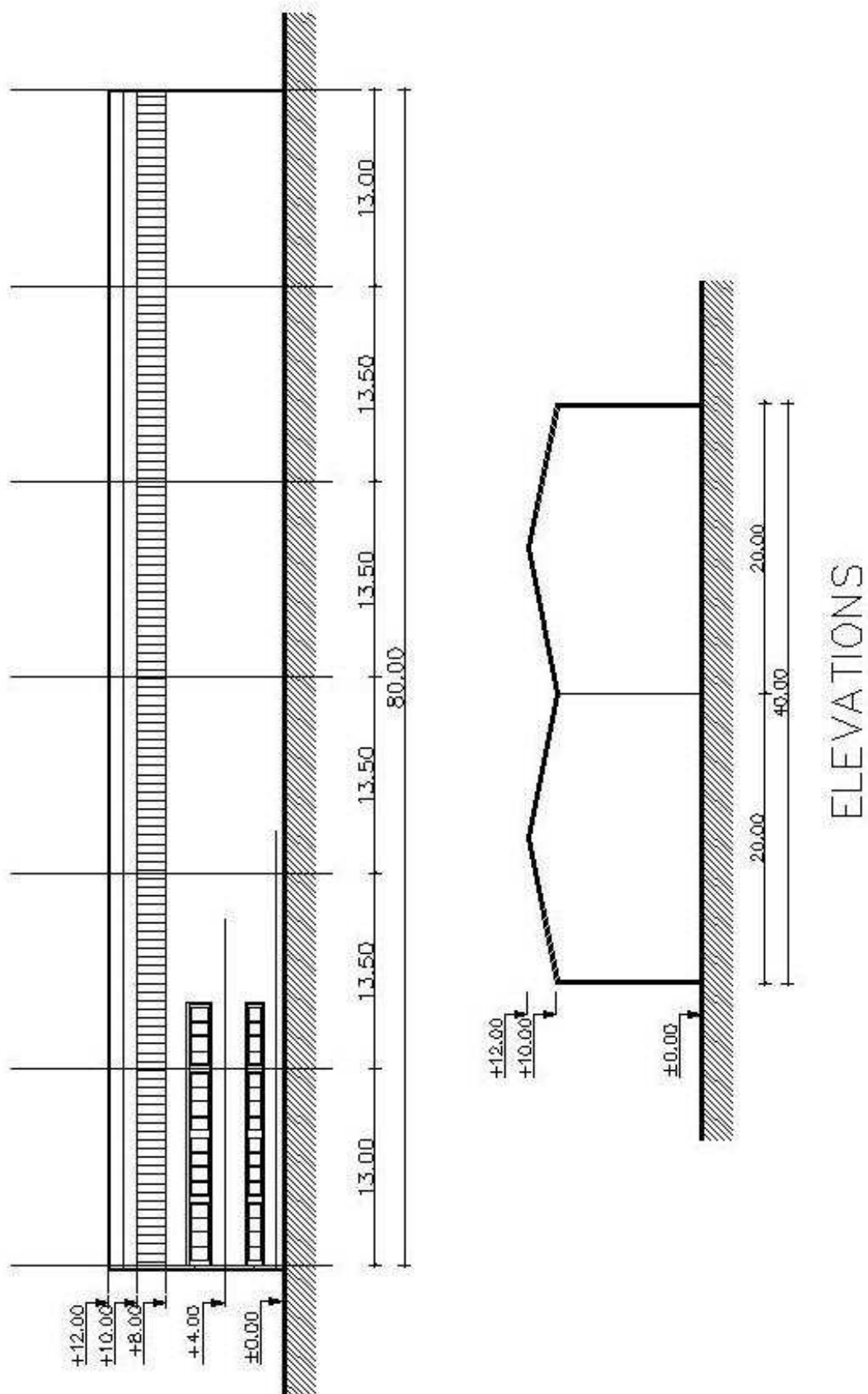


Fig. 6.6 Elevations (dimensions in meters)

7. Parametric Fire Scenarios

The main aim of this study is to analyze the impact of non-structural “damage”, on the development of natural fire in the building. In this case the damage is considered to be a result of an earthquake, as it is almost certain that after a mid to high intensity earthquake many of the non-structural elements of the building will be damaged, as they are not specially designed to sustain seismic displacements. In the analysis three main types of non-structural “damage” are introduced in the model:

- window breakage, which modifies ventilation conditions
- fireproof door damage which modifies ventilation and alters the fire compartmentation
- overall / partial malfunction of the water sprinkler system.

In total, 14 fire scenarios were tested. Of those, 12 included variations in the ventilation conditions by changing the number and placement of the broken windows and damage of the fireproof door. The remaining two had full and half operational the water sprinkler system. A visual description of the scenarios is provided in Fig. 7.1. For every scenario, the following parameters are given:

- percentage of broken openings to the total area of openings in the storage compartment which is affected by natural fire
- percentage of the broken openings to the total wall area
- position of the broken openings and
- percentage of the operational water sprinkler system.

The windows in the model are divided into 19.00 m² sections representing 7.1% of the total compartment window area. In Fig. 7.1 the position of the broken windows section is marked with an X symbol. In the scenario with the 50% active water sprinkler system the functional part is presented in Fig. 7.2. The parameters of every fire scenario are also presented in Table 7.1.

Fire Scenarios	broken window area	broken window area	broken window /wall area	functional water sprinkler system
	(m ²)	(%)	(%)	(%)
SC-00	0	0.00	0.00	0
SC-07	19	7.12	0.92	0
SC-015a	38	14.23	1.84	0
SC-015b	38	14.23	1.84	0
SC-015c	38	14.23	1.84	0
SC-030a	72	26.97	3.50	0
SC-030b	72	26.97	3.50	0
SC-030c	72	26.97	3.50	0
SC-045	114	42.70	5.53	0
SC-060a	152	56.93	7.38	0
SC-060b	152	56.93	7.38	0
SC-100	267	100.00	12.96	0
SC-100sp1	267	100.00	12.96	100
SC-100sp2	267	100.00	12.96	50

Table 7.1 Parametric Fire Scenarios








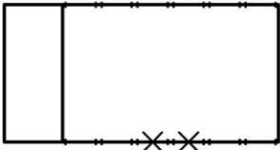







<u>Fire scenario description</u>	<u>Scenario name</u>		
	% of damaged openings		
	% of damaged openings / wall area		
	% of operational water sprinkler system		
<u>SC - 00</u>		<u>SC - 030c</u>	
0 %		27 %	
0 %		3.50 %	
0 %		0 %	
<u>SC - 07</u>		<u>SC - 045</u>	
7 %		43 %	
0.92 %		5.53 %	
0 %		0 %	
<u>SC - 015a</u>		<u>SC - 060a</u>	
14 %		57 %	
1.84 %		7.38 %	
0 %		0 %	
<u>SC - 015b</u>		<u>SC - 060b</u>	
14 %		57 %	
1.84 %		7.38 %	
0 %		0 %	
<u>SC - 015c</u>		<u>SC - 100</u>	
14 %		100 %	
1.84 %		12.96 %	
0 %		0 %	
<u>SC - 030a</u>		<u>SC - 100sp1</u>	
27 %		100 %	
3.50 %		12.96 %	
0 %		100 %	
<u>SC - 030b</u>		<u>SC - 100sp2</u>	
27 %		100 %	
3.50 %		12.96 %	
0 %		50 %	

Fig. 7.1 Parametric Fire Scenarios

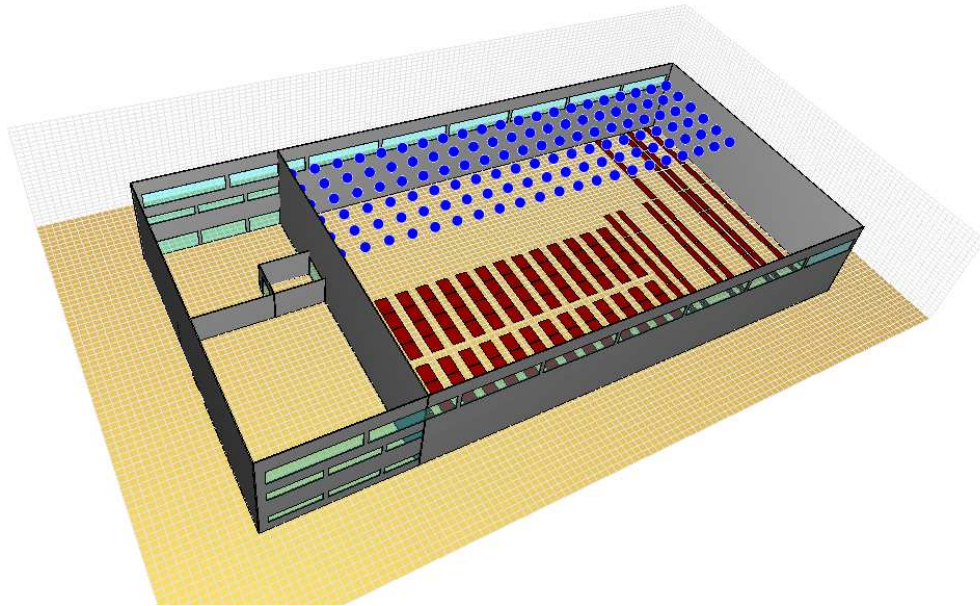


Fig. 7.2 Position of the 50% functional part of the water sprinkler system

8. Simulation

The simulation of the natural fire event in the industrial building is performed on a full scale model of the building with dimensions 80.00 x 40.00 x 12.00 m extended 10.00 m around the structure and 3.00 m above, for a better representation of the ambient atmospheric conditions and a more realistic simulation and visualization of the heat transfer and smoke movement on the exterior environment of the building. The basic geometry of the fire compartments is described, including the inclined two ridge roof and the windows' positions. The thermal properties of the construction materials are entered and the burning behavior of the combustible materials in the storage area is given. The position and properties of the sprinkler heads is inserted in the model and finally the boundary conditions are defined. After the model is constructed, the position and type of the output quantities is selected before the beginning of the simulation. The real simulation time of the fire scenarios is about one hour.

8.1 Computational domain – Grid Sensitivity

The phenomena that need to be considered in an analysis of fire dynamics vary in scale from the level where the chemical process of combustion takes place (10^{-4} m) to the actual size of a building (10^1 m). So the dimension scale that needs to be covered is of the order of 10^5 . It is evident that the simulation is a very difficult process and all the results ought to be interpreted in the context of all these conditions. For fire design purposes where the study of the phenomena of the smaller scale is not the objective, the Large Eddy Simulation technique is preferred. LES assumes that the eddies that account for most of the turbulent mixing of the gaseous fuel and combustion products are large enough to be calculated with reasonable accuracy from the equations of fluid dynamics and small scale eddy motion is modeled separately outside of the computational grid.

Considering the information given above, the most important numerical parameter of the simulation is the grid size. The discretization of the numerical grid defines the spatial and temporal accuracy of the discretized partial differential equations. FDS is second-order accurate in space and time, so by halving the grid cell size the discretization error will decrease in the governing equations by a factor of 4. However, because of the non-linearity of the equations, the decrease in discretization error does not necessarily translate into a comparable decrease in the error of a given FDS output quantity.

In the present study, a grid sensitivity test is performed in order to decide on the final mesh that is used for the analysis. The grid is refined in steps until the output results reach a point that the differences are acceptable for the purpose of this study, compared to the computational time required for the simulation. It needs to be mentioned that with each halving of the grid cell size, the time required for the simulation increases by a factor of $2^4 = 16$ (a factor of two for each spatial coordinate, plus time). A compromise between accuracy and corresponding computer capacity is necessary.

In the present analysis the grid size that was used varied from a grid cell size of 200x200x200cm to 83x80x60cm which is eventually the grid cell size that was used. In Table 8.1 a description of the grid cell sizes is given along with computational time that was required for the analysis. In all simulations, the real fire simulation time is one hour and the calculation time step was set not to exceed 0.1 sec, allowed to be decreased by the solver if it was necessary for the calculation convergence. In the models that the water sprinkler system was implemented the computational time exceeded 120 hours and a slightly coarser mesh was used for the simulation. In Figures 8.1 and 8.2 point temperature and HRR time-histories for different mesh discretization are compared.

MESH	cell size (cm)			total number of mesh cells	computational time (h:min:sec)
	x- axis	y-axis	z-axis		
MESH-200	200	200	188	12000	0:38:39
MESH-150	154	150	150	26000	1:33:24
MESH-125	125	125	125	46080	3:11:33
MESH-100	100	100	100	90000	7:35:59
MESH-080	80	80	83	162000	15:09:13
MESH-080B	83	80	60	225000	31:06:58

Table 8.1 Grid size and corresponding computational time required for the analysis of one fire scenario

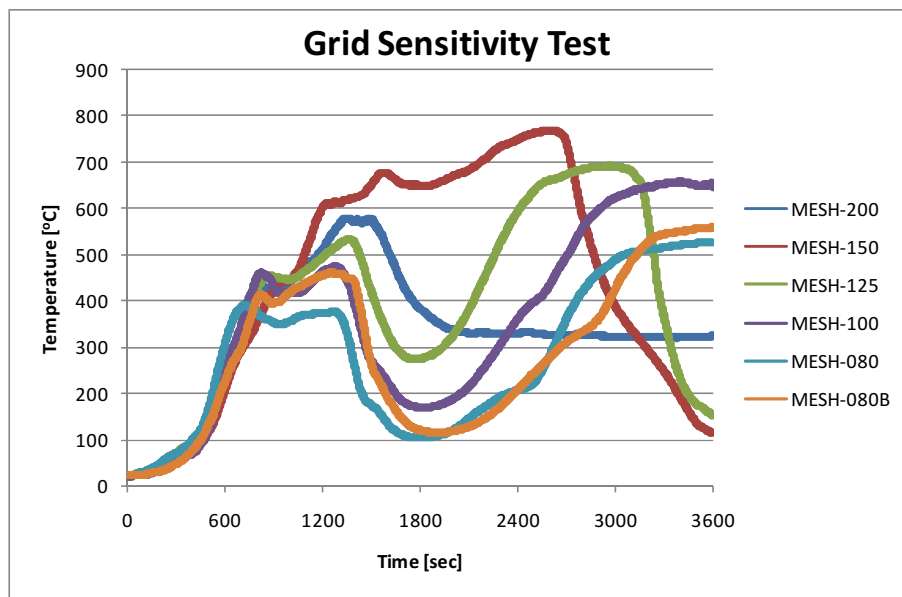


Fig. 8.1 Point temperature time-histories for different mesh-cell dimensions

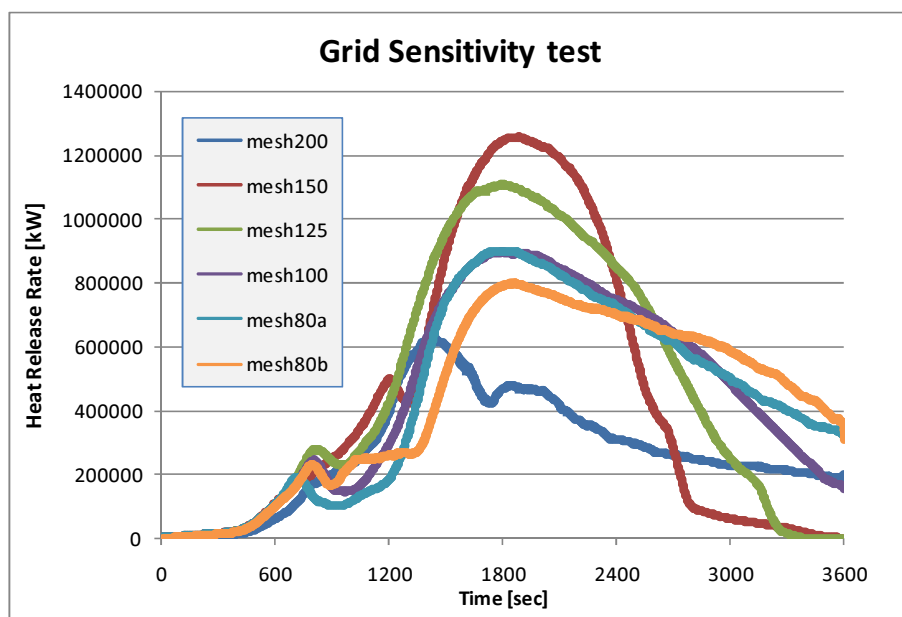


Fig. 8.2 Heat Release Rate for different mesh-cell dimensions

8.2 Structural materials

In the model three main structural materials are used in the analysis and these are concrete, steel and typical insulation. The concrete is assigned to the base floor of the building and to the slab dividing the storeys of the two story section. Steel and insulation is used to describe the cross section of the typical industrial insulation panels that cover the walls and the roof of the building. The cross section of the insulation panels is given in Fig. 8.3, and its total thickness is 10.00 cm. The connection of one panel to another is considered to be airproof so there is no extra ventilation from the walls into the compartment. The thermal properties of the materials are given in Tables 8.2, 8.3 and 8.4.

The windows, for simplification purposes, are either considered as a void in the wall when they are open/damaged, or either are considered to be of the same material of the wall, when they are closed/ undamaged. Use of a material such as glass was not necessary because the main function of the windows is to act as vents changing the ventilation conditions of the compartment. Any radiation loss through the undamaged/closed windows is negligible, due to the position of the windows which is high under the ceiling and their small area compared to the overall wall area of the storage compartment.

Insulation		
Density (kg/m ³)	208.0	
Emissivity	0.9	
Specific heat (kJ/(kg·K))	Temperature (°C)	Specific heat (kJ/(kg·K))
	20.0	0.8
	677.0	2.0
Absorption Coefficient (1/m)	50000	
Conductivity (W/(m·K))	Temperature (°C)	Specific heat (kJ/(kg·K))
	20.0	0.05
	377.0	0.1
	677.0	0.2

Table 8.2 Thermal properties of insulation

Concrete	
Density (kg/m ³)	2280.0
Emissivity	0.9
Specific heat (kJ/(kg·K))	1.04
Absorption Coefficient (1/m)	50000
Conductivity (W/(m·K))	1.80

Table 8.3 Thermal properties of concrete

Steel	
Density (kg/m ³)	7850.0
Emissivity	0.95
Specific heat (kJ/(kg·K))	0.46
Absorption Coefficient (1/m)	50000
Conductivity (W/(m·K))	45.8

Table 8.4 Thermal properties of steel

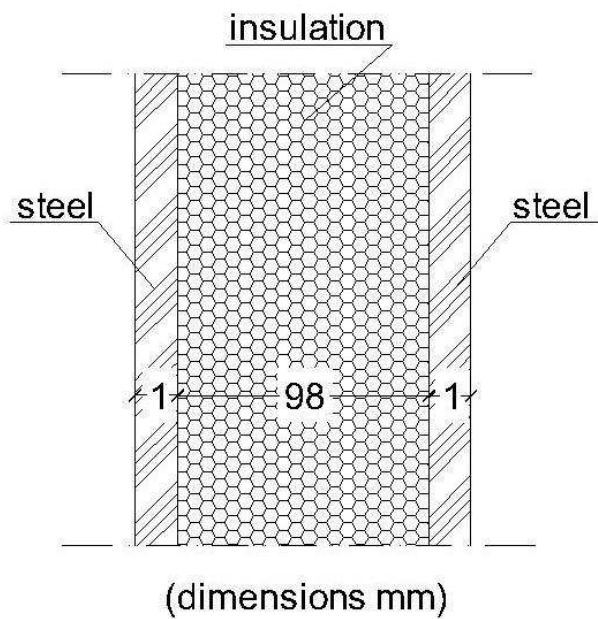


Fig. 8.3 Typical insulation panel cross section

8.3 Modeling of fire and fire spread

Concerning the fire phenomenon a distinction needs to be made between gas phase combustion and solid phase pyrolysis.

- **Pyrolysis** is the irreversible decomposition or transformation of a compound caused by heat that produces the gaseous fuel. It is the first chemical reaction that occurs in the burning of many solid fuels, like wood, cloth, paper, and plastic.
- **Gas phase combustion** refers to the exothermic chemical reactions between the gaseous fuel and oxygen accompanied by the production of heat and light in the form of flames.

So the combustion is the actual chemical process of the burning of the gaseous fuels, which could be the result of pyrolysis and that is what we finally perceive as fire. A solid fuel does not combust directly. (Fig. 8.4)

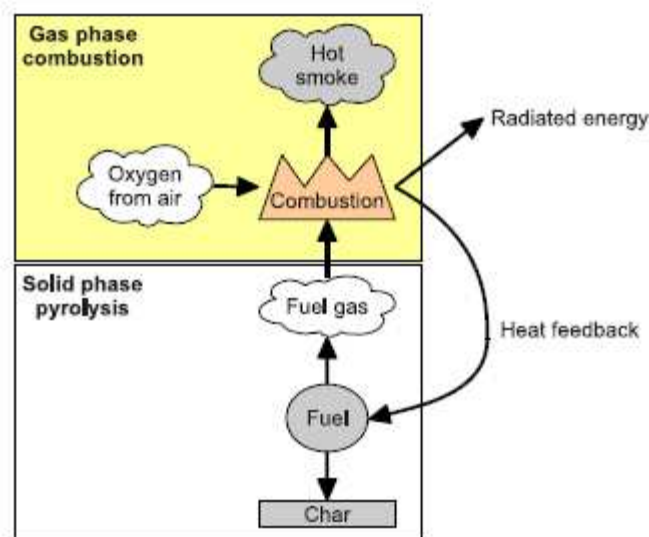


Fig. 8.4 Combustion and pyrolysis (Gissi,2010)

In FDS there are two ways to model the fire. The first is to directly specify the Heat Release Rate Per Unit Area (HRRPUA), which could be either constant or changing with time. The second is to allow FDS to predict the energy released from the fire by specifying the thermo-physical properties of the materials that act as fuels. In both cases the mixture fraction combustion model is used by default to simulate the actual combustion.

In the first case FDS creates a gas burner whose fuel flow is controlled by the prescribed Heat Release Rate (HRR) curve that is specified by the user. The gas that is used is propane as a default fuel, and its flow is adjusted accordingly. However, for combustion to take place regardless of the fuel flow the fuel/oxygen mixture fraction needs to be within the limits that allow for its occurrence. If for example oxygen is not enough for the combustion there will be no heat release coming from the gas burner. Generally this is a fairly straightforward method by which you have almost full control of the fire parameters.

The second method is considerably more complex as it tries to simulate both the pyrolysis process with its produced gases and after that the actual combustion. It is understood that pyrolysis takes place in a much smaller scale than the grid that is usually used for the simulation of fires in buildings of regular dimensions in the scale of tens of meters. For a more accurate solution of the pyrolysis equations a very fine grid is needed, which would be

inappropriate for most civil engineering cases. Apart from the need for a very fine mesh, also the thermal properties and detailed composition of the materials need to be known which is not usually available, as in most fires there is a large variety of objects whose properties are not well known, except maybe in the case of experiments where the burning items may be more accurately known.

FIRE MODELING

In the industrial building that is subjected to fire simulation, the materials that are stored in the 6.25 m high shelving units are mainly electrical appliances and spare parts. Their composition is both unknown and definitely not uniform as there are numerous types of electrical appliances. Moreover, they consist of many different materials such as plastic, wood, PVC, steel, in formations that are very difficult to model, so as to predict their pyrolysis rate. In this specific case the use of the second method would induce many uncertainties in the analysis and due to the buildings dimensions an appropriate mesh would render the analysis unsolvable concerning the computational time. So the method with the prescribed HRR curve was preferred.

The most important parameter in the modeling of natural fire in an industrial building used as a storage facility is to use a HRR curve that would realistically represent the way items burn when are placed in industrial storage units. Much experimental work has been done on rack storage fires and fire spread in warehouses in the Brandforsk project in Sweden (Lönnermak and Ingason, 2005). In a series of 1:5 scale experiments fire development in rack storages was investigated. Fire spread from rack to rack was examined in correlation to the dimensions of the enclosure, the composition and placement of burning materials, the rack height, the ceiling height and the ventilation conditions. These tests were almost a match to the storage arrangement in the building under examination so it was decided that the Heat Release Rate curves of these experiments would be used for the simulations, after the necessary transformations to account for the correct scale.

As the aim of the Brandforsk experiments was to study rack fires in general, the fuel that was used was cardboard boxes stacked in multiple layers to represent typical commodities that are usually stored in warehouses. The position of the rack units was also set in way to represent the typical distance that is kept in industrial premises from one rack unit to another. In Fig. 8.5, 8.6 and 8.7 the experimental set up of the rack units is presented. In Table 8.5 a scale correlation between the experiment and the real scale of the rack units in the building under examination is provided.

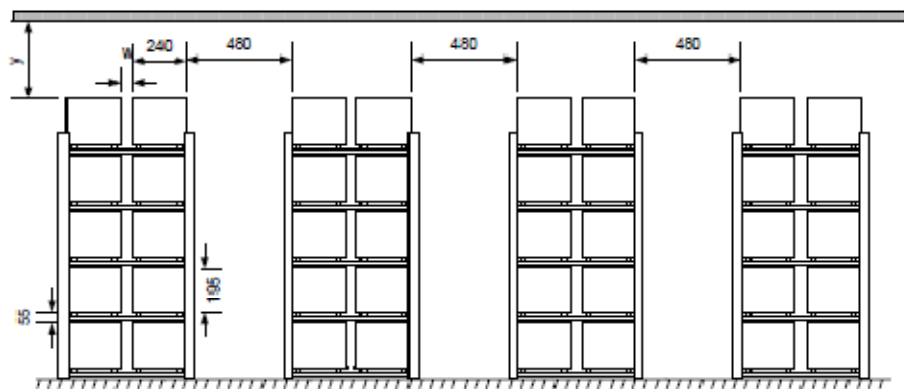


Fig. 8.5 Experimental setup of the rack units (Lönnermak and Ingason,2005)

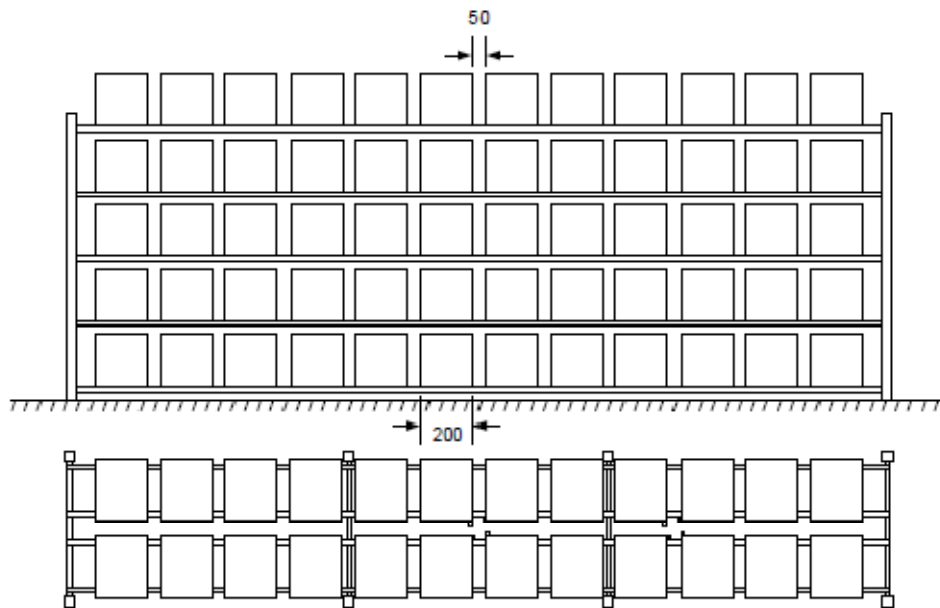


Fig. 8.6 Experimental setup of the rack units (Lönnermak and Ingason,2005)



Fig. 8.7 Experimental setup of the rack units (Lönnermak and Ingason,2005)

Scale 1/5	Experiment (mm)	Corresponding Real scale (m)	Building (m)
Rack height	1250	6.25	6.25
Rack length	1655	8.28	8.00
Rack width	535	2.68	2.70
Rack distance	480	2.40	2.40
Ceiling height	600	3.00	3.75

Table 8.5 Scale comparison between experiment setup and real building

As it is described in Table 8.5 the experiment is quite similar to the dimensions of the building arrangement and the Heat Release Rate curve of the experiments could represent satisfactorily the actual Heat Release Rate in the building after it is scaled according to the dimensional analysis scaling laws.

In the experiment the HRR curve that was recorded was produced by the burning of racks whose actual floor area of burning material was 1.42m^2 producing the heat release rate curve given in Fig. 8.8 with a peak value of approximately 4128 kW.

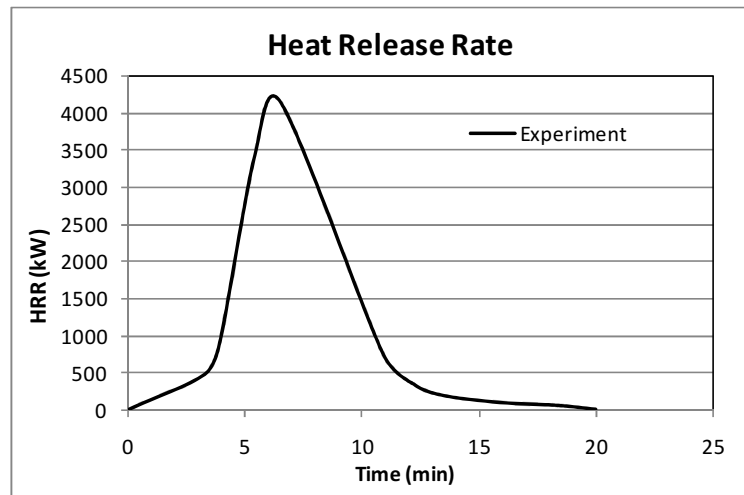


Fig. 8.8 Experiment Heat Release Rate curve

In order to use this curve as input in the real model simulation it needs to be scaled both in the energy and the time domain. The equations for the transformation are the following (Fong Y.Y. and Fong N.K. ,2003):

Transformation of the Heat Release Rate:

$$\frac{Q_M}{Q_R} = \left(\frac{L_M}{L_R}\right)^{5/2} \quad (8.1)$$

and in the time domain:

$$\frac{t_M}{t_R} = \left(\frac{L_M}{L_R}\right)^{1/2} \quad (8.2)$$

So the peak HRR value is transformed to 230771 kW for a corresponding area of $1.42 \times 5^2 = 35.5 \text{ m}^2$, because the area also needs to be scaled accordingly. This results in a peak value of 6593 kW/m² in real scale.

After the transformation in the time domain the overall duration is extended from 20min to 44min and the Real scale curve is obtained (Fig. 8.9)

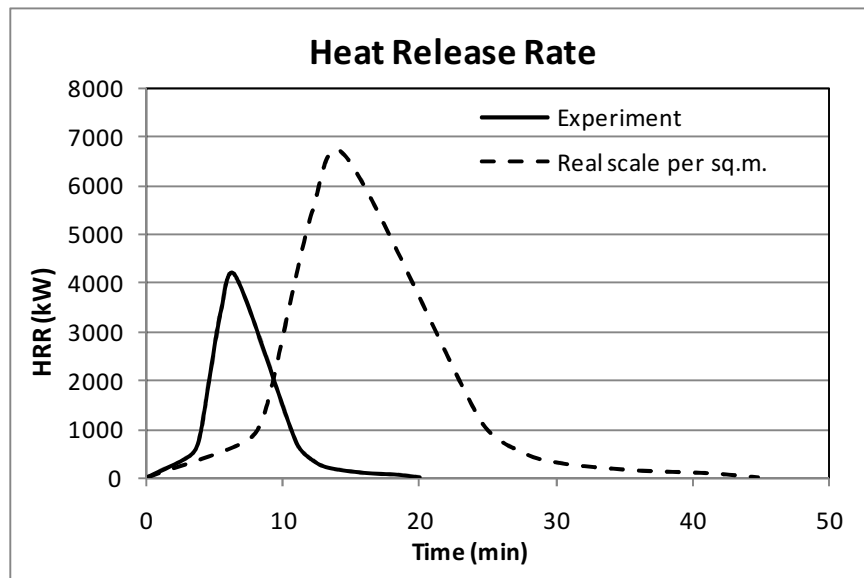


Fig. 8.9 Experiment and Real scale Heat Release Rate curves

The produced Heat Release Rate curve is assigned to 156 Heat Release sections that represent the rack units of the compartment placed in the exact position that is indicated by the architectural plan (Fig 8.10). When each section is activated it starts to release heat in the prescribed manner, given that the oxygen is enough to support the combustion. The next key issue of the fire modeling is to simulate how fire spreads from one rack unit to another, and when each Heat Release section is activated.

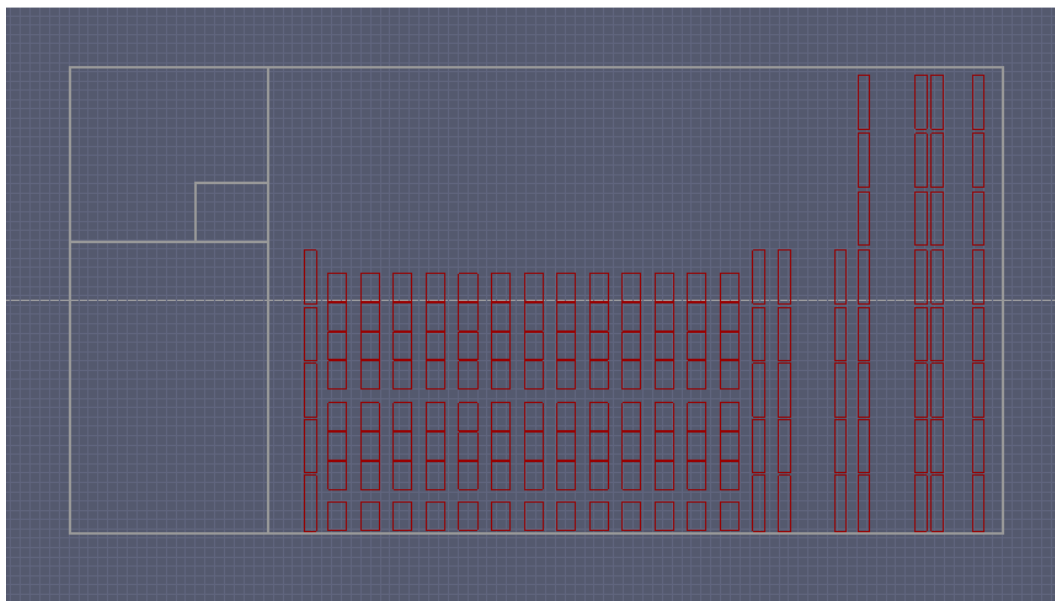


Fig. 8.10 Layout of the 156 Heat Release Rate sections

MODELING OF THE FIRE SPREAD

The ignition of the fire is implemented by activating one rack unit in the middle of the top row from the beginning of the simulation, so as to allow for a symmetrical heat release in the x direction and allowing fire to spread in both directions.

In reality the physical sequence of the fire spread between organic, solid materials at a distance is: ignition, temperature rise, pyrolysis, and then combustion of the gases created

from the pyrolysis process. Apart from direct ignition through flames, a condition necessary for fire spread between materials at a distance is temperatures high enough near the surface of the object to start the pyrolysis reaction. This concept is implemented in the simulation by connecting the activation of each heat release section to a temperature sensor. The sensor is situated 3.00 meters above the center of each section, recording the temperature arising in the middle of the height of each rack. A section is activated only when the temperature of the sensor exceeds 250°C, which is approximately the auto-ignition temperature of wood (Babrauskas,2002) (Graf,1949). The auto-ignition temperature of wood and paper was chosen because the electrical appliances were stored inside cardboard boxes or on wooden pallets so at this temperature either the cardboard boxes or the wooden pallets would ignite and spread the fire in the rack. Again it is noted that combustion would take place only if the oxygen index is >0.15.

8.4 Sprinklers and particle materials

A sprinkler system is installed in the storage compartment, with a total number of 252 sprinkler heads placed under the ceiling at 9.50m, at a grid of 3.00 meters. Each sprinkler head is able to release 100L of water per minute. The sprinkler head is activated at 74°C releasing water in all direction at a latitude angle from 60° to 75°. In the simulation the water is released in the form of water particles whose material properties are given in Table 8.6. When a droplet strikes a solid surface, it sticks and is reassigned a new speed and direction. If the surface is horizontal, the direction is randomly chosen. If vertical, the direction is downwards. Modeling suppression of a fire by a water spray is challenging because the relevant physical mechanisms occur at length scales smaller than a single mesh cell. In the gas phase, flames are extinguished due to lowered temperatures and dilution of the oxygen supply. For the solid phase, water reduces the fuel pyrolysis rate by cooling the fuel surface and also changing the chemical reactions that release fuel gases from the solid.

Water particles	
Density (kg/m ³)	1000.0
Specific heat (kJ/(kg·K))	4.184
Vaporization temperature (°C)	100
Heat of Vaporization (kJ/(kg))	1.80
Droplet median diameter (µm)	500
Droplets per second	5000
Insertion interval (sec)	0.1

Table 8.6 Properties of the water particles

Due to the fact that no actual burning materials are placed in the compartment for the simulation and the fire is modeled by Heat Release sections, the effect of the sprinklers on the fire suppression is implemented through an extinguishing coefficient applied to the HR section. It is assumed that water impinging on the fuel surface takes energy away from the pyrolysis process and thereby reduces the burning rate of the fuel. In FDS a parameter needs to be specified that governs the suppression of the fire by water because this type of simulated fire essentially acts like a gas burner whose flow rate is explicitly specified. An empirical way to account for fire suppression by water is to characterize the reduction of the pyrolysis rate in terms of an exponential function. The local mass loss rate of the fuel is expressed in the form

$$\dot{m}_f''(t) = \dot{m}_{f,0}''(t)e^{-\int k(t)dt} \quad (8.3)$$

Here $\dot{m}_{f,0}''(t)$ is the user-specified burning rate per unit area when no water is applied and k is a function of the local water mass per unit area, \dot{m}_w'' , expressed in units of kg/m^2 .

$$k(t) = E_{\text{COEFFICIENT}}\dot{m}_w''(t) \quad [\text{s}^{-1}] \quad (8.4)$$

The parameter $E_{\text{COEFFICIENT}}$ must be obtained experimentally, and it is expressed in units of $\text{m}^2/\text{kg}/\text{s}$. Usually, this type of suppression algorithm is invoked when the fuel is complicated, like a cartoned commodity.

The value that was chosen for the extinguishing coefficient is 0.4 and this value was a result of a three-year research project of Jukka Vaari et al. (2012) on experimental and simulation fire suppression with a goal to improve and enhance the capabilities of the NIST Fire Dynamics Simulator to describe water spray dynamics, discharge of large water based fire suppression systems, gas phase cooling by water sprays, flame extinguishment, and the suppression of large complex solid fire loads. The value 0.4 resulted in the best qualitative overall agreement between experimental and simulated data, of the water suppression of a burning stack of wooden pallets.

8.5 Boundary conditions

FDS contains some predefined boundary conditions: INERT, OPEN, and MIRROR.

An INERT boundary condition represents an isothermal wall with the temperature INERT fixed at ambient temperature. INERT allows for heat loss and is not the same as an adiabatic surface. An INERT solid is something that never heats up, like a piece of steel that has cold water constantly flowing across its back side. In general, this boundary condition should not be used, as it is better to assign actual material properties to everything.

An OPEN boundary condition assumes that ambient conditions exist beyond. OPEN can only be prescribed at an exterior boundary of the computational domain. The flow in and out is treated naturally as part of the solution of the governing equations.

A MIRROR boundary condition denotes a symmetry plane. A MIRROR should span an entire face of the computational domain, essentially doubling the size of the domain. The flow on the opposite side of the MIRROR is exactly reversed. From a numerical point of view, a MIRROR is a no-flux, free-slip boundary. MIRROR can only be prescribed at an exterior boundary of the computational domain.

In the model the computational mesh is extended 10 meters around the building allowing the simulation to take into account in the calculations the ambient conditions around the building. At the outer limits of the mesh in $-x$, $+x$, $-y$, $+y$ and $+z$ directions OPEN boundary conditions are applied (Fig 8.11). In the $-z$ direction there was not allowed any interaction with the soil.

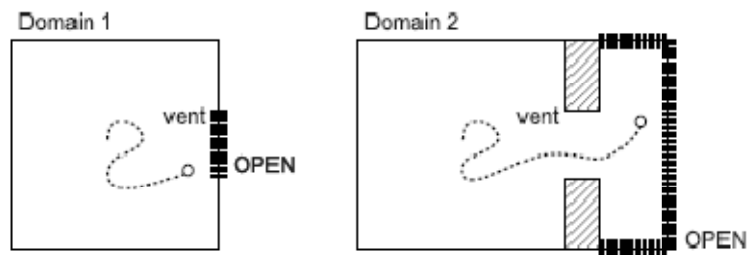


Fig. 8.11. Mesh of the type 2 was applied extending the computational domain beyond the windows and limits of the building in all directions (Gissi,2010)

8.6 Results data acquisition

In FDS it is necessary to prescribe from the beginning of the simulation what kind of data needs to be recorded as you would do in a physical experiment. In this study the parameters that were recorded are:

- Temperature time histories in specific positions near the steel frames
- Temperature distributions with time in certain planes in the interior and exterior of the building (Temperature plane slices)
- Velocity fields in certain planes in the interior and exterior of the building
- Pressure fields in certain planes in the interior and exterior of the building.
- Smoke movement
- Total Heat Release Rate of the analysis

TEMPERATURE TIME HISTORIES

The most important result in a fire simulation for a structural engineer is the temperature distributions near the structural elements of the building. For this reason the gas temperature was recorded in 64 points around every frame (Fig. 8.12).

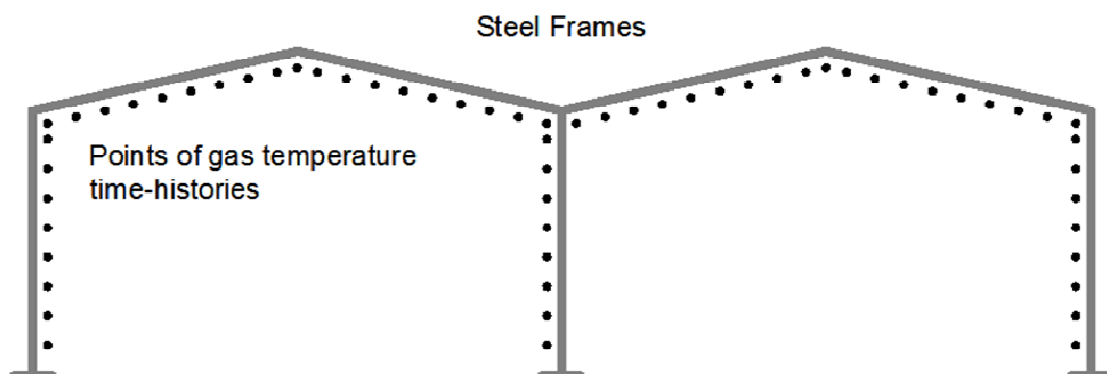


Fig. 8.12 Points where the gas temperatures time histories were recorded around the structural members during the fire simulation at a distance of 1.00 m.

PLANE SLICES

In FDS you can define certain slices where specific data is recorded. In the analysis such slices were specified that recorded temperature, velocity (vector form) and pressure with the evolution of time. A detailed description of the quantities measured is given in Table 8.7 and a visual presentation in Fig. 8.13. These slices are used by Smokeview to animate the evolution of the fire simulation.

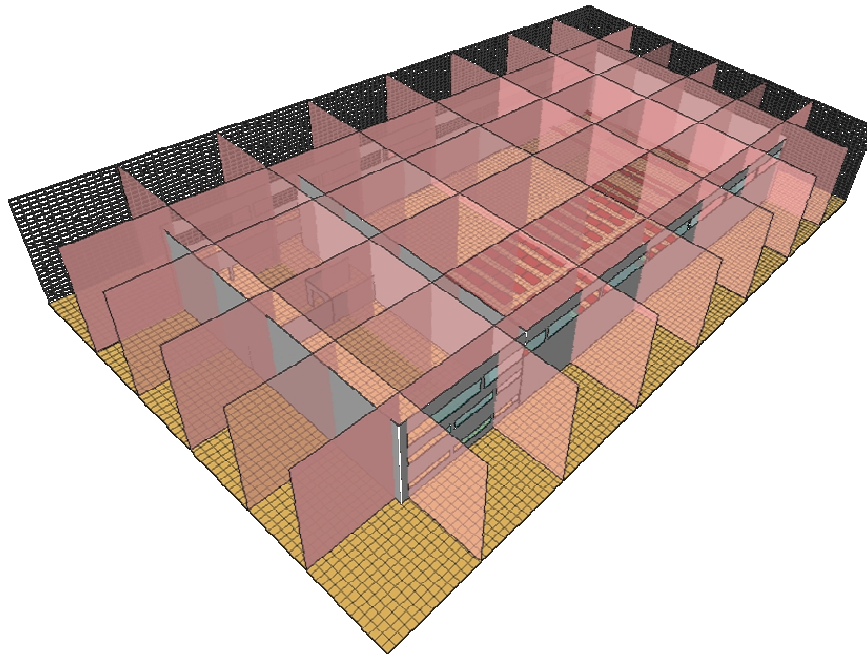


Fig. 8.13 Slices where the temperature distribution, velocity vector field and pressure is recorded with the evolution of time

XYZ Plane	Plane value	Gas Phase Quantity
X	-39.0	Temperature
X	-27.0	Temperature
X	-13.5	Temperature
X	0.0	Temperature
X	13.5	Temperature
X	27.0	Temperature
X	39.0	Temperature
Y	-19.0	Temperature
Y	-10.0	Temperature
Y	0.0	Temperature
Y	10.0	Temperature
Y	19.0	Temperature
Y	-19.0	Pressure
Y	0.0	Pressure
Y	19.0	Pressure
Y	-19.0	Velocity
Y	19.0	Velocity
Z	9.5	Temperature

Table 8.7 Plane slices and recorded quantities

SMOKE PRODUCTION AND MOVEMENT

By default, FDS assumes that the smoke from a fire is generated in direct proportion to the heat release rate. The “smoke” is not explicitly tracked by FDS, but rather is assumed to be a function of the mixture fraction combustion model. A value of SOOT_YIELD defines the percentage of the soot yield in regard to the fuel burning rate. The default soot yield value for the default mixture fraction is 0.01 kg/kg and this value was used in the simulation.

9. Simulation Results

In total 14 fire scenarios were simulated and results of temperature time-histories, total Heat Release Rate and pressure, velocity and temperature spatial distributions were acquired.

9.1 Processing of the temperature time-histories

For each of the seven steel frames 64 point gas temperature time- histories were obtained, so in total 448 temperature time histories around the interior of the compartment were obtained for every fire scenario. The data was recorded in a time frame of 2 sec so each time history was composed of 1800 pairs of values.

These temperature time-histories displayed very high fluctuations of the temperature values, and also very much variation between the different points of each frame. High variance of the temperature values was also observed between the temperature values for the seven different frames, especially to the ones that were inside the storage compartment that was under fire (Fig 9.1). This fact alone shows that temperature distribution is not homogenous in a compartment under fire, as it is assumed in the one/two-zone models that are used for the prediction of temperature evolution caused by natural fire.

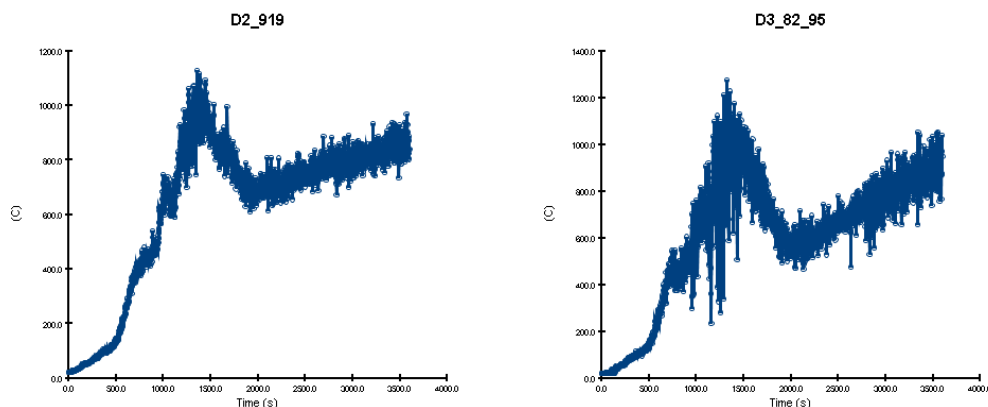


Fig. 9.1 Fluctuation in the temperature time-histories.

Direct comparison between the temperature time histories was very difficult and no direct conclusions could be attained in a strict mathematical manner, regarding the severity of each fire scenario on the building as a whole. A way to compare the various time histories was to transform them into a kind of scalar value that would represent the heat exposure that the evolving temperature values described.

A way to accomplish that, was to calculate for every separate time-history the duration that the temperature surpassed the levels of 600°C, 700°C, 800°C, 900°C and 1000°C respectively. As a result, the time-history was condensed to five scalar values, which were considerably easier to compare. These values expressed for how long the corresponding point of the frame was exposed to a certain temperature.

The second step of the process was to calculate from the values related to each structural member the exposure duration of the three structural member types (two columns and a beam) that formed each sub-frame. This was achieved by selecting the highest duration value for every temperature level. It is assumed that if any point of the structural member fails due to the heat exposure, the corresponding sub-frame will fail as well. As a result, a group of five durations were associated to each sub frame, depicting the effect that the fire had on it. In total

there were seven double span, steel frames in the building, but two of them were situated in the adjacent compartment and their temperatures did not exceed 500°C, so it was decided that they would not be included further in the data processing, and only the 10 sub frames of the storage compartment sustaining the fire would be used to determine the fire severity and its effect on the structural system of the building.

The third step in the processing of the results was to calculate a value that would represent the severity of each fire scenario. This was executed by calculating the average duration and standard deviation of the heat exposure of the 10 sub-frames for every temperature level and every scenario. The average duration is indicative of the magnitude of the thermal exposure and the standard deviation denotes how uniform (lower value of st. dev.), or dispersed (higher value of st. dev.) is the influence of the fire on the structural system. Among the scenarios with the highest average, the most severe is determined by the smallest standard deviation which indicates that more uniformly the frames are affected by the fire and contribute to the average temperature duration. The temperature durations (in minutes) of the 10 sub-frames for the five temperature levels, for all the fire scenarios are presented in Tables 9.1, 9.2, 9.3, 9.4 and 9.5 and a summary of the average durations and st. deviations for all temperature levels in Table 9.6. The color scale corresponds to the value displayed.

minutes over 600 °C		Frames										AVERAGE (min)	ST.DEV. (min)
		A1	A2	B1	B2	C1	C2	D1	D2	E1	E2		
Fire scenarios	SC-00	0	2	4	2	0	3	0	0	0	0	1.1	1.4
	SC-07	8	2	4	4	0	2	0	0	0	0	2.1	2.7
	SC-015a	7	2	12	7	6	2	0	0	0	0	3.6	4.0
	SC-015b	2	4	3	14	2	4	0	0	0	0	2.9	4.0
	SC-015c	5	8	5	5	0	2	6	0	17	0	4.9	5.0
	SC-030a	30	20	44	36	29	26	10	9	6	4	21.3	13.1
	SC-030b	8	28	7	20	18	4	40	12	41	20	19.8	12.4
	SC-030c	8	30	10	36	6	19	3	5	0	3	11.9	11.6
	SC-045	13	28	15	38	14	38	7	37	13	32	23.4	11.6
	SC-060a	42	37	46	44	42	41	38	38	35	26	38.9	5.3
	SC-060b	43	46	42	40	37	33	37	39	37	38	39.3	3.4
	SC-100	20	23	21	36	17	23	15	18	15	16	20.4	6.0
	SC-100SP1	0	0	0	0	0	0	0	0	0	0	0.0	0.0
SC-100SP2	0	0	0	5	0	0	0	0	0	0	0.5	1.6	

Table 9.1 Duration (min) of temperature exceeding 600°C near the steel frames for every fire scenario

minutes over 700 °C		Frames										AVERAGE (min)	ST.DEV. (min)
		A1	A2	B1	B2	C1	C2	D1	D2	E1	E2		
Fire scenarios	SC-00	0	0	0	2	0	0	0	0	0	0	0.2	0.6
	SC-07	0	2	2	3	0	0	0	0	0	0	0.7	1.1
	SC-015a	0	3	9	4	0	0	0	0	0	0	1.5	2.7
	SC-015b	0	6	2	7	0	2	0	0	0	0	1.7	2.4
	SC-015c	0	4	1	3	0	0	0	0	11	0	1.9	3.4
	SC-030a	8	2	31	20	11	10	0	0	0	0	8.2	10.0
	SC-030b	0	11	3	10	0	2	25	1	23	6	8.2	8.8
	SC-030c	2	10	5	12	2	8	0	2	0	0	4.1	4.1
	SC-045	5	12	6	13	4	11	0	16	0	16	8.4	5.9
	SC-060a	17	16	42	29	38	26	34	17	9	2	23.2	12.2
	SC-060b	39	26	32	20	7	8	32	18	29	17	22.8	10.1
	SC-100	18	21	18	31	15	18	14	15	13	14	17.8	4.9
	SC-100SP1	0	0	0	0	0	0	0	0	0	0	0.0	0.0
	SC-100SP2	0	0	0	4	0	0	0	0	0	0	0.4	1.2

Table 9.2 Duration (min) of temperature exceeding 700°C near the steel frames for every fire scenario

minutes over 800 °C		Frames										AVERAGE (min)	ST.DEV. (min)
		A1	A2	B1	B2	C1	C2	D1	D2	E1	E2		
Fire scenarios	SC-00	0	0	0	2	0	0	0	0	0	0	0.2	0.6
	SC-07	0	0	0	2	0	0	0	0	0	0	0.2	0.6
	SC-015a	0	0	6	3	0	0	0	0	0	0	0.8	1.8
	SC-015b	0	0	5	5	0	0	0	0	0	0	0.9	1.9
	SC-015c	0	4	0	2	0	0	0	0	14	0	2.0	4.1
	SC-030a	0	0	18	10	2	3	0	0	0	0	3.3	5.7
	SC-030b	0	7	2	5	0	0	25	0	12	0	5.1	7.5
	SC-030c	2	5	4	4	0	4	0	0	0	0	1.9	2.0
	SC-045	3	6	5	7	2	9	0	8	0	7	4.5	3.1
	SC-060a	3	5	27	12	27	14	20	9	0	0	11.8	9.7
	SC-060b	23	11	13	10	0	3	21	10	16	11	11.9	6.9
	SC-100	16	20	16	26	14	16	12	14	12	13	15.9	3.9
	SC-100SP1	0	0	0	0	0	0	0	0	0	0	0.0	0.0
	SC-100SP2	0	0	0	5	0	0	0	0	0	0	0.5	1.6

Table 9.3 Duration (min) of temperature exceeding 800°C near the steel frames for every fire scenario

minutes over 900 °C		Frames										AVERAGE (min)	ST.DEV. (min)
		A1	A2	B1	B2	C1	C2	D1	D2	E1	E2		
Fire scenarios	SC-00	0	0	0	2	0	0	0	0	0	0	0.2	0.6
	SC-07	0	0	0	2	0	0	0	0	0	0	0.2	0.7
	SC-015a	0	0	0	2	0	0	0	0	0	0	0.2	0.7
	SC-015b	0	0	6	6	0	0	0	0	0	0	1.2	2.3
	SC-015c	0	4	0	2	0	0	0	0	2	0	0.8	1.4
	SC-030a	0	0	13	6	0	0	0	0	0	0	1.9	4.1
	SC-030b	0	5	3	4	0	0	24	0	3	0	3.8	6.8
	SC-030c	0	4	3	3	0	3	0	0	0	0	1.3	1.6
	SC-045	2	5	4	5	0	5	0	5	0	4	3.1	2.3
	SC-060a	2	2	13	10	18	9	21	8	0	0	8.3	7.0
	SC-060b	20	9	9	5	0	0	18	9	13	11	9.4	6.3
	SC-100	15	18	15	20	13	10	12	8	7	3	12.0	4.9
	SC-100SP1	0	0	0	0	0	0	0	0	0	0	0.0	0.0
SC-100SP2	0	0	0	3	0	0	0	0	0	0	0.3	1.0	

Table 9.4 Duration (min) of temperature exceeding 900°C near the steel frames for every fire scenario

minutes over 1000 °C		Frames										AVERAGE (min)	ST.DEV. (min)
		A1	A2	B1	B2	C1	C2	D1	D2	E1	E2		
Fire scenarios	SC-00	0	0	0	2	0	0	0	0	0	0	0.2	0.5
	SC-07	0	0	0	2	0	0	0	0	0	0	0.2	0.5
	SC-015a	0	0	0	2	0	0	0	0	0	0	0.2	0.7
	SC-015b	0	0	4	4	0	0	0	0	0	0	0.8	1.7
	SC-015c	0	3	0	2	0	0	0	0	0	0	0.5	0.9
	SC-030a	0	0	11	5	0	0	0	0	0	0	1.6	3.4
	SC-030b	0	0	3	3	0	0	15	0	0	0	2.0	4.4
	SC-030c	0	3	2	3	0	2	0	0	0	0	1.0	1.2
	SC-045	0	3	3	4	0	3	0	3	0	5	2.0	1.7
	SC-060a	0	0	11	7	19	4	16	5	0	0	6.2	6.7
	SC-060b	19	5	5	5	0	0	16	8	5	5	6.8	5.9
	SC-100	13	9	9	9	8	3	6	4	6	0	6.6	3.4
	SC-100SP1	0	0	0	0	0	0	0	0	0	0	0.0	0.0
SC-100SP2	0	0	0	1	0	0	0	0	0	0	0.1	0.4	

Table 9.5 Duration (min) of temperature exceeding 900°C near the steel frames for every fire scenario

Duration over (minutes)		600 °C		700 °C		800 °C		900 °C		1000 °C	
		average	st. dev.	average	st. dev.	average	st. dev.	average	st. dev.	average	st. dev.
Fire scenarios	SC-00	1.1	1.4	0.2	0.6	0.2	0.6	0.2	0.6	0.2	0.5
	SC-08	2.1	2.7	0.7	1.1	0.2	0.6	0.2	0.7	0.2	0.5
	SC-015a	3.6	4.0	1.5	2.7	0.8	1.8	0.2	0.7	0.2	0.7
	SC-015b	2.9	4.0	1.7	2.4	0.9	1.9	1.2	2.3	0.8	1.7
	SC-015c	4.9	5.0	1.9	3.4	2.0	4.1	0.8	1.4	0.5	0.9
	SC-030a	21.3	13.1	8.2	10.0	3.3	5.7	1.9	4.1	1.6	3.4
	SC-030b	19.8	12.4	8.2	8.8	5.1	7.5	3.8	6.8	2.0	4.4
	SC-030c	11.9	11.6	4.1	4.1	1.9	2.0	1.3	1.6	1.0	1.2
	SC-045	23.4	11.6	8.4	5.9	4.5	3.1	3.1	2.3	2.0	1.7
	SC-060a	38.9	5.3	23.2	12.2	11.8	9.7	8.3	7.0	6.2	6.7
	SC-060b	39.3	3.4	22.8	10.1	11.9	6.9	9.4	6.3	6.8	5.9
	SC-100	20.4	6.0	17.8	4.9	15.9	3.9	12.0	4.9	6.6	3.4
	SC-100SP1	0.0	0.0	0.0	0.0	0.0	0.0	0.0	0.0	0.0	0.0
	SC-100SP2	0.5	1.7	0.4	1.2	0.4	1.2	0.4	1.1	0.1	0.4

Table 9.6 Average duration (min) and st. deviation of temperature levels near the steel frames

9.2 Total Heat Release Rate

During the simulation, the Total Heat Release Rate in the building is recorded. The total Heat Release Rate is indicative of the energy that is released by the combustion in the compartment. The evolution of the Total Heat Release Rate of all the fire scenarios is displayed in Figure 9.2 and a selection of the seven most representative fire scenarios is given in Fig 9.3.

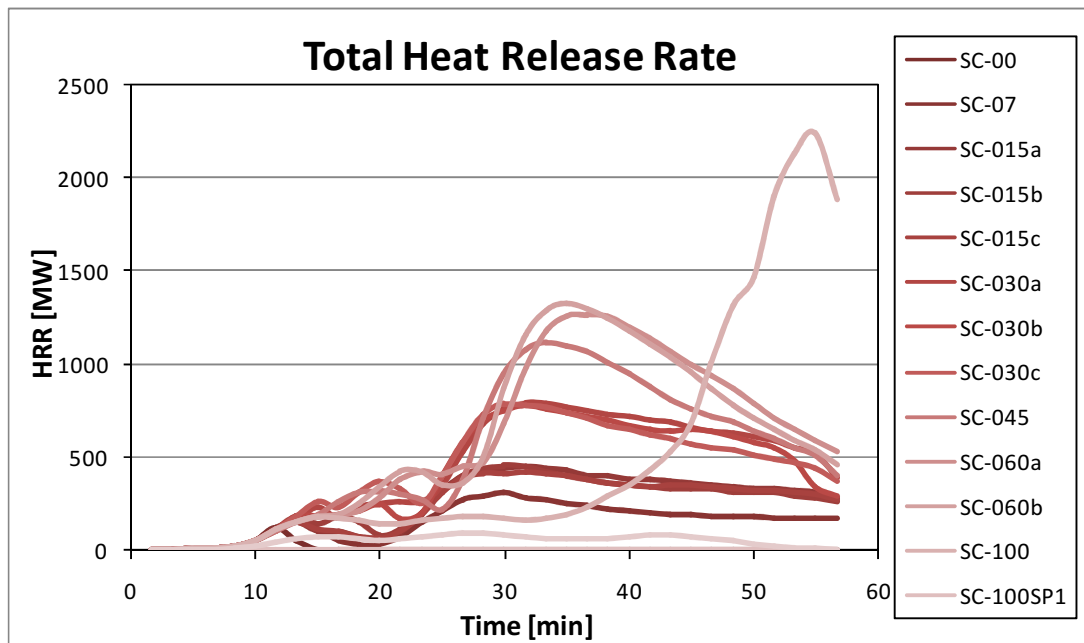


Fig. 9.2 Total heat release rate of all the considered fire scenarios

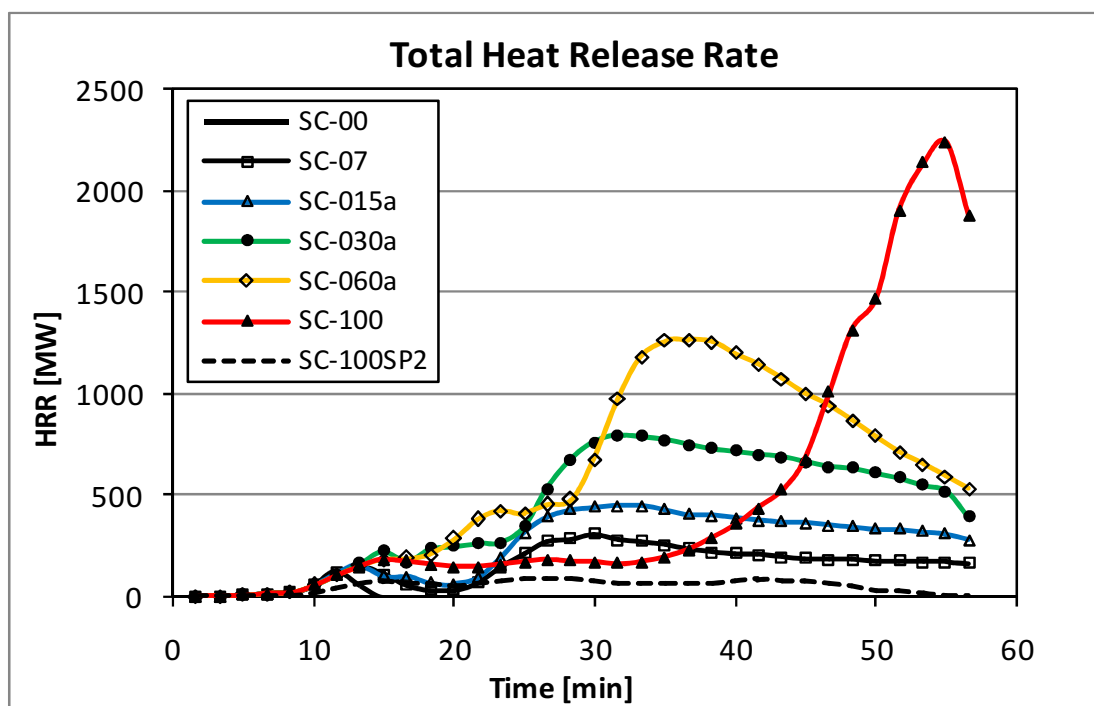


Fig. 9.3 Total heat release rate of the seven most representative fire scenarios

9.3 Pressure, velocity and temperature spatial distributions

During the simulation pressure, velocity and temperature data of the defined slices of the computational volume is recorded. This is used by the companion program Smokeview to create animations of the simulation, which are a valuable aid in the study and comprehension of the simulation and its results. Some distinctive frames of these animations that present characteristic aspects of every fire scenario are presented in the next figures.

FIRE SCENARIO SC-00

In this fire scenario, no windows are damaged, so there is no ventilation to the compartment. The fire is suppressed within 10 minutes due to oxygen depletion. In Figures 9.4 and 9.5 a slice of the temperature distribution and a visualization of the area where the Heat Release Rate per Unit Volume (HRRPUV) is greater than 27 kW/m^3 are depicted. This could be interpreted as the area where most of the combustion takes place. The water sprinkler system is considered fully damaged.

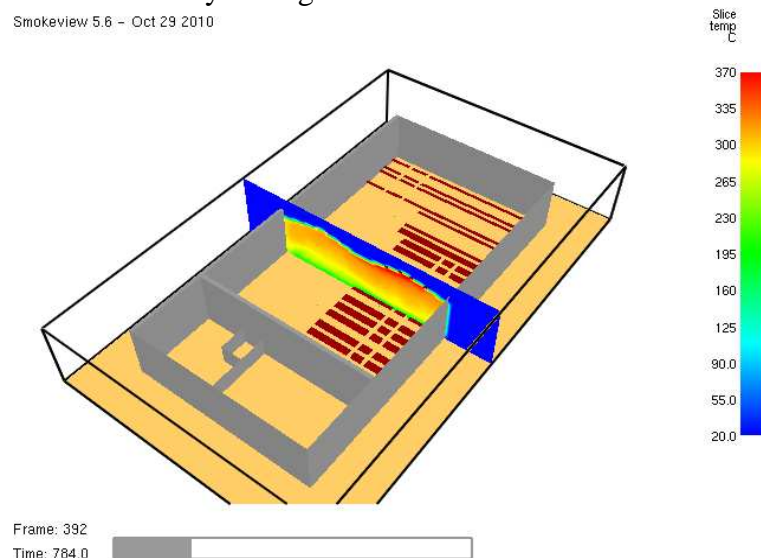


Fig. 9.4 Slice of temperature distribution in the compartment – SC-00

Smokeview 5.6 - Oct 29 2010

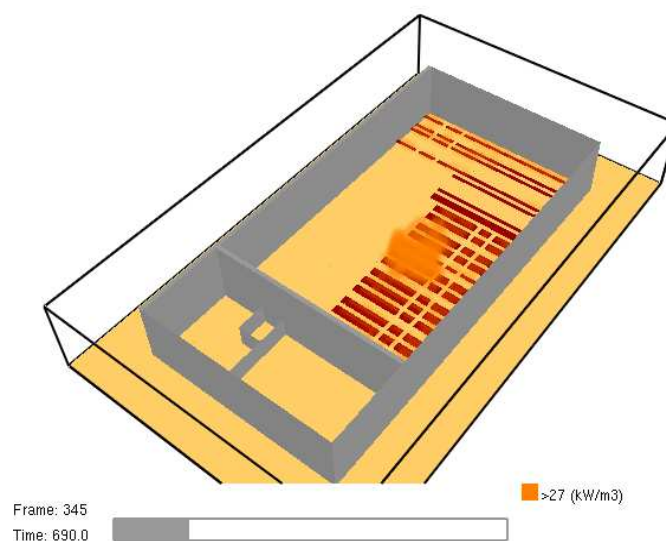


Fig. 9.5 Area of Heat Release Rate per Unit Volume $> 27 \text{ kW/m}^3$ – SC-00

FIRE SCENARIO SC-07

In this scenario there is only one damaged/open window and no water sprinkler system.

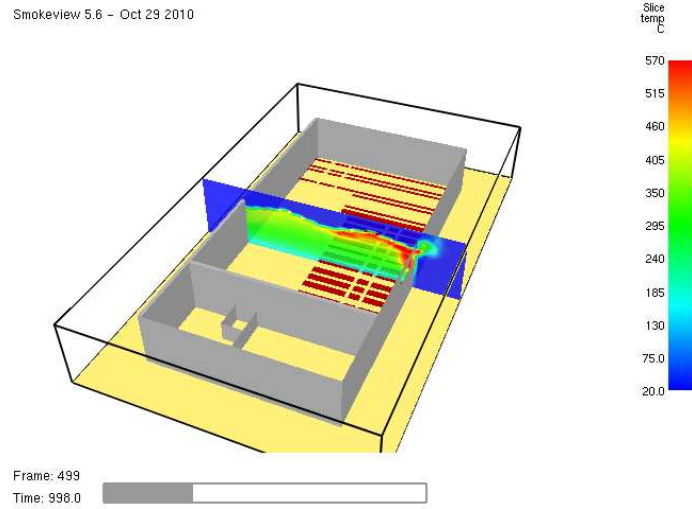


Fig. 9.6 Slice of temperature distribution in the compartment – SC-07

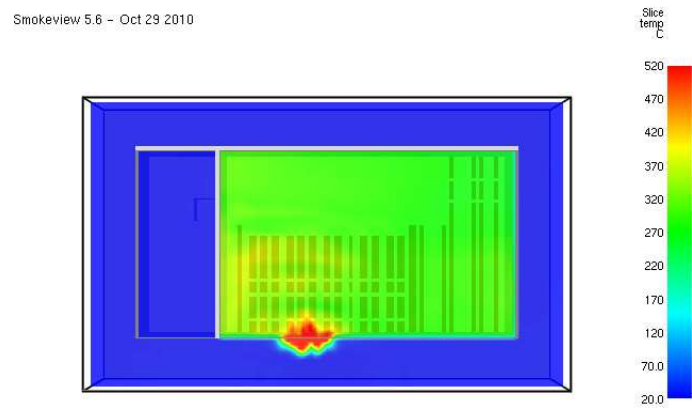


Fig. 9.7 Slice of temperature distribution under the roof – SC-07

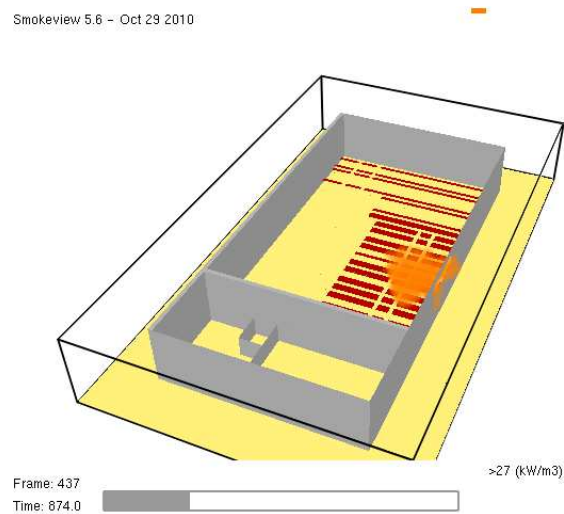


Fig. 9.8 Area of Heat Release Rate per Unit Volume > 27 kW/m³ – SC-07

FIRE SCENARIO SC-015a

In this scenario the damage to the windows is 15%. The area of the highest temperatures is double compared to the SC-07 fire scenario.

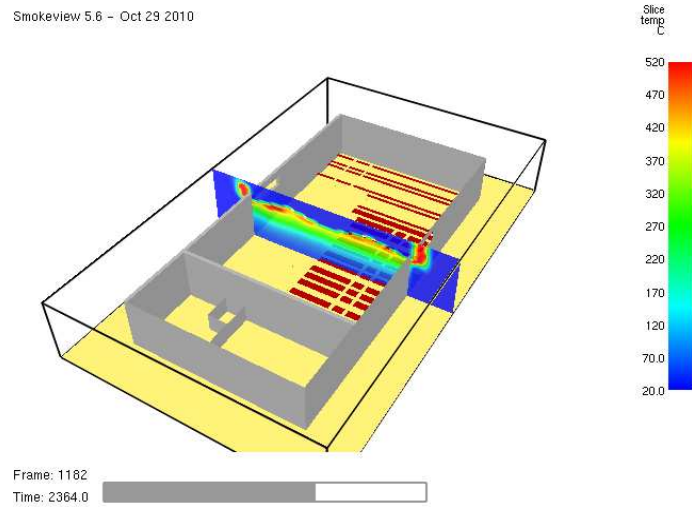


Fig. 9.9 Slice of temperature distribution in the compartment – SC-015a

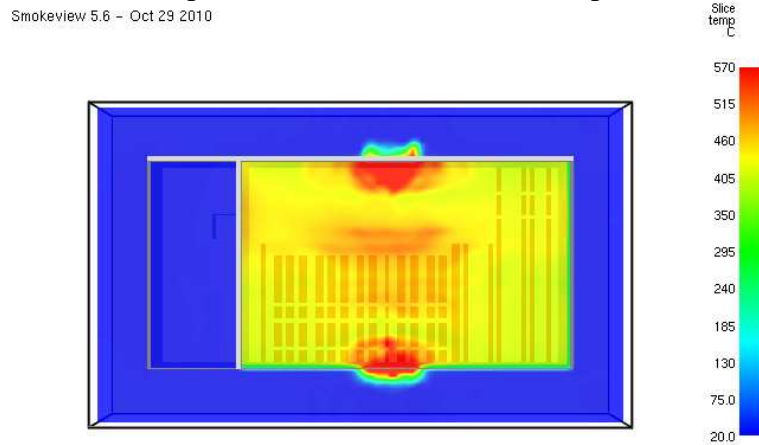


Fig. 9.10 Slice of temperature distribution under the roof – SC-015a

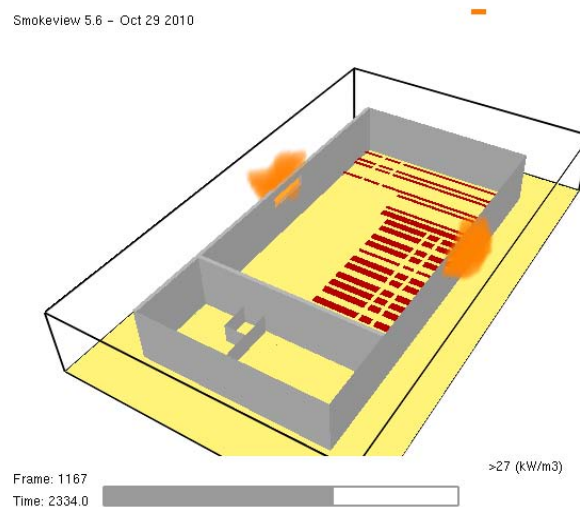


Fig. 9.11 Area of Heat Release Rate per Unit Volume > 27 kW/m³ – SC-015a

FIRE SCENARIO SC-015b

This scenario has the same parameters with the previous scenario with different position of the damaged/open windows which are placed next to each other on the same side of the building.

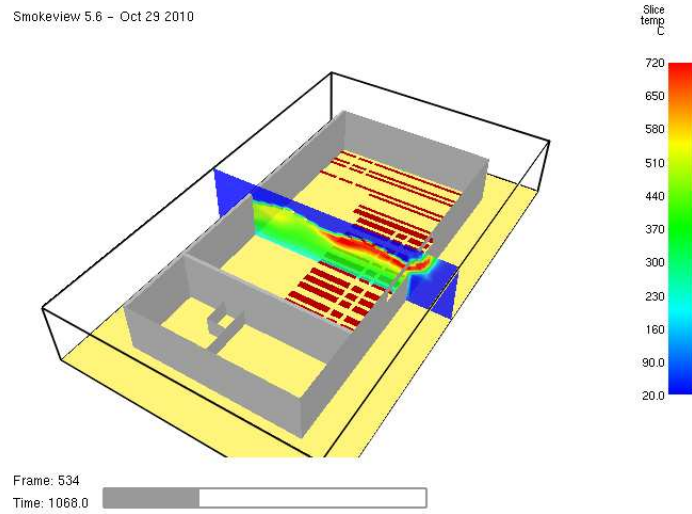


Fig. 9.12 Slice of temperature distribution in the compartment – SC-015b

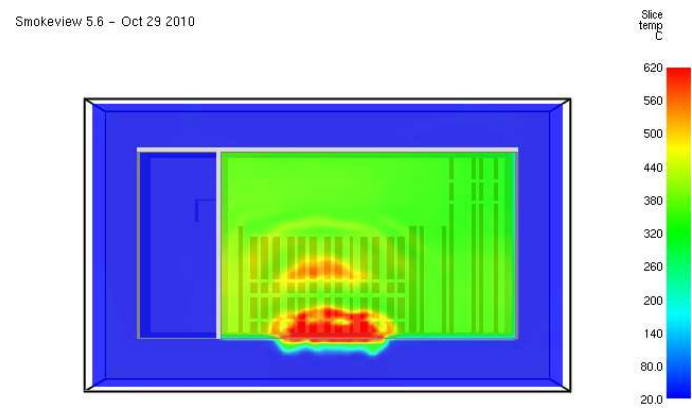


Fig. 9.13 Slice of temperature distribution under the roof – SC-015b

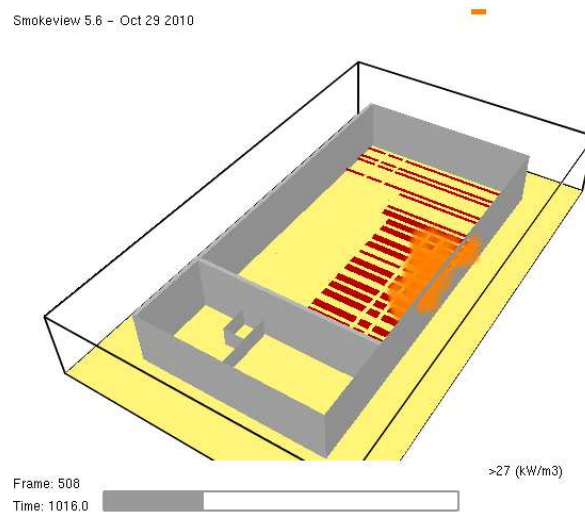


Fig. 9.14 Area of Heat Release Rate per Unit Volume $>27 \text{ kW/m}^3$ – SC-015b

FIRE SCENARIO SC-015c

Again, in this scenario, the level of window damage is the same but with a different configuration. The windows are placed on opposite corners on the opposite walls of the compartment.

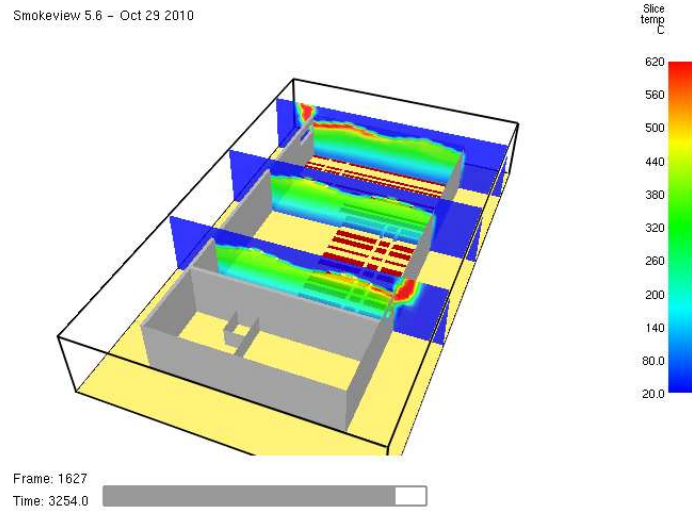


Fig. 9.15 Slice of temperature distribution in the compartment – SC-015c

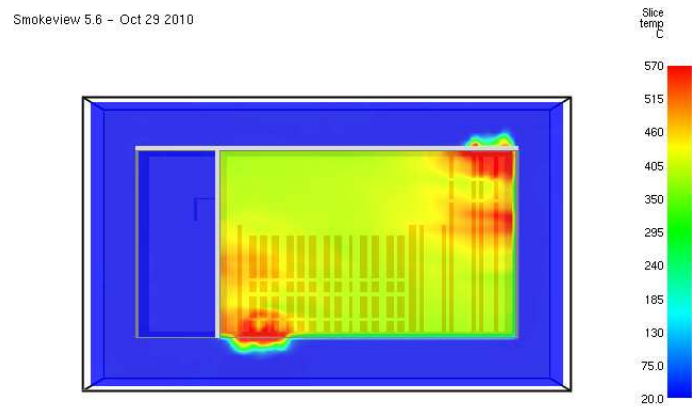


Fig. 9.16 Slice of temperature distribution under the roof – SC-015b

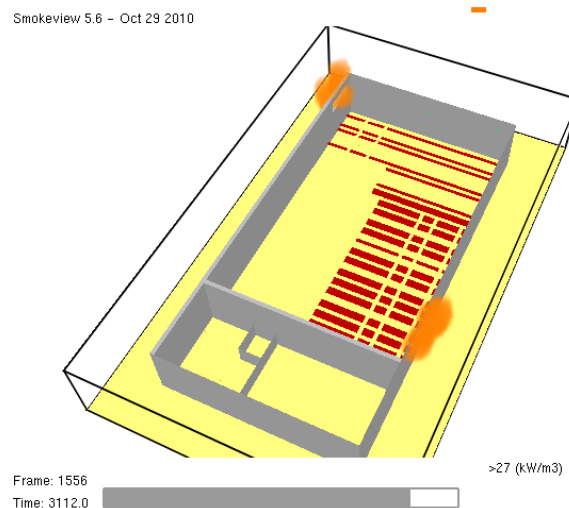


Fig. 9.17 Area of Heat Release Rate per Unit Volume > 27 kW/m³ – SC-015c

FIRE SCENARIO SC-030a

In this scenario the level of non structural window damage is 30%.The windows are placed symmetrically on the opposite walls. Temperatures get higher in the compartment.

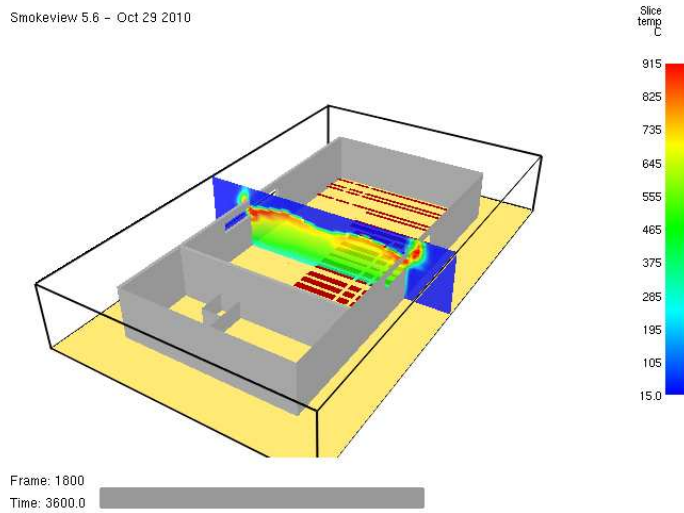


Fig. 9.18 Slice of temperature distribution in the compartment – SC-030a

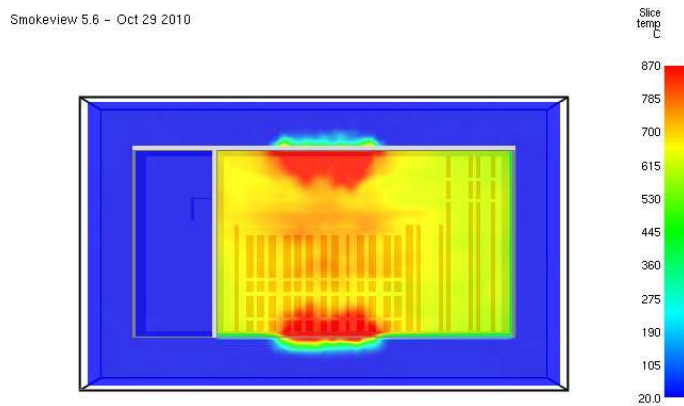


Fig. 9.19 Slice of temperature distribution under the roof – SC-030a

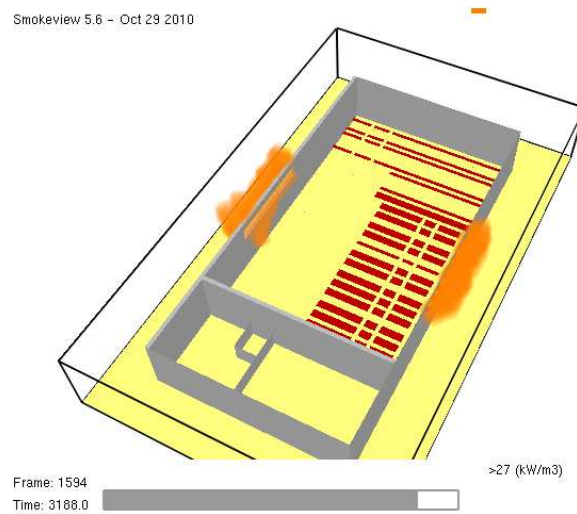


Fig. 9.20 Area of Heat Release Rate per Unit Volume > 27 kW/m³ – SC-030a

FIRE SCENARIO SC-030b

In this scenario there is 30% of the windows broken and are placed diagonally on the two opposite walls. The temperatures are slightly lower.

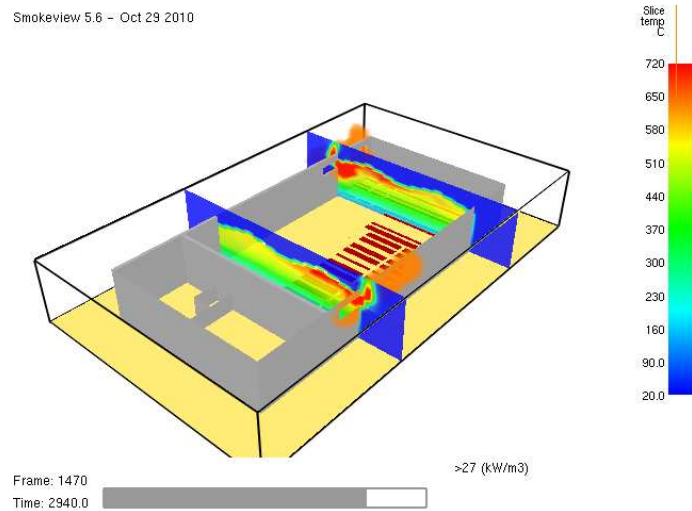


Fig 9.21 Slice of temperature distribution in the compartment – SC-030b

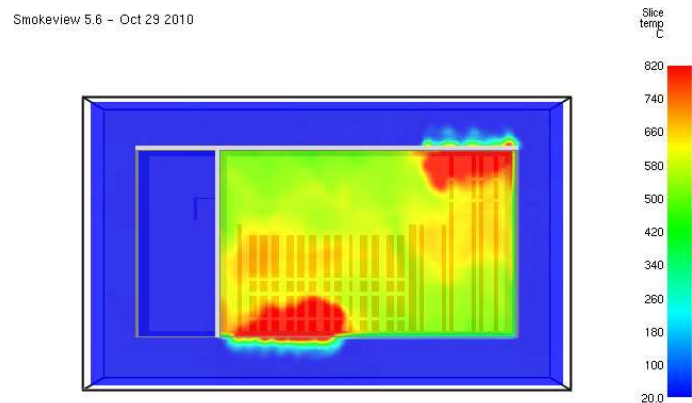


Fig 9.22 Slice of temperature distribution under the roof – SC-030b

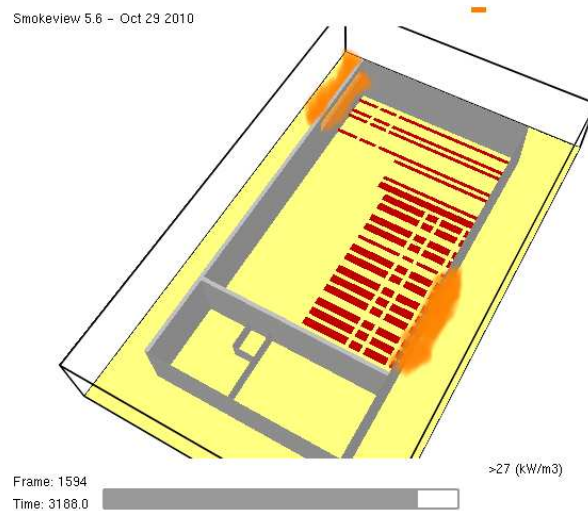


Fig 9.23 Area of Heat Release Rate per Unit Volume > 27 kW/m³ – SC-030b

FIRE SCENARIO SC-030c

In this scenario there is the same level of damage (30%) but the windows are placed on the one side of the building.

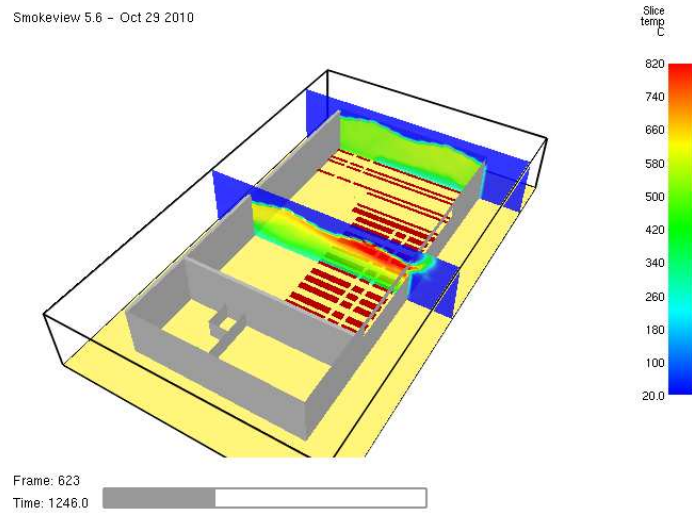


Fig. 9.24 Slice of temperature distribution in the compartment – SC-030c

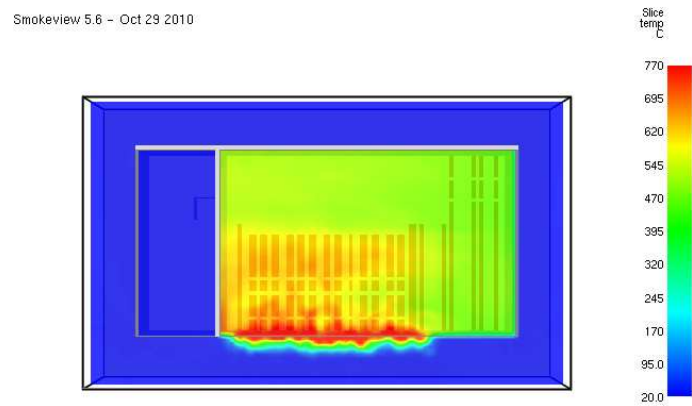


Fig. 9.25 Slice of temperature distribution under the roof – SC-030c

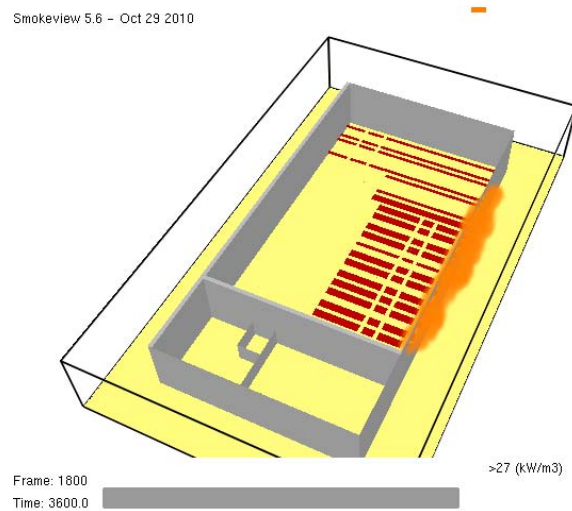


Fig. 9.26 Area of Heat Release Rate per Unit Volume > 27 kW/m³– SC-030c

FIRE SCENARIO SC-045

In this scenario almost all the windows on the one side of the compartment are damaged (45% windows damage).

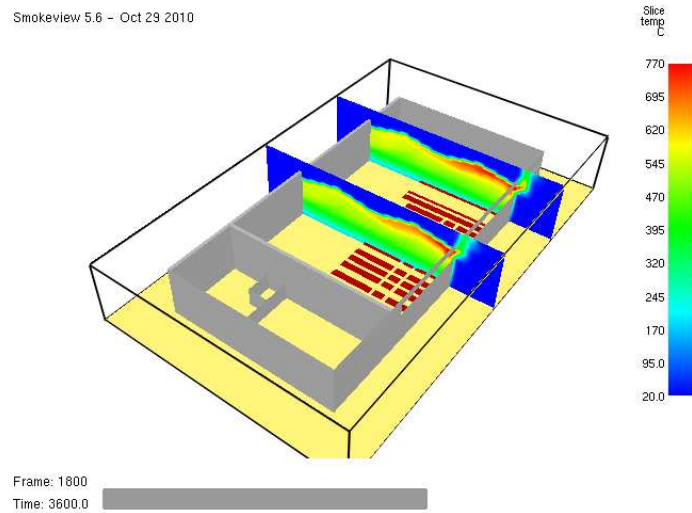


Fig. 9.27 Slice of temperature distribution in the compartment – SC-045

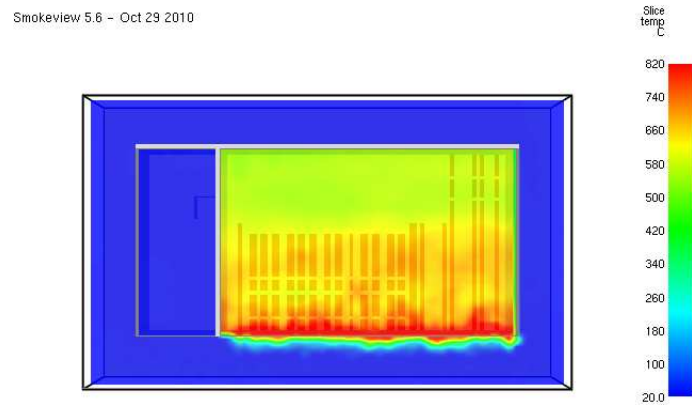


Fig. 9.28 Slice of temperature distribution under the roof – SC-045

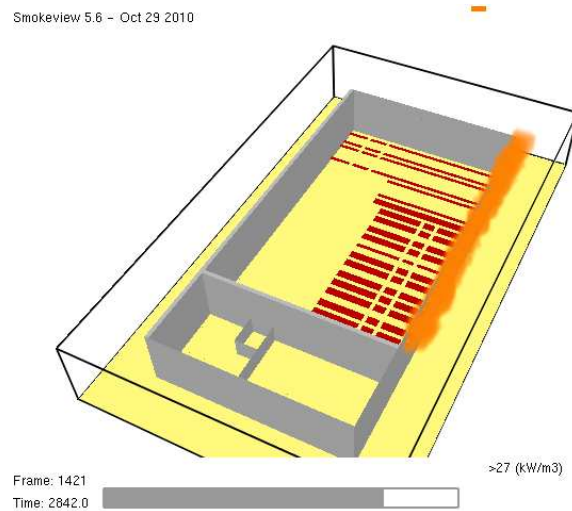


Fig. 9.29 Area of Heat Release Rate per Unit Volume > 27 kW/m³ – SC-045

FIRE SCENARIO SC-060a

In this scenario 60% of the compartment windows are damaged. The temperatures get higher in the compartment.

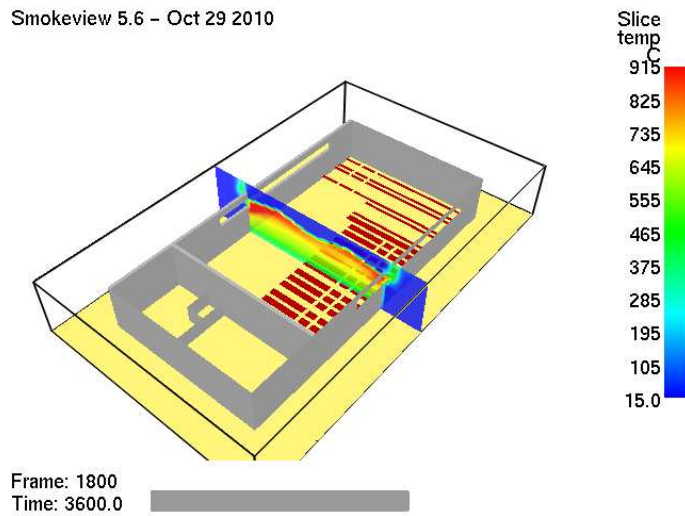


Fig. 9.30 Slice of temperature distribution in the compartment – SC-060a

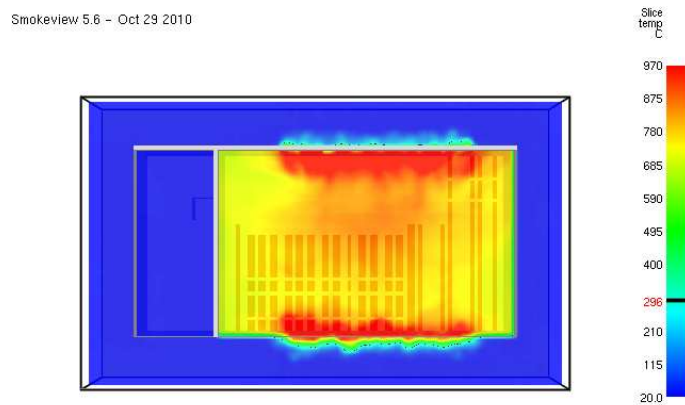


Fig. 9.31 Slice of temperature distribution under the roof – SC-060a

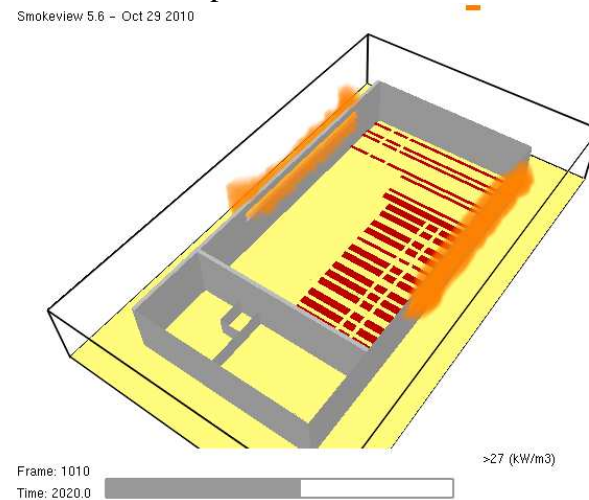


Fig. 9.32 Area of Heat Release Rate per Unit Volume > 27 kW/m³ – SC-060a

FIRE SCENARIO SC-060b

Again in this scenario there is 60% damage but the windows are placed in the four corners of the compartment.

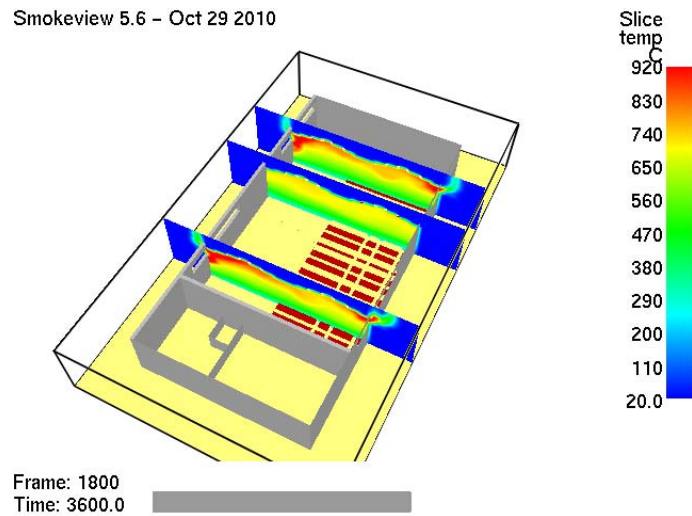


Fig. 9.33 Slice of temperature distribution in the compartment – SC-060b

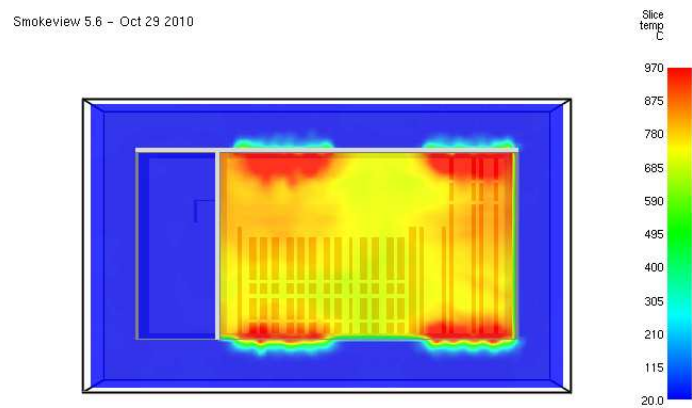


Fig. 9.34 Slice of temperature distribution under the roof – SC-060b

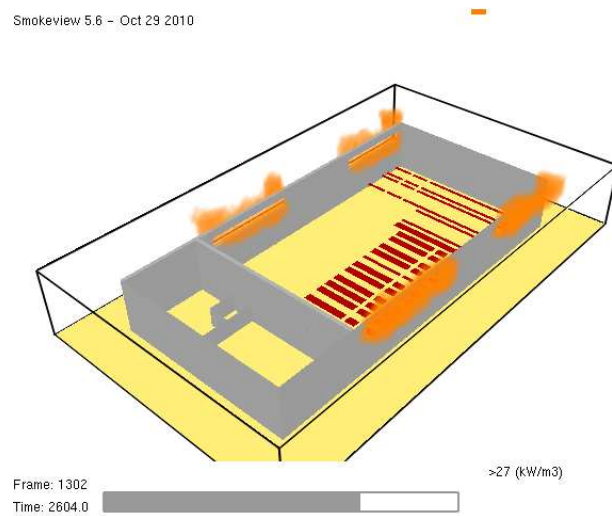


Fig. 9.35 Area of Heat Release Rate per Unit Volume > 27 kW/m³ – SC-060b

FIRE SCENARIO SC-100

In this fire scenario it is considered that all the windows of the compartment are damaged plus the fireproof door that divides the compartments.

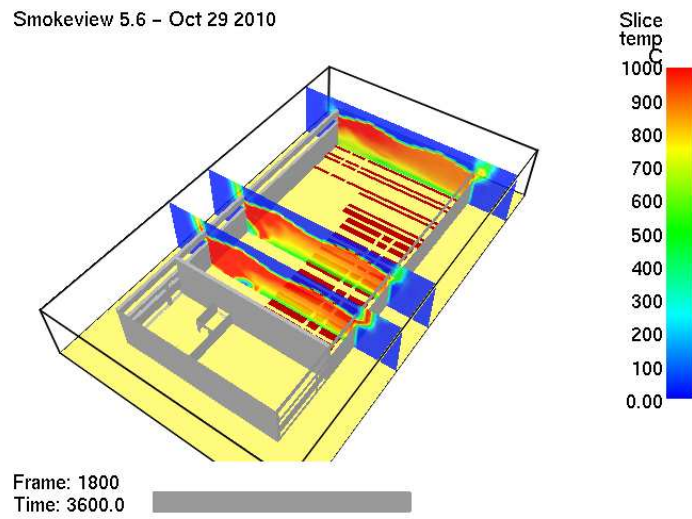


Fig. 9.36 Slice of temperature distribution in the compartment – SC-100

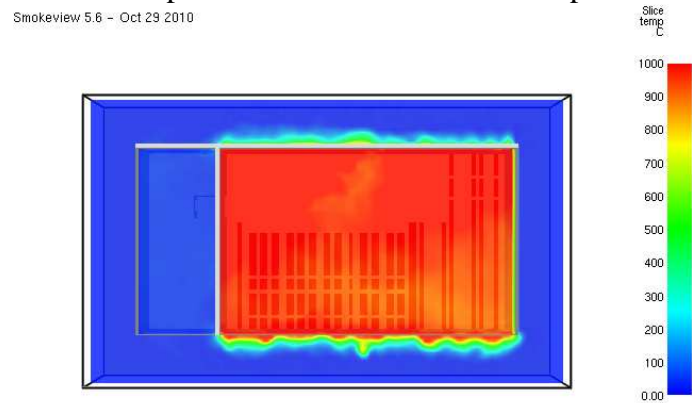


Fig. 9.37 Slice of temperature distribution under the roof – SC-100

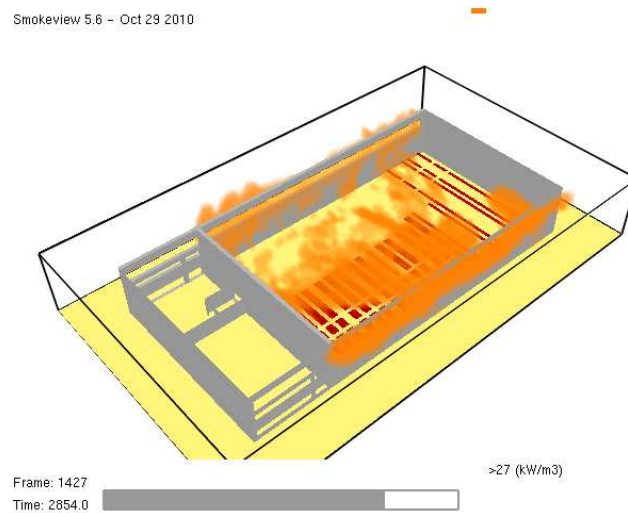


Fig. 9.38 Area of Heat Release Rate per Unit Volume > 27 kW/m³ – SC-100

FIRE SCENARIOS SC-100SP1 AND SC-100SP2

In all the previous fire scenarios the water sprinkler system was considered completely damaged. In fire scenario SC-100SP1 the sprinkler system is fully functional and in scenario SC-100SP2 50% of the sprinkler system is functional. Also all the compartment windows are considered damaged. Regarding the results of the analysis, in the full functional sprinkler system scenario the fire is immediately suppressed. In SC-100SP2, the fire is controlled by the sprinklers resulting in considerably lower temperatures.

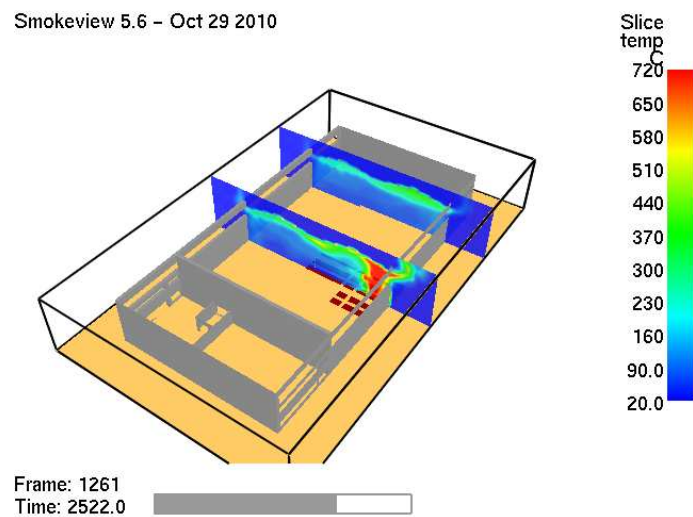


Fig. 9.39 Slice of temperature distribution in the compartment – SC-100SP50
50% operational water sprinkler system.

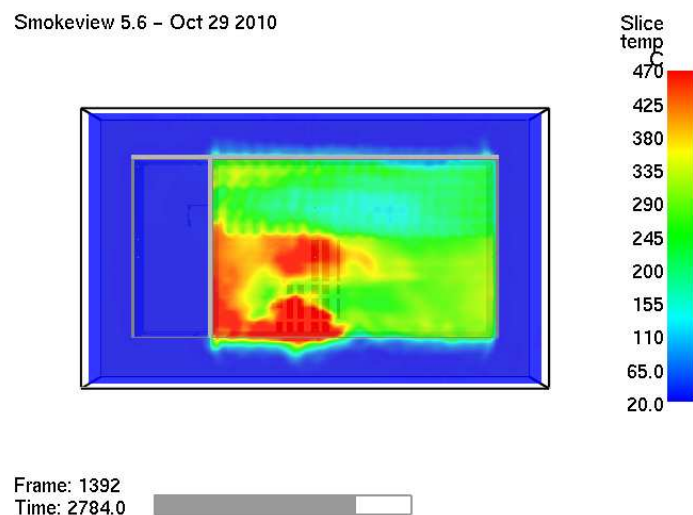


Fig. 9.40 Slice of temperature distribution under the roof – SC-100SP50
50% operational water sprinkler system.

10. Discussion

From the simulations and the analysis results it is evident that the most influential factor in the fire development is the function/malfunction of the water sprinkler system. If it is functional, the fire is either almost immediately suppressed or considerably controlled but that highly depends on whether the functional part covers the fire ignition point. The fire develops only in the part of the building that is not covered by the sprinklers. In the absence of an active fire suppression system, the ventilation conditions are the second most influential factor of the fire development, given that the fuel type and fuel quantity do not change.

In Tables 9.5 to 9.6, it is evident that as the number of open/broken windows increases, the thermal exposure of the steel frames rises, making the fire scenarios of 60% and 100% “damage” the most severe ones. In the summarized results of Table 9.6, where the average duration of all the temperature levels for all the fire scenarios are displayed, it is observed that for the lower temperature levels of 600°C and 700°C scenario SC-60a/b is the most critical (60% level of non structural damage) and for the higher temperature levels of 800°C, 900°C and 1000°C the SC-100 fire scenario results in more heat exposure. As it was expected open windows provide more fresh air into the compartment to sustain the combustion. The cause for the decrease that is observed in the heat exposure for the temperature levels of 600°C and 700°C in SC-100 can be explained by the evolution of the Heat Release Rate in table 9.3. For the SC-100 fire scenario there is a delay in the fire growth for about 40 minutes and then a very steep increase. The result of that is that for the first hour of the fire development that is examined in this study, the increase in the temperature values lasts only for about 20 minutes, and, consequently, there is only a 20 minute window for temperatures greater than 600°C to be recorded. However, the temperatures in the compartment rise very rapidly and in this 20 minute growth period, surpass 800°C for 15.9 minutes, 900°C for 12.0 minutes and 1000°C for 6.6 minutes, which are the longest durations recorded, compared to all the scenarios. If the fire was studied for a longer period it is expected that the 100% damage scenario would result in the longest durations for all temperature levels as the fire curve in all the other fire scenarios has reached the decaying phase within this one hour. However in the SC-100 fire scenario the HRR has just passed its peak point. Yet, by studying only the first hour of the fire development we can observe that, if for example, the level of 600°C or 700°C is critical for the stability of the structure, then the 60% damage scenario would be the most hazardous one, because it causes such temperatures in the compartment much quicker than the 100% damage scenario. If the structure could maintain its stability for 600°C and 700°C, then the fire scenario of 100% damage would be the most hazardous. If not, the 60% damage would be the critical one.

As it was mentioned there is a delay of 40 minutes in the fire growth in the 100% damage scenario. This delay is caused by the ventilation conditions. When windows are open at the beginning of the fire, during the first stages of the fire growth they act as vents, removing hot gases and smoke from the interior due to the difference in the pressure inside and outside of the compartment. This process results in reduced temperatures in the compartment and hinders fire growth as the heat feedback from the hot layer is very low and the pyrolysis process slows down. The phenomenon, though, can't last for long as at some point the pressure difference is balanced. The delay that is caused in the fire development is very important as it provides a time window during which the fire can be suppressed or extinguished by human intervention with conventional fire suppressing means or by the actions of the fire fighting crew.

Apart from the global degree of ventilation of the building, the position of the broken/open windows plays also a major role in the heat exposure of the steel frames. The frames that are mostly affected by the fire are the ones that are near the open windows. The

position of the affected frames could result either in a local or a global collapse of the structure. This is observed by comparing the scenarios that have the same level of damage but a different configuration of the broken openings.

In fire scenarios SC-030a/b/c the level of damage is 30% but in the SC-030a scenario the broken windows are placed opposite each other, in SC-030b diagonally on the opposite corners and in SC-030c on one side of the compartment (Fig. 10.1). The temperature durations are displayed in Table 10.1.

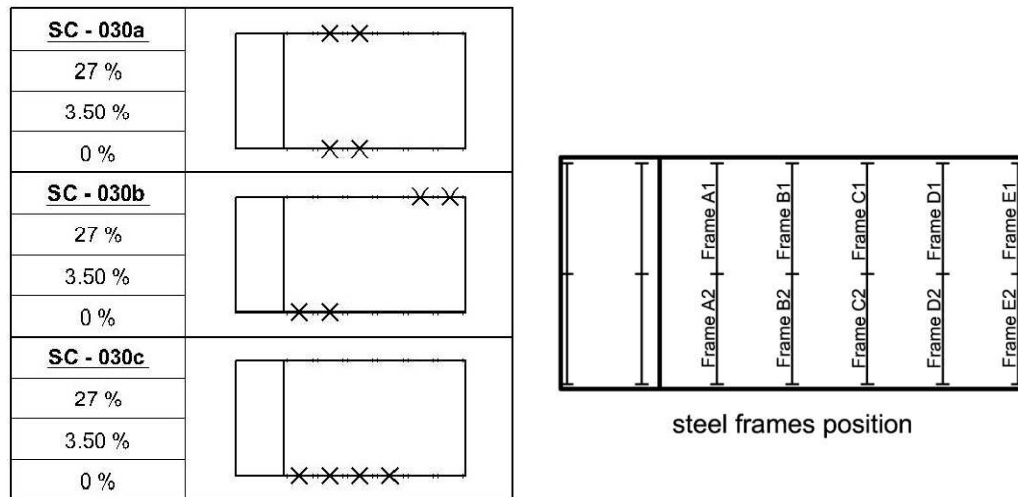


Fig. 10.1 Fire scenarios SC-030a/b/c and steel frames' position

minutes over 600°C	Frames										AVERAGE (min)	ST.DEV. (min)
	A1	A2	B1	B2	C1	C2	D1	D2	E1	E2		
SC-030a	30	20	44	36	29	26	10	9	6	4	21.3	13.1
SC-030b	8	28	7	20	18	4	40	12	41	20	19.8	12.4
SC-030c	8	30	10	36	6	19	3	5	0	3	11.9	11.6

Table 10.1 Duration (min) of temperature exceeding 600°C near the steel frames for fire scenarios SC-030a/b/c

It is evident in all scenarios that the sub-frames that are mostly affected are the ones next to the broken windows. In fire scenario SC-030a frames B1 and B2 are more affected because they have windows on both sides. In fire scenario SC-030b most affected are frames A2, B2 and D1 and E1 which are situated diagonally next to the open windows. In scenario SC-030c the frames A2, B2, C2, that are situated next to the open windows on one side of the building are subjected to 600°C for longer durations. The reason for this outcome is that after the oxygen within the compartment is consumed, fresh air and oxygen is present at the vicinity of the open windows and therefore, after some time, the combustion takes place near the openings inside and outside the building and affects more significantly the nearby frames. Also, as it is already mentioned, only the gases that are caused by the pyrolysis process are able to combust and thus combustion can take place away from the solid fuels. The temperature distributions under the roof of the building for scenarios SC-030a/b/c, where the above mentioned phenomenon can be visualized, are given in Fig. 10.2.

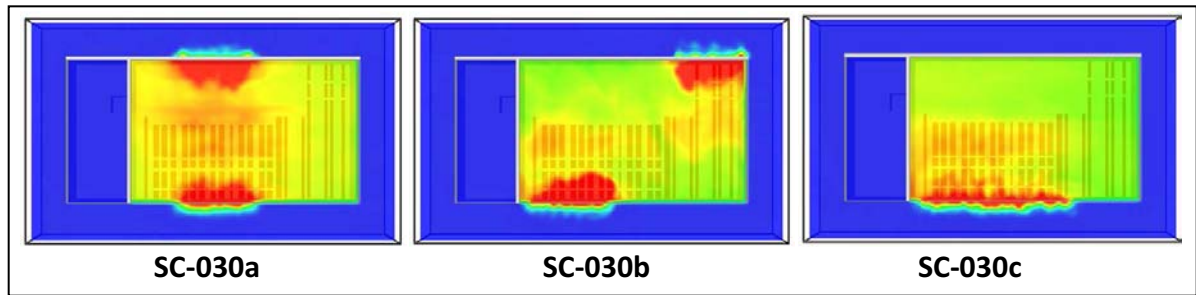


Fig. 10.2 Temperature distribution under the roof of the building for scenarios SC-030a/b/c

The same behavior can be observed also in the other scenarios (SC-07, SC-015a/b/c, SC-045) displayed in Table 10.2 and Fig 10.3. The phenomenon becomes less prominent as the total ventilation increases and the combustion becomes more global as the oxygen is present almost everywhere.

minutes over 600 °C	Frames										AVERAGE (min)	ST.DEV. (min)
	A1	A2	B1	B2	C1	C2	D1	D2	E1	E2		
SC-07	8	2	4	4	0	2	0	0	0	0	2.1	2.7
SC-015a	7	2	12	7	6	2	0	0	0	0	3.6	4.0
SC-015b	2	4	3	14	2	4	0	0	0	0	2.9	4.0
SC-015c	5	8	5	5	0	2	6	0	17	0	4.9	5.0
SC-045	13	28	15	38	14	38	7	37	13	32	23.4	11.6

Table 10.2 Duration (min) of temperature exceeding 600°C near the steel frames for fire scenarios SC-07, SC-015a/b/c and SC-045

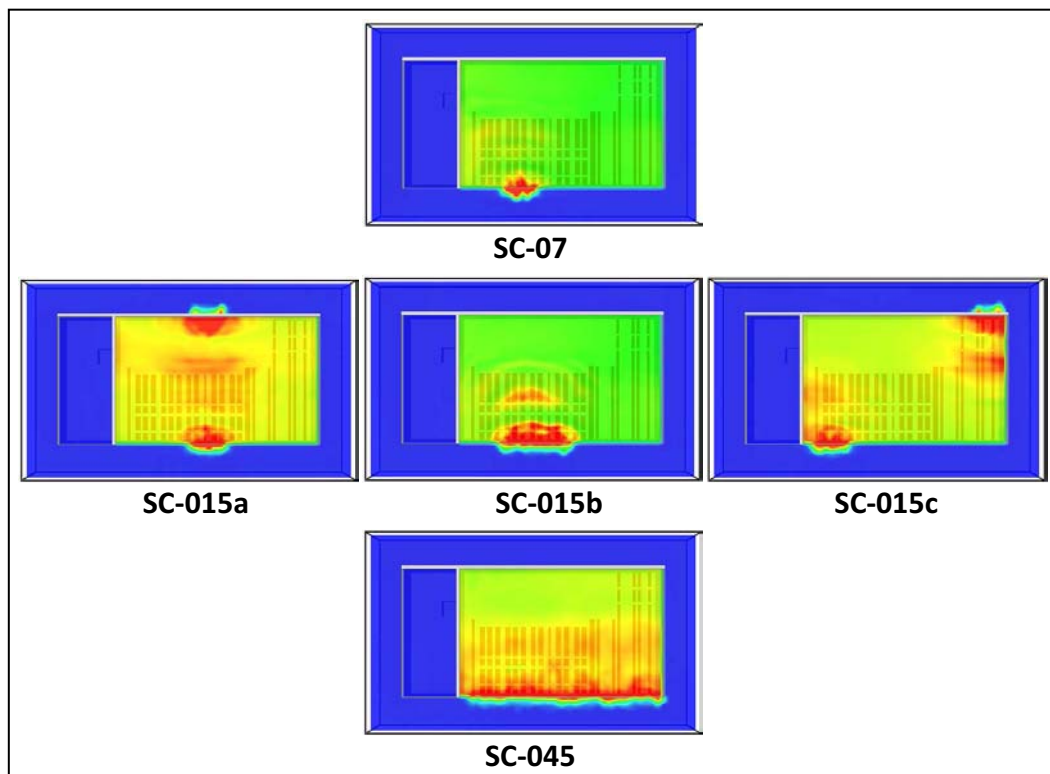


Fig. 10.3 Temperature distribution under the roof of the building for scenarios SC-07, SC-015a/b/c and SC-045

In fire scenario SC-07, where there is only one group of windows damaged/open only frames A1, A2, B1 and B2 are exposed to temperatures over 600°C and the rest are not affected at all. The heat exposure is small (8 mins maximum) because in general the fire isn't very harsh. In the group of scenarios of 15% non-structural damage (SC-015a/b/c) the different ventilation configuration leads to different heat exposure distribution among the frames. In the first scenario (SC-015a), where the windows are placed on opposite sides, the average heat exposure of the frames over 600°C is 3.6 min, while in scenario SC-015b is lower (2.9 minutes). There is a difference though, on the maximum value of heat exposure duration on separate frames and on the number of frames that are most affected. In the first scenario there is a more even distribution among frames A1, B1, B2 and C1 with a peak value of 12min, and in the second, frame B2 which is next to the open window is exposed for 14 minutes with the rest 5 frames only exposed for 2-4 minutes. The third scenario (SC-015c) has a higher average duration of 4.9 mins but with a higher value of st. dev., meaning that there is more dispersion of the duration of heat exposure among the frames of the compartment. The frame that is most affect, however, is exposed to temperatures over 600°C for 17 minutes, the longest among the three fire scenarios.

In scenario SC-045, where the damage level is higher (45%) and the windows are placed only on one side, the average duration of the heat exposure increases considerably to 23.4 min and the frames on the side of the open windows are approximately exposed to temperatures over 600°C for 20 minutes longer than the frames on the other side.

As the degree of damage increases further, heat exposure increases as an average value for all fire scenarios. The differences in the heat exposure of the frames still exists but isn't so significant. The differences, though, in the roof temperature distribution and the exposure duration of the frames can be observed in Table 10.3 and Fig. 10.4 for fire scenarios SC-060a/b for the temperature level of 800°C. The frames that are more affected are in the middle of the compartment in SC-060a, where in scenario SC-060b the middle frames are barely exposed to temperatures over 800°C.

minutes over 800 °C	Frames										AVERAGE (min)	ST.DEV. (min)
	A1	A2	B1	B2	C1	C2	D1	D2	E1	E2		
SC-060a	3	5	27	12	27	14	20	9	0	0	11.8	9.7
SC-060b	23	11	13	10	0	3	21	10	16	11	11.9	6.9

Table 10.3 Duration (min) of temperature exceeding 800°C near the steel frames for fire scenarios SC-060a/b

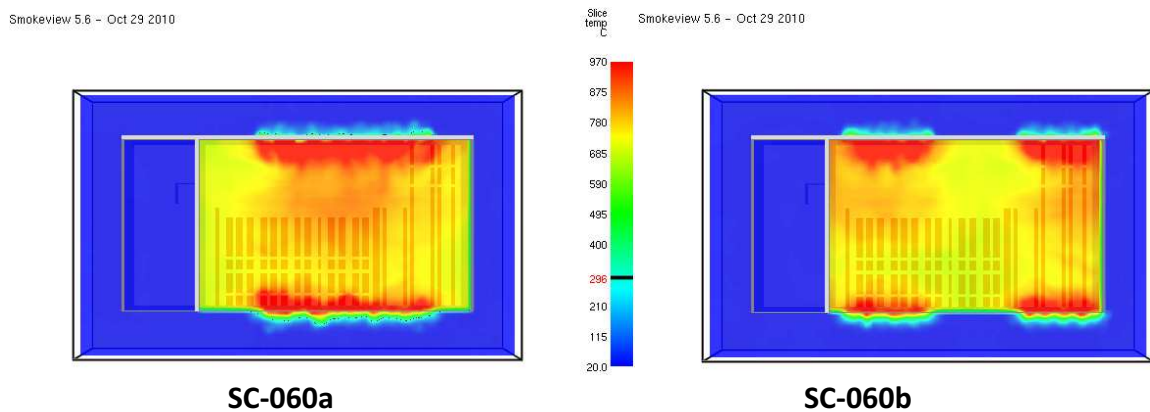


Fig. 10.4 Temperature distribution under the roof of the building for scenarios SC-060a/b

For the 100% broken windows scenario, the highest heat exposure durations with the most uniform distributions among the frames were observed. This is reflected in the low values of st. deviation for all the temperatures levels that are calculated for this scenario (Table 10.4 and Table 9.6 in previous Chapter).

Duration over (minutes)	600 °C		700 °C		800 °C		900 °C		1000 °C	
	average	st. dev.	average	st. dev.	average	st. dev.	average	st. dev.	average	st. dev.
SC-100	20.4	6.0	17.8	4.9	15.9	3.9	12.0	4.9	6.6	3.4

Table 10.4 Average duration (min) and st. deviation of temperature levels near the steel frames for scenario SC-100

Regarding each fire scenario's temperature time-history, as it was already mentioned in the beginning of Chapter 9, the time-histories that were recorded varied significantly both in time and space. There is not a unique temperature time-history for every fire scenario. There is even significant variance in the heat exposure of the frames within the same fire scenario. Even a creation of a separate temperature time-history for every frame would be an averaging procedure, and still in this case a decision needs to be made whether a different temperature time-history would be created for every frame element. But even in the case of one temperature time-history per frame beam for example, would result in numerous temperature time-histories for all the considered fire scenarios. This is the reason that the post processing of the results was done in terms of scalar durations of heat exposure. Otherwise it would be very difficult to reach any conclusions regarding the severity of the fire scenarios on the structure as a whole. A full CFD-thermal-structural analysis by a coupled CFD and thermo-mechanical analysis is the best solution, but apart from the great problems regarding the interface of the CFD and thermo-mechanical analysis, from the computational point of view is extremely expensive.

In the next diagrams, indicative average temperature time-histories of the span of the frame, which was the most affected component in each fire scenario, are presented. Every time history is created by averaging in every time frame the gas temperature of 20 point temperature time-histories near the span of the frame. The scenarios are divided in two diagrams for display purposes in Fig. 10.5 and 10.6 and the temperature time histories are plotted against the nominal ISO-834 temperature curve that is most commonly used for the fire design of structural elements. It can be observed that, as the level of damage increases, the peak temperature increases as well. Moreover, the average gas temperature around the beam in all fire scenarios, except the 100% damage scenario, remains below 1000 °C, varies with the evolution of time and towards the end of the simulation reaches a steady, slightly increasing temperature value. Also, apart from some peak values, the curves remain in general closely under the ISO curve, having though chronically a slower growth branch.

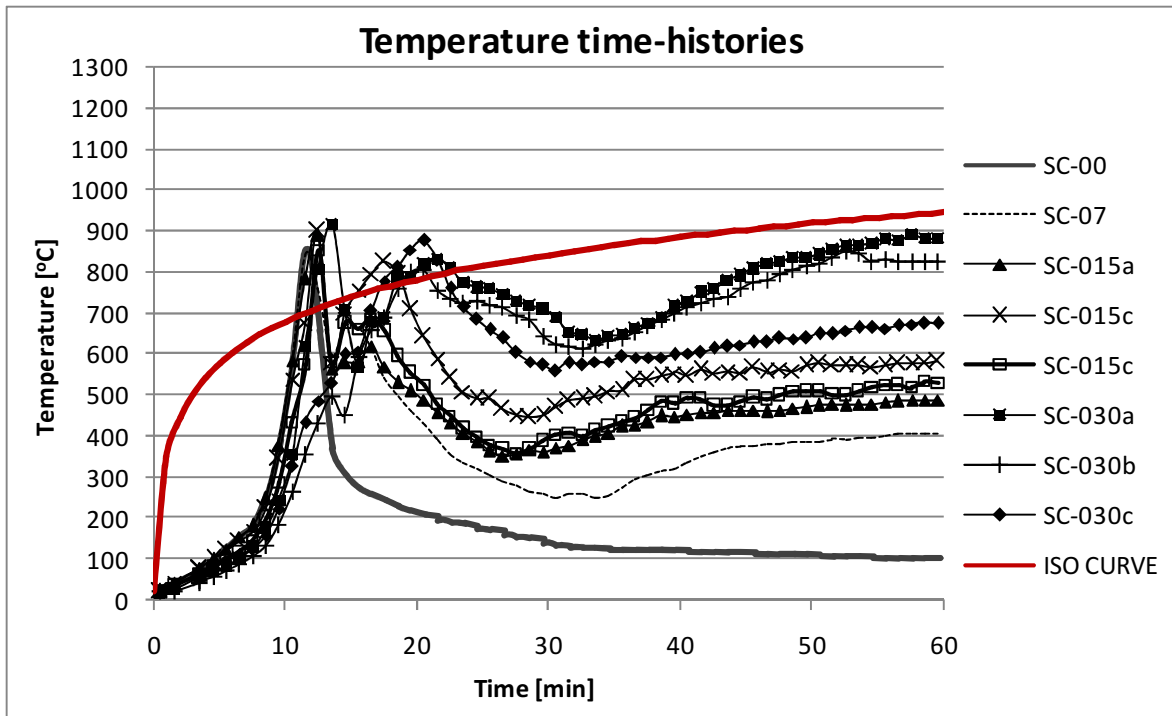


Fig. 10.5 Average gas temperature time-histories around the beam of the most affected frame by the fire

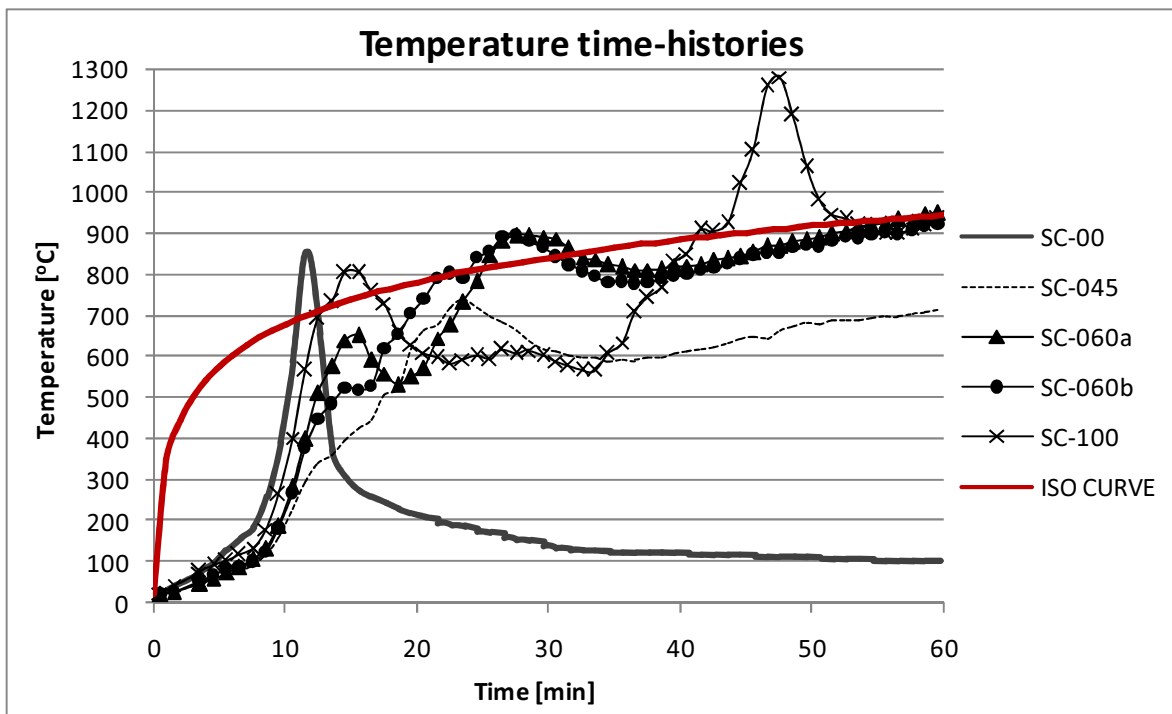


Fig. 10.6 Average gas temperature time-histories around the beam of the most affected frame by the fire

11. Conclusions

In the present study a numerical simulation of natural fire in an industrial building was performed with the aid of Computational Fluid Dynamics. A full 3-d model of the building, that is used mainly as a storage facility, was constructed in Fire Dynamic Simulator software, and its properties regarding the geometry, compartmentation, openings, construction materials and fire load were described. In total 14 fire scenarios of natural fire were simulated, each one corresponding to a different level of non-structural damage, which consisted of window breakage, fireproof door damage and water sprinkler system malfunction. Special attention was given to the simulation of the burning behavior of the combustible materials that were contained in the storage compartment. The fire development was studied, and gas temperature, pressure, velocity and Heat Release Rate time-histories were recorded. The goal of the study was to assess the impact that the non-structural damage can have on the development of natural fire in the storage compartment.

From the analysis of the results, it is observed that the temperature distribution inside the compartment varies significantly both in time and space. Such a variation cannot be simulated with the more simplistic one/two zone models, which are also considered a more advanced procedure in regard to the nominal temperature-time curves found in Eurocode 1, but less advanced than CFD modeling.

The most influential parameter of the fire development is the malfunction of the water sprinkler system. Sprinklers, even partially functional, can control or suppress the fire, however its extinguishing effect highly depends on whether the ignition point of the fire is covered. These systems are not specifically designed to withstand seismic forces, but in a fire-after-earthquake event, if designed with earthquake performance in mind, could prevent the building's destruction.

Ventilation is the second most influential parameter of the fire development, especially in the absence of an active fire extinguishing system. Window breakage changes the ventilation conditions of the compartment and can result in much higher temperatures than the ones considered during the fire design process, where all the systems are considered undamaged and fully functional. For the specific building, the scenario with all the windows damaged, which is a very probable event after an earthquake, leads to temperatures which are much higher compared to the ones occurring when there is no damage at the building. However more ventilation from the beginning of the fire provides a 40 minutes time window for the fire to be suppressed by human intervention, before the fire starts growing out of control.

The steel frames that are situated next to open windows are considerably more affected than the ones that have no ventilation near them. The position of the openings is never considered during the structural design of the building especially in the ones of industrial purpose. An open window however during a fire near the structural element could increase greatly the heat exposure of the element.

Regarding the fire design process, though both earthquake and fire are considered accidental events and should not be considered simultaneously for the structural design of the building, it is observed that there is correlation between post-earthquake non-structural damage and the way natural fire develops in the building. In some cases it would be advisable to consider the change in the structure's fire behavior caused by non-structural damage.

This type of analysis could not be performed without the use of Computational Fluid Dynamics which proves to be very useful, both as a research and design tool for the engineer. Specifically in the field of fire engineering it can aid the fire design of buildings which do not conform to the provisions for a simpler design approach, though it should be used with extreme caution, as is the case for all advanced computational methods.

References

- Babrauskas V., (2002), Ignition of Wood: A Review of the State of the Art, *J. Fire Protection Engineering* 12, 163-189
- Drysdale, D. (1999), *An Introduction to Fire Dynamics*, 2nd edition, Wiley, Chichester
- EN 1991-1-2, Eurocode 1: Actions on structures – Part 1-2: General actions – Actions on structures exposed to fire.
- Fire Dynamics Simulator and Smokeview, FDS-release5.5.3 SMV-release5.6, website: <http://code.google.com/p/fds-smv/>, (2012)
- Fong, Y.Y. and Fong N.K. (2003), “Scale Modelling of Smoke Movement in Linear Atrium”, *International Journal on Engineering Performance-Based Fire Codes*, Volume 5, Number 4, p.149-151.
- Gissi, E. (2010), *An introduction to Fire Simulation with FDS and Smokeview*, Creative Commons Licence, <http://www.emanuelegissi.eu/>
- Graf S. H., (1949), *Ignition Temperatures of Various Papers, Woods, and Fabrics* (Oregon State College Bull. 26), Oregon State College, Corvallis
- JukkaVaari, SimoHostikka, Topi Sikanen & Antti Paajanen,(2012), *Numerical simulations on the performance of water-based fire suppression systems*, VTT Technology 54
- Karlson, B. and Quintiere, J. (2000), *Enclosure Fire Dynamics*, CRC Press, Boca Raton
- Lönnermark, A. and Ingason, H.,(2005), *Fire Spread in Large Industrial Premises and Warehouses*, SP Swedish National Testing and Research Institute, 2005
- McGrattan, K. et al, (2007), *Fire Dynamics Simulator (Version 5) Technical Reference Guide Volume 1: Mathematical Model*, NIST Special Publication 1018-5, NIST, U.S. Government Printing Office, Washington
- McGrattan, K. et al, (2007), *Fire Dynamics Simulator (Version 5) User’s Guide*, NIST Special Publication 1019-5, NIST, U.S. Government Printing Office, Washington
- Ohnishi, K., (1996), “Causes of the great fires following the Great Hanshin-Awaji Earthquake survey” in “Thirteenth meeting of the UJNR panel on fire research and safety, March 1996, Volume 2, pg 337-344, NISTIR 6030.
- Scawthorn, Ch., (1996), “Fires following the Northridge and Kobe earthquakes”, in “Thirteenth meeting of the UJNR panel on fire research and safety, March 1996, Volume 2, pg 325-334. NISTIR 6030.
- Wiscombe, W.J.,(1980), “Improved Mie Scattering Algorithms”. *Applied Optics*, 19(9):1505–1509